PNNL-28064
DVZ-RPT-0010 Rev 0

Pacific Northwest
NATIONAL LABORATORY

Evaluation of Remediation Technologies for Iodine-129: FY18 Bench Scale Results

September 2018

JE Szecsody	EC Gillispie
C Pearce	AR Lawter
KJ Cantrell	BN Gartman
NP Qafoku	CF Brown
G Wang	

U.S. DEPARTMENT OF
ENERGY

Prepared for the U.S. Department of Energy
under Contract DE-AC05-76RL01830

PACIFIC NORTHWEST NATIONAL LABORATORY
operated by
BATTELLE
for the
UNITED STATES DEPARTMENT OF ENERGY
under Contract DE-AC05-76RL01830

Printed in the United States of America

Available to DOE and DOE contractors from the
Office of Scientific and Technical Information,
P.O. Box 62, Oak Ridge, TN 37831-0062;
ph: (865) 576-8401
fax: (865) 576-5728
email: reports@adonis.osti.gov

Available to the public from the National Technical Information Service
5301 Shawnee Rd., Alexandria, VA 22312
ph: (800) 553-NTIS (6847)
email: orders@ntis.gov <http://www.ntis.gov/about/form.aspx>
Online ordering: http://www.ntis.gov

PNNL-28064
DVZ-RPT-0010 Rev 0

Evaluation of Remediation Technologies for Iodine-129: FY18 Bench Scale Results

September 2018

JE Szecsody
C Pearce
KJ Cantrell
NP Qafoku
G Wang
EC Gillispie
AR Lawter
BN Gartman
CF Brown

Prepared for
the U.S. Department of Energy
under Contract DE-AC05-76RL01830

Pacific Northwest National Laboratory
Richland, Washington 99352

Executive Summary

At the U.S. Department of Energy's (DOE's) Hanford Site, located in southeastern Washington State, ^{129}I was produced as a byproduct of nuclear fission in the site's nine Pu production reactors. Currently, there are large dilute ^{129}I groundwater plumes at Hanford, including a groundwater plume in the 200-UP-1 operable unit (OU) located within the Central Plateau. The interim Record of Decision (ROD) for the 200-UP-1 OU requires that DOE evaluate potential treatment options for I-129 before a final ROD is issued. A remedy evaluation plan was subsequently published and identified the approach for this effort. The laboratory evaluation reported herein is part of the remedy evaluation. This report builds from information gathered in previous literature reviews of potential remedy technologies and provides laboratory testing results for promising candidates in support of determining which candidates warrant additional evaluation through treatability testing.

Based on samples of 200 West Area groundwater, iodine is present in the plume as a mix of iodide (I^-), iodate (IO_3^-), and organo-I species, with iodate as the dominant species in most groundwater samples analyzed to date. Thus, evaluation of technologies focused on the two most common iodine species, iodide and iodate. Candidate in situ technologies and materials for use in aboveground treatment processes (e.g., as part of a pump-and-treat [P&T] system) were tested in the laboratory to evaluate their effectiveness under conditions relevant to the 200-UP-1 OU. Within this report, the technologies are organized into three broad categories: in situ sequestration or removal of iodine from groundwater, in situ mobilization of iodine to enhance extraction efficiency, and ex situ removal of iodine from groundwater to support P&T operations.

For in situ sequestration, co-precipitation of iodate with calcium carbonate was investigated using three methods. The first method evaluated iodate uptake as a function of calcite precipitation rate. The second method explored the impact of solution chemistry on iodate uptake by calcite, and the final approach examined the impact of surface area on iodate uptake. While all three investigations demonstrated the ability to remove iodate from Hanford-representative solutions at relevant total iodine solution concentrations, none of the approaches were effective at removing more than 70% iodate from solution. This presents a serious shortcoming for in situ application; therefore, further testing of in situ formation of calcite for remediation of ^{129}I is not recommended.

Precipitation of initially amorphous calcium-phosphate (which slowly crystallizes to apatite), another potential in situ treatment approach, inconsistently removed a small amount of iodate from solution at pH 11 and above, and none at pH 9.0 and 7.5. In the 40 experiments performed as part of this study, many showed greater uptake during initial amorphous calcium phosphate precipitation, and less iodate uptake as the precipitate crystallized to hydroxyapatite. Iodate removal from solution via either sorption onto or incorporation into apatite was insufficient to meet the maximum contaminant level of 1 pCi/L in groundwater; therefore, further testing of this technology for remediation of ^{129}I is not recommended.

A series of batch adsorption/desorption experiments was also conducted to determine the effectiveness of several organic materials for sequestering iodate and iodide from Hanford groundwater. The organic materials that were evaluated in this study were chitin, lignin, and humic acid sorbed to a representative Hanford sediment. Of the three organic carbon materials tested, only chitin showed potential as an in situ remediation technology for iodide (average K_d value of 74.9 ± 4.3 mL/g). However, iodine within the groundwater at 200-UP-1 is primarily in the form of iodate, which limits the effectiveness of chitin as a removal technology. As such, further testing of this technology is not recommended.

Laboratory results indicated that iodate and iodide are effectively removed from Hanford groundwater by iron oxides, especially HFO, either through sorption or co-precipitation processes. The high sorption

capacity at neutral pH conditions, low cost, and likely ability to precipitate HFO in situ, indicate that this approach is a promising candidate for iodate and iodide remediation in the 200-UP-1 OU. Further testing of this technology is recommended.

The use of dithionite was identified as a potential remedial approach for enhancing pump-and-treat extraction. Results demonstrated that dithionite treated sediments enabled much greater (4x or more) and rapid (one to three orders of magnitude) leaching of iodine from the sediment compared to leaching of untreated sediment. This technology is a promising candidate to accelerate removal of iodine from the surface by P&T in areas where sorption limits extraction efficiency. Further testing of this technology is recommended for this type of application.

A wide range of materials for above ground treatment were also tested for their capacity to remove iodate from groundwater. Synthetic groundwater was used in the experiments to evaluate iodate removal in the presence of the competing anions. Ferrihydrite, bismuth oxy(hydroxide), and bismuth-cobalt-aluminum are the most promising materials, and the observed batch-test removal efficiency is sufficient to reduce concentrations of I-129 from 30 pCi/L to 1 pCi/L, even in the presence of a total iodine concentration loading due to the presence of stable iodine (I-127) in the groundwater at concentrations 1000 times higher than I-129. Hence, these materials are recommended for column testing with relevant influent concentrations to verify removal efficiency.

Acknowledgments

This document was prepared by the Deep Vadose Zone – Applied Field Research Initiative at Pacific Northwest National Laboratory. Funding was provided by the U.S. Department of Energy (DOE) Richland Operations Office. Pacific Northwest National Laboratory is operated by Battelle Memorial Institute for the DOE under Contract DE-AC05-76RL01830.

Acronyms and Abbreviations

AGW	artificial groundwater
BBB	1,4-bis(bromomethyl)benzene
BTC	1,3,5-benzenetricaboxylate
CAC	Carbon Activated Corporation
COPC	contaminant of potential concern
CPN	cationic polymeric network
CPS	calcium polysulfide (CaS_x)
DDI	double de-ionized
DDW	degassed and deionized water
DOE	U.S. Department of Energy
EDS	energy dispersive X-ray spectroscopy
GAC	granulated activated carbon
HA	humic acid
HF	Hanford fine sand
HFO	2-line-ferrihydrite
IC	inorganic carbon
ICP-OES	inductively coupled plasma – optical emission spectroscopy
ICP-MS	inductively coupled plasma – mass spectrometry
MOF	metal organic framework
NAPL	non-aqueous phase liquids
OU	operable unit
P&T	pump-and-treat
PDA	polydopamine
PNNL	Pacific Northwest National Laboratory
PV	pore volume
ROD	record of decision
SAGW	sediment with artificial groundwater
SEM	scanning electron microscopy
SSA	specific surface area
TIPE	1,1,2,2-tetrakis(4-(imidazolyl-4-yl) phenyl)ethene
TOC	total organic carbon
VZPW	synthetic vadose zone porewater
XAS	X-ray absorption spectroscopy
XPS	X-ray photoelectron spectroscopy
XRD	X-ray diffraction

Contents

Figures

Tables

1.0 Introduction

Due to its long half-life (15.7 Ma) and relatively unencumbered migration in subsurface environments (Sheppard et al. 1995; Bird and Schwartz 1997; Cantrell et al. 2003; Um and Serne 2005), ^{129}I has been recognized as a contaminant of concern at numerous federal and international nuclear facilities (DOE 1996; Hou et al. 2003; Kekli et al. 2003; Hartman et al. 2004). At the U.S. Department of Energy's (DOE's) Hanford Site, located in southeastern Washington State, ^{129}I was produced as a byproduct of nuclear fission in the site's nine Pu production reactors. Release of waste solutions (both purposeful and inadvertent) to the environment has resulted in ^{129}I being the second-most widespread radionuclide in the Hanford groundwater system (DOE 2016). Currently, there are large, dilute ^{129}I groundwater plumes, including a groundwater plume in the 200-UP-1 operable unit (OU) located within the Central Plateau (Figure 1.1). The interim Record of Decision (ROD) for the 200-UP-1 OU requires that DOE evaluate potential treatment options for I-129 before a final ROD is issued (DOE 2012). A remedy evaluation plan was subsequently published and (DOE 2017) identified the approach for this effort. The laboratory evaluation reported herein is part of the remedy evaluation. This report builds from information gathered in a literature review of potential remedy technologies (Strickland et al. 2017a,b) and provides laboratory testing results for promising candidates in support of determining which candidates warrant additional evaluation through treatability testing.

Based on samples of 200 West Area groundwater, iodine is present in the plume as a mix of iodide (I^-), iodate ($IO3^-$), and organo-I species, with iodate as the dominant species in most groundwater samples analyzed to date. Thus, evaluation of technologies focused on the two most common iodine species, iodide and iodate. Candidate in situ technologies and materials for use in aboveground treatment processes (e.g., as part of a pump-and-treat [P&T] system) were tested in the laboratory to evaluate their effectiveness under conditions relevant to the 200-UP-1 OU. Detailed descriptions of the ^{129}I plume and factors important for remediation technologies are provided in a series of reports describing the conceptual model for iodine behavior in the Hanford Site subsurface (Truex et al. 2015, 2016, 2017; Qafoku et al. 2017), and were considered in designing the laboratory tests used to evaluate technologies.

Strickland et al. (2017a) identified several potential technologies. The set of technologies evaluated was expanded based on a literature review by Strickland et al. (2017b). Within this report, the technologies are organized into three broad categories: in situ sequestration or removal of iodine from groundwater, in situ mobilization of iodine to enhance extraction efficiency, and ex situ removal of iodine from groundwater to support P&T operations. Evaluated technologies are summarized in the following sections.

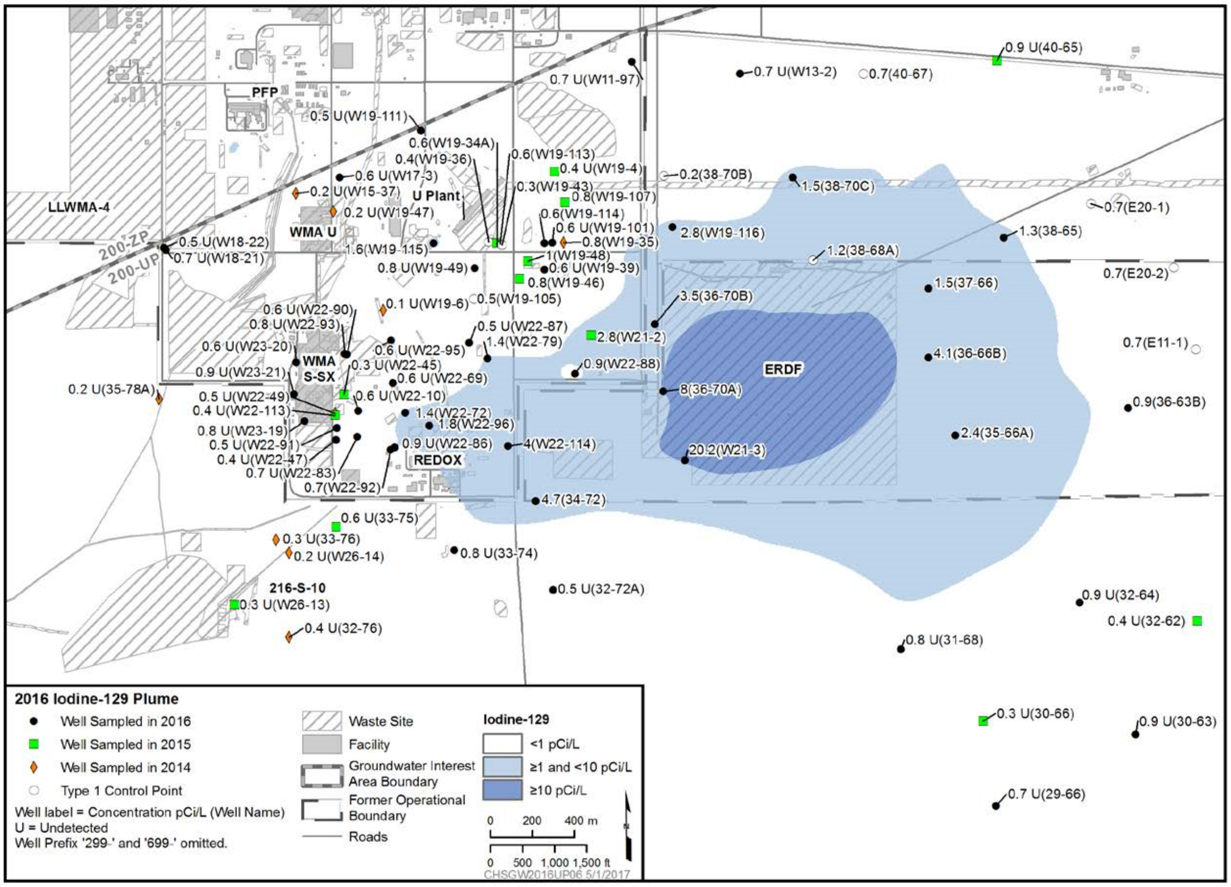

Figure 1.1. 2016 I-129 plume map (from DOE-RL 2016).

1.1 Category 1: In Situ Sequestration or Removal of Iodine from Groundwater

1.1.1 Co-precipitation and Enhanced Sorption by Calcite

The laboratory study focused on evaluating methods to induce calcite precipitation in situ over a large radial distance from an injection well. Key to this effort was ensuring a suitable precipitate mass to create slow-release conditions for iodate while not clogging aquifer pores. Previous calcite precipitation experiments showed removal of iodine by incorporation into calcite during calcite precipitation (50% aqueous iodate removed) (Truex et al. 2016). However, there was a need to further increase iodate uptake by calcite to make this a viable in situ remediation strategy. The calcite precipitation method used during previous years was modified to determine if iodate uptake could be increased. Modifications included calcite formation in synthetic vadose zone porewater (VZPW) instead of double de-ionized (DDI) water, precipitation of nano-calcite to increase surface area, and use of alternative precipitation methods to enhance iodate sorption/uptake.

1.1.2 Co-precipitation and Enhanced Sorption by Iron Oxides

Interaction of iodide and iodate with iron oxides was evaluated, building on the work by Couture and Seitz (1983) and Fuhrman et al. (1998). Laboratory-scale efforts focused on two tasks: (1) understanding the interactions of iodate/iodide with iron oxides (sorption/desorption, and co-precipitation), and (2) evaluating methods to induce iron oxide precipitation in situ over a large radial distance from an injection well and at a suitable mass to create enhanced sorption and slow-release conditions for iodine species without clogging aquifer pores. For task 1, batch experiments were conducted to investigate the immobilization of iodine through association with iron oxides (in terms of distribution coefficient K_d). Building on the previous test results that focused on iodate/iodide sorption onto pure iron oxides in artificial groundwater (AGW) (Strickland et al. 2017a), testing was expanded to include reversibility testing (i.e., desorption) of iodate/iodide on iron oxides in AGW, as well as iodate/iodide behavior during iron oxide transformation between different phases, such as ferrihydrite to goethite or to magnetite. Experiments also involved 1-D flow through soil columns using amendments identified to induce iron oxide precipitation in situ.

1.1.3 Enhanced Sorption by Organic Carbon

These laboratory tests focused on evaluating types of organic carbon that could be injected as a permeable reactive (sorption) barrier. Candidates included chitin, lignin, and humic/fulvic acids sorbed to a Hanford sediment. Batch partitioning and desorption studies were conducted for the candidate materials. In the case of humic/fulvic acids sorbed to Hanford sediment, both as is and sterilized sediments were evaluated to determine potential impacts of microbial activity. Selected samples were analyzed for iodine speciation to determine if any changes in iodine speciation occurred during the course of the experiments.

1.1.4 Co-precipitation and Enhanced Sorption by Apatite

Previous work (Campayo et al. 2011) identified up to 7% iodate incorporation into solid apatite with a pH 10 to 12 solution. Apatite technology evaluation focused on adapting and testing this technology under Hanford groundwater conditions. Tests were conducted by adding apatite forming chemicals to solutions containing iodate and iodide. The loss of iodine from solution was monitored as a function of time. Additionally, adsorbed iodine species and measurement of incorporated iodine species were quantified through analysis of the solid-phase materials (by acid dissolution of the precipitated apatite). The test matrix included multiple tests to evaluate the effect of pH, iodine concentration, iodine/phosphate ratio, and the addition of carbonate on iodine species uptake.

1.2 Category 2: In Situ Mobilization of Iodine to Enhance Extraction Efficiency

1.2.1 Dithionite-Enhanced Mobility

The enhanced mobility screening tests focused on using a low concentration solution of sodium dithionite to reduce iodide to iodate, thereby reducing its sorption potential by up to a factor of four (Xu et al. 2015; Truex et al. 2016). This technology is targeted at accelerating removal of iodine from the surface by P&T in areas where sorption limits extraction efficiency. This laboratory study focused on identifying appropriate concentration ranges of dithionite to release and maintain iodine mobility by converting iodate to iodide and by dissolving iron oxides on sediment surfaces, releasing iodine species to aqueous solution. Batch experiments were conducted to bound the appropriate concentration ranges and evaluate potential analytical interferences with iodine quantification. Samples were also analyzed to determine the magnitude of other constituents released by the dithionite treatment. Soil column experiments were used to quantify water quality after treatment and to determine if released ferrous iron that is oxidized downgradient of the treatment would sequester the iodine and nullify the enhanced mobilization.

1.3 Category 3: Ex Situ Removal of Iodine from Groundwater to Support Pump and Treat Operations

1.3.1 Materials for Iodine Immobilization

The objective of this task was to conduct a set of batch sorption experiments with selected materials for ex situ iodate immobilization in a representative synthetic Hanford groundwater. The materials that were evaluated in this study included iron oxides (ferrihydrite, micro-magnetite, nano-magnetite, goethite, ferrous hydroxide), sulfides (potassium metal sulfide, iron sulfide), organoclays (PM-199 and MRM, Cetco), bismuth-based materials (bismuth nitrate), metal organic frameworks (SCU-101, SCU-102, SCU-CPN, FeBTC-PDA) and aerogels (sulfur functionalized aerogels, copper-functionalized aerogels). These materials were tested alongside the baseline materials currently used in the 200 West PP&T Plant (Purolite A530E Ion Exchange Resin and Carbon Activated Corporation 011-55 Granulated Activated Carbon), because previous work has demonstrated that strong base anion exchange resins can remove iodine from Hanford groundwater (Parker et al. 2014; Levitskaia et al. 2017). Silver-based materials were not included for testing because silver is a *Resource Conservation and Recovery Act* metal and its use for remediation activities may be restricted. It is notable that an in-situ treatment zone created through injection of submicron silver chloride particle is being evaluated at the Savannah River Site (Denham and Eddy-Dilek 2016).

2.0 Co-Precipitation with Calcite

Previous experiments have shown removal of iodine by incorporation into calcite during precipitation (~50% aqueous iodate removed); however, there is a further need to increase iodate uptake for this approach to be a viable remediation strategy. Various modifications to the calcite co-precipitation approach were made to determine if iodate uptake could be improved. Modifications included calcite formation in the presence of silica gel, which slows down the rate of calcite precipitation, and is expected to result in greater iodate incorporation into calcite. The effects of other background solutions on iodate incorporation into calcite (including synthetic VZPW and/or AGW instead of DDI) were evaluated. In addition, methods to precipitate nano-calcite to increase surface area with the aim of greater iodate incorporation were assessed.

2.1 Experimental Methods

2.1.1 Iodate Co-Precipitation with Calcite in the Presence of Si Gel

Iodate-doped calcium carbonate in a sodium metasilicate gel was synthesized using a modified procedure described by Podder et al. (2017). The starting materials included analytical grade sodium metasilicate (Na_2SiO_3; 18 mesh granular and purity ≥95.0% Alfa Aesar), calcium chloride ($CaCl_2$; ≥97% Sigma-Aldrich), ammonium carbonate ($(NH_4)_2CO_3$; Purity Grade Fisher Scientific), sodium iodate ($NaIO_3$; ≥99% Acros Organics), acetic acid ($C_2H_4O_2$; ACS Grade ≥99.7% Fisher Scientific), and Milli-Q water (18.2 MΩ cm at 21°C). Five batches of Na_2SiO_3 + 1 M acetic acid were made, which corresponded to five concentrations of iodate spiked in calcite. First, 2.5 g Na_2SiO_3 was added in 50 mL of distilled deionized water, stirred for 30 min, and then left undistributed for another 30 min. Subsequently, a 1 M acetic acid solution was prepared and stirred for 15 min. In order to prepare the Na_2SiO_3 gel (specific gravity of approximately 1.05 g/cm^3), the 50 mL Na_2SiO_3 solution was added drop wise to 50 mL of 1 M acetic acid in 150 mL high-density polyethylene bottles (Fisher Scientific, USA) using a transfer pipette, while constantly stirring the solution at 100 rpm. One hundred milliliters of 0.1 M ammonium carbonate was impregnated into the gel solutions for each batch. Additionally, $NaIO_3$ at the concentrations of 100 (0.51 μM), 250 (1.3 μM), 500 (2.5 μM), and 395784 (2.0 mM) μg/L was added to the gel solution separately. Concentrations between 100 and 500 μg/L were chosen in order to closely mimic elevated environmental levels and the 2.0 mM concentration was the lowest concentration used in Podder et al. (2017) and chosen for a comparison of technique. Approximately 25 mL of each combined solution was slowly placed into five 50 mL polypropylene centrifuge tubes (Corning Incorporated) and left to settle (ca. 5 min). Each tube was then covered with 20 mL of 0.1 M $CaCl_2$, gently agitated, and capped. Solutions gelled after roughly 2 weeks and small amounts of calcite precipitation occurred after 4 weeks.

To quantify the amount of iodine from calcite precipitation, the solution was centrifuged (Thermo Electron Corporation; HN-SII Bench-Top) from gel + calcite material at approximately 2500 rpm, decanted, filtered (0.2 micron), and measured for total iodine using inductively coupled plasma mass spectrometry (ICP-MS). Currently, there are no effective methods for complete separation of calcite from Si gel matrix. Therefore, several techniques were tested for complete separation and evaluated below.

2.1.1.1 Separation Considerations

Several techniques (i.e., centrifuging, sonication, rinsing and filtration, dissolution) were considered to separate solution and calcite from Si gel. Centrifuging the samples twice, once to extract the bulk solution and a second time to extract any remaining solution within the gel, was an effective technique to remove all solution from the remaining gel. Most solutions were fully separated from the gel + calcite material after only one time centrifuging (20 min, ca. 2500 rpm). During this process, calcite appeared uniformly trapped in the gel and no visible calcite was present or decanted with the solution. Due to the novelty of this technique, it was assumed that iodate captured in the gel + calcite material would be immobilized in field conditions whether bound to calcite or the Si gel. Additionally, it is likely that calcite would have a greater affinity for iodate than silicate, and therefore iodine is expected to be mostly bound to calcite. However, it will be important to better understand the mechanism of immobilization prior to deploying Si gel as a remediation tool.

Sonication was considered as a possible technique to further separate calcite from Si gel. A 50 mL centrifuge tube with solution, Si gel, and calcite was placed into a rack and put into a bench top sonicator (Fisher Scientific; FS30H) filled with DDI water and left to sonicate for 15 minutes. After 15 minutes, some Si gel migrated toward the bottom of the centrifuge leaving roughly 5 mL of solution as a layer at the top. Due to the amount of time it would take to separate the solution from gel using this technique, and the fact that calcite still remains in the gel, centrifuging is a better technique for solution separation. Further tests could be conducted to evaluate just gel and calcite separation using either a bench sonicator or sonic dismembrator.

Calcite and Si gel material were placed onto a 0.45 micron filter (Millipore Express®; Stericup vacuum driven disposable filtration system), rinsed with DDI water during vacuum, and set aside to air dry in a fume hood. After a week, solids appeared to be crystalized calcite minerals, where the crystallization could have incorporated small amounts of silica. This technique has the potential to separate out calcite from Si gel; however, further tests need to be conducted to determine if the mass balance of iodate uptake matches that from solution and if the chemical composition of the solid is pure calcite or contains silica impurities. Qualitative analyses of the initial tests suggest that not all of the Si gel is removed with the process of rinsing and drying.

2.1.1.2 Differences from Podder et al. Synthesis and Separation Methods

According to Podder et al. (2017), solid products were washed with deionized water and air dried. Once dry, samples were examined under a microscope and were hand-picked to separate calcium carbonate minerals. Based on testing, washing of solid products did not effectively separate gel material from calcite and the calcite was too well mixed and small in size to be hand-picked. This approach would likely result in loss of the majority of calcite and thus be an inadequate representation of the amount of iodine that was co-precipitated with calcite.

Additionally, iodine in calcite and vaterite was dissolved using HF-HNO_3, which could result in the volatilization of iodine due to the extreme acidic conditions and loss of total iodine actually found in these minerals. Therefore, samples were digested using alkaline fusion and analyzed via ICP-MS.

2.1.2 Iodate Co-Precipitation with Calcite from VZPW and AGW

Calcite was precipitated in Hanford VZPW and AGW to test the extent of iodate uptake in calcite. Calcite forming solutions were prepared in VZPW and AGW and contained 0.1 M $CaCl_2$ and 0.1 M $(NH_4)_2CO_3$ (Truex et al., 2017). The VZPW solution comprised of 12 mM $CaSO_4*2H_2O$ (Acros Organics), 1.7 mM NaCl (ACS Grade Spectrum Chemical, 0.4 mM $NaHCO_3$ (ACS Grade Fisher Scientific), 3.4 mM $NaNO_3$ (≥99% Sigma-Aldrich), 2.6 mM $MgSO_4$ (J.T. Baker), 2.4 mM $MgCl_2*6H_2O$ (ACS Grade Fisher Scientific), and 0.7 mM KCl (ACS Grade Fisher Scientific) adjusted to a pH of 7.14 (Serne et al. 2015) (Table 2.1). The AGW solution comprised of 0.20 mM $H_2SiO_3*nH_2O$, 0.11 mM, KCl, 0.15 mM $MgCO_3$, 0.26 mM NaCl, 0.49 mM $CaSO_4$, and 1.5 mM $CaCO_3$ and measured a pH value range of 7.5-7.6 (Table

2.2). In addition to VZPW and AGW, calcite was precipitated in DDI water spiked with and without iodate as controls. Iodate uptake during calcite precipitation was tested by spiking VZPW, AGW, and DDI water solutions with 100 (0.51 µM), 250 (1.3 µM), 500 (2.5 µM), and 395784 (2.0 mM) µg/L $NaIO_3$, concentrations consistent with those discussed in section 2.1. Batch experiments were conducted in duplicate in 250 mL high-density polyethylene bottles (Fisher Scientific, USA).

The VZPW was made by addition of the reagents in Table 2.1 to DDI water in the order identified in Table 2.1. Once the reagents had all been added, the solution pH was adjusted with the addition of sodium hydroxide or sulfuric acid to a final pH of between 7.0 and 7.2.

Table 2.1. Vadose zone porewater (VZPW) simulant recipe (from Serne et al. 2015).

Order to Dissolve	M	Reagent	MW	g/L
1	0.012	$CaSO_4*2H_2O$	172.1723	2.0661
2	0.0017	NaCl	58.4430	0.0994
3	0.0004	$NaHCO_3$	84.0068	0.0336
4	0.0034	$NaNO_3$	84.9948	0.2890
5	0.0026	$MgSO_4$	120.3660	0.3130
6	0.0024	$MgCl_2*6H_2O$	203.3034	0.4879
7	0.0007	KCl	74.5515	0.0522

Adjust pH to 7.0 to 7.2 with sodium hydroxide or sulfuric acid.

The AGW was made by addition of the reagents in Table 2.2 to DDI water in the order identified in the table. Once the chemicals were dissolved, an excess of calcium carbonate ($CaCO_3$) was added and the solution was stirred. After approximately one week, the solution was filtered to remove excess $CaCO_3$ using a 0.45-µm filter.

Table 2.2. Artificial Hanford groundwater (AGW).

Constituent	Conc. (mg/L)	Mass for 1 L (g)
$H_2SiO_3*nH_2O$, silicic acid	15.3	0.0153
KCl, potassium chloride	8.20	0.0082
$MgCO_3$, magnesium carbonate	13.0	0.0130
NaCl, sodium chloride	15.0	0.0150
$CaSO_4$, calcium sulfate	67.0	0.0670
$CaCO_3$, calcium carbonate	150	0.1500

After the VZPW and/or AGW were prepared, the calcite forming solutions were made. To remain consistent with previous calcite formation studies (Truex et al. 2017), 1M or 0.1M $CaCl_2$ and $(NH_4)_2CO_3$ were used as the calcite forming solutions. These calcite forming solutions were prepared in VZPW, AGW, and/or DDI water. Table 2.3 provides the appropriate amount of each chemical added for the two molarities.

Table 2.3. Calcite forming solutions.

Constituent	Molarity	Mass for 1 L (g)
$CaCl_2$, calcium chloride	0.1M	11.098
	1M	110.98
$(NH_4)_2CO_3$, ammonium carbonate	0.1M	19.218
	1M	192.18

To precipitate calcite, equal volumes of the $CaCl_2$ and $(NH_4)_2CO_3$ solutions of equal molarity were slowly added together in a PTFE poly bottle (e.g., 50 to 250 mL of each solution). Iodate spikes (from a stock $NaIO_3$ solution to achieve concentrations in the range 100 to 500 µg/L) was added to the $CaCl_2$ solution prior to the $(NH_4)_2CO_3$ addition. Once the calcite forming solutions were combined, calcite precipitation was visible immediately. Calcite was precipitated from solutions made in DDI water, as well as DDI water without calcite forming solutions (but spiked with $NaIO_3$) to serve as controls for these experiments.

After the calcium carbonate precipitation started, pH was measured and 2 ml of supernatant was sampled at approximately 0, 4, 24, and 72 hours, and then weekly for a minimum period of 28 days. The 2 mL samples were filtered with a 0.2 µm syringe filter. The contents of the bottles were gently swirled daily during regularly scheduled workdays, and were otherwise undisturbed between samplings. Following the completion of sampling events, the contents of the poly bottles were filtered with a 0.45 µm vacuum filter to collect the produced solids. After drying in a fume hood, the solids were collected for solid phase characterization by alkaline fusion and scanning electron microscopy (SEM) energy dispersive X-ray spectroscopy (EDS).

2.1.3 Iodate Co-Precipitation with Nano-Calcite

Nano-sized calcite was synthesized using a modified procedure from Montes-Hernandez et al. (2007). A 1M calcium hydroxide ($Ca(OH)_2$) solution was made by adding 1.85 g of $Ca(OH)_2$ (> 96% purity; Sigma-Aldrich) to a volumetric flask and filling up to 25 mL with DDI. A 25 mL Parr pressure reactor (Parr Instrument Company) was used to react the $Ca(OH)_2$ solution with CO_2 (800 psi) at 30°C. A rigid mantle heater with a heat controller receiving feedback directly from a J-type thermocouple (OMEGA Engineering Inc.; Precision Fine Wire) was used to maintain the reactor at 30°C. Solutions were spiked with either 100 or 500 µg/L sodium iodate and reacted for 4 and 24 h.

Samples were centrifuged and the solution decanted. Solids were dried at 80°C for 48 h. The weight of the decanted solution was recorded and a 4 mL aliquot was filtered using a 0.2 µm syringe filter (Merck Millipore; Millex – GV) and analyzed for total iodine using ICP-MS.

2.1.4 Analyses

2.1.4.1 Elemental Analyses

Total iodine was analyzed on two different ICP-MS instruments based on equipment availability. The first instrument was an X-Series II ICP Mass Spectrometer from Thermo Fisher Scientific and the second instrument was an ELAN DRC II ICP Mass Spectrometer from PerkinElmer. The detection limit for total iodine is 0.0126 µg/L for both instruments.

A suite of elements were analyzed based on the VZPW - aluminum, calcium, magnesium, potassium, silicon, sodium, sulfur, and tin. Detection limits for each element were 16, 33, 2.7, 161, 54, 44, 47, and 13 µg/L respectively.

2.1.4.2 Scanning Electron Microscope

The SEM instrument used for calcite size and morphology was a FEI Helio 600 dual beam. Samples were prepped by attaching double sticky carbon (C) tape to aluminum holders (Ted Pella) and sprinkling a small amount of sample powder to the C tape. Samples were then coated with a 10 nm C layer using a sputter coater to avoid charging.

2.1.4.3 Alkaline Fusion

Alkaline fusion was used to solubilize iodine from calcite using a PNNL Technical Procedure (No. PNNL-ESL-Fusion Rev. 2). In short, the calcite sample was mixed with a potassium hydroxide-potassium nitrate (KOH-KNO_3) solution in a nickel (Ni) crucible (Metal Technology; 20-0075HC) and dried. The crucible was then heated at approximately 550°C in a furnace (OMEGALUX; LMF – 3550) for about 60 minutes. KNO_3 is used as an oxidant to improve the dissolution potential of the flux. To recover samples from the crucibles after heating, samples were cooled and then rinsed with DDI and 5 mL of sulfuric acid into funnels over 50 mL polypropylene centrifuge tubes (Corning Incorporated) and brought to a volume of 30-35 mL. All Ni crucibles were new and cleaned by washing the crucibles and lids with 2% nitric acid (HNO_3), rinsed with DDI water, pre-heated in an oven (Thermo Scientific) to 150-200 °C, cleaned again, and air dried. All chemicals were ACS grade or equivalent. Each fusion process had 1 to 3 samples, a blank, a blank spike, at least one duplicate of a sample, and a sample matrix spike. An aliquot was then filtered using a 0.2 µm syringe filter and analyzed for total iodine using ICP-MS.

2.2 Results

2.2.1 Iodate Co-Precipitation with Calcite in the Presence of Si Gel

Iodate co-precipitation with calcite in the presence of Si gel was chosen as a potential method of iodate removal in the subsurface due to Si gel's ability to slow down the rate of formation of calcium carbonate minerals. In general, calcite formation is almost instantaneous and preliminary data has shown that the majority of iodate uptake occurs during this time. By slowing the precipitation of calcite, it is possible that more iodate could be removed over time. Results demonstrated that in the presence of Si gel, greater than 50% of total iodine in solution is removed within the calcite and gel mixture for all concentrations of iodate. Figure 2.1 shows that compared to initial spiked concentrations, calcite in Si gel removed the most iodine when the initial spike was 500 µg/L. Overall, 84% of iodine was removed when initial concentrations were 500 µg/L and 56% at 100 and 250 µg/L concentrations.

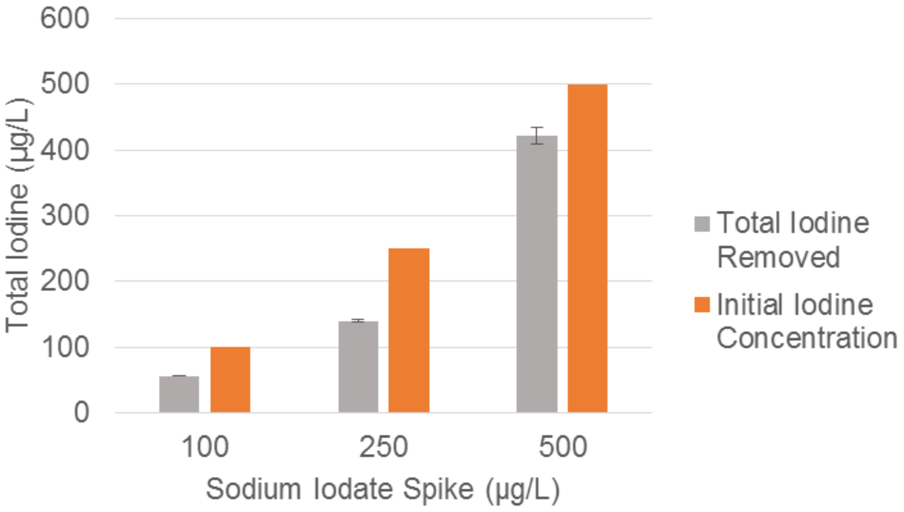

Figure 2.1. Removal of iodate after calcite precipitation in metasilicate gel. Treatments of Si gel and calcite were spiked with 100, 250, and 500 µg/L sodium iodate in a stock solution relative to the spike. Five replicates of each treatment were performed and left to sit for approximately five weeks until calcite formation. Orange bars represent initial iodine concentrations spiked into solutions. Gray bars represent the difference between the average measured iodine concentration and the original spike amount, assuming that the spike and solution were distributed evenly throughout the five centrifuge tubes. Error bars represent the standard deviation of the replicates for total iodine in solution.

As the concentration of iodate in solution increased (i.e., increase in spike), calcite removed the same percentage of iodate in both 100 and 250 µg/L treatments, yet the amount of iodine co-precipitated with calcite increased (Figure 2.1; Table 2.4). This suggests that calcite can indeed remove and bind more iodine but that other chemical mechanisms are having an effect, such as equilibrium between how much iodine is in the system and how much gets sorbed. Furthermore, an elevated concentration of iodine was tested (396 ppm) to compare to the lowest concentration of Podder et al. (2017). Results were similar to spikes with 100 and 250 µg/L iodine, where approximately 58% of iodine was removed from solution and resulted in 1129 µg of iodine loaded onto 1 g of calcite (Table 2.4).

Table 2.4. Iodine concentrations in calcite precipitated in Si gel.

Sodium Iodate Spike (µG/L)-	Total Iodine in Solution (µG/L)	Amount of Iodine Removed (µG IO_3^-/G of calcite)
100	44 ± 0.5	0.278
250	110 ± 1.2	0.689
500	79 ± 13	1.59
395784	167800 ± 2588	1129

2.2.2 Iodate Co-Precipitation with Calcite from VZPW and AGW

Various concentrations of sodium iodate were introduced into Hanford VZPW and AGW to better understand the effect of the chemical composition of solution on iodine removal in the presence of calcite. Our results indicate that the greatest amount of iodine was removed over time in VZPW at any given concentration and that removal of iodine was almost instantaneous for all solutions (Figure 2.2). After 28 days, calcite VZPW had removed 71, 168, 324, and 51284 µg/L of iodine for each respective spike (100, 250, 500, and 39,5784 µg/L), whereas calcite in AGW removed only 46, 121, 224, and 32,784 µg/L. Overall, the calcite in VZPW treatment removed 15-20% more iodate than in AGW or DDI. For treatments with 100 and 250 µg/L iodate, calcite in VZPW was able to remove up to 80% of the iodate in solution, whereas AGW removed 46 and 48% respectively and DDI 32 and 36%, respectively. When concentrations were extremely elevated with iodine (i.e., 396 ppm spike), only 8-12% of the iodine was removed across all solutions. Despite the differences in iodine removal, all solutions removed most of the iodine within the first 4 h but slightly increased in removal by day 28 (Figure 2.2). Varying iodate concentrations without calcite were also mixed with VZPW, AGW, and DDI, and no significant difference was noticed between samples on any iodine removal and concentrations remained at the initial levels (Figure 2.3).

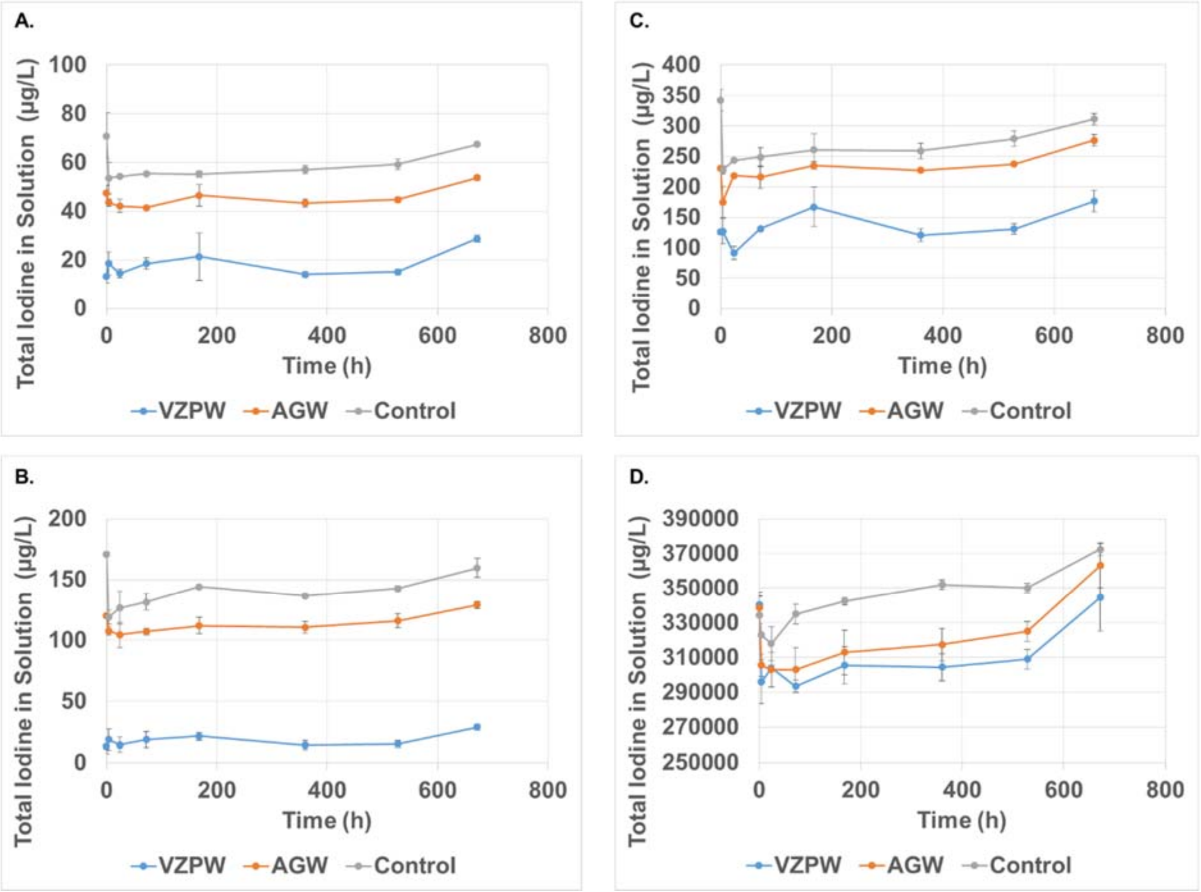

Figure 2.2. Iodine in solution after calcite precipitation in VZPW and AGW over time. Four concentrations of iodine - 100 µg/L (A), 250 µg/L (B), 500 µg/L (C), and 39,5784 µg/L (D) - were added to VZPW (blue line) and AGW (orange line) in the presence of calcium carbonate. Total iodine in solution was measured over a period of 28 days and sampled at 0 h, 4 h, 24 h, 3 d, 7 d, 15 d, 22 d, and 28 d. Gray lines represent iodine concentrations over time in DDI in the presence of calcite. Samples were performed in duplicate. Error bars represent the standard deviation of replicates for each time point.

Results from SEM images reveal that AGW and DDI produced purely calcite minerals, where VZPW produced a mixture of calcite and aragonite (Figure 2.4). This can be seen by the needle-like structures of aragonite and cubic structure of calcite. These results could suggest that the solution chemical composition and mineralogy of calcium carbonate has an impact on the effectiveness of iodate uptake. Within the chemical composition of VZPW, concentrations of the constituents, especially magnesium (Mg), were at much high molarities than in AGW (Table 2.5). Because of this, it is possible that a more complex structure composed of aragonite and calcite might be better in removing iodate than if just calcite was present. Lastly, alkaline fusion digestions were performed on VZPW, AGW, and DDI solutions with calcite spiked at 500 µg/L and resulted in 66.5, 48.5, and 40.9 µg/g of iodine present in calcite from the VZPW, AGW, and DDI solutions respectively.

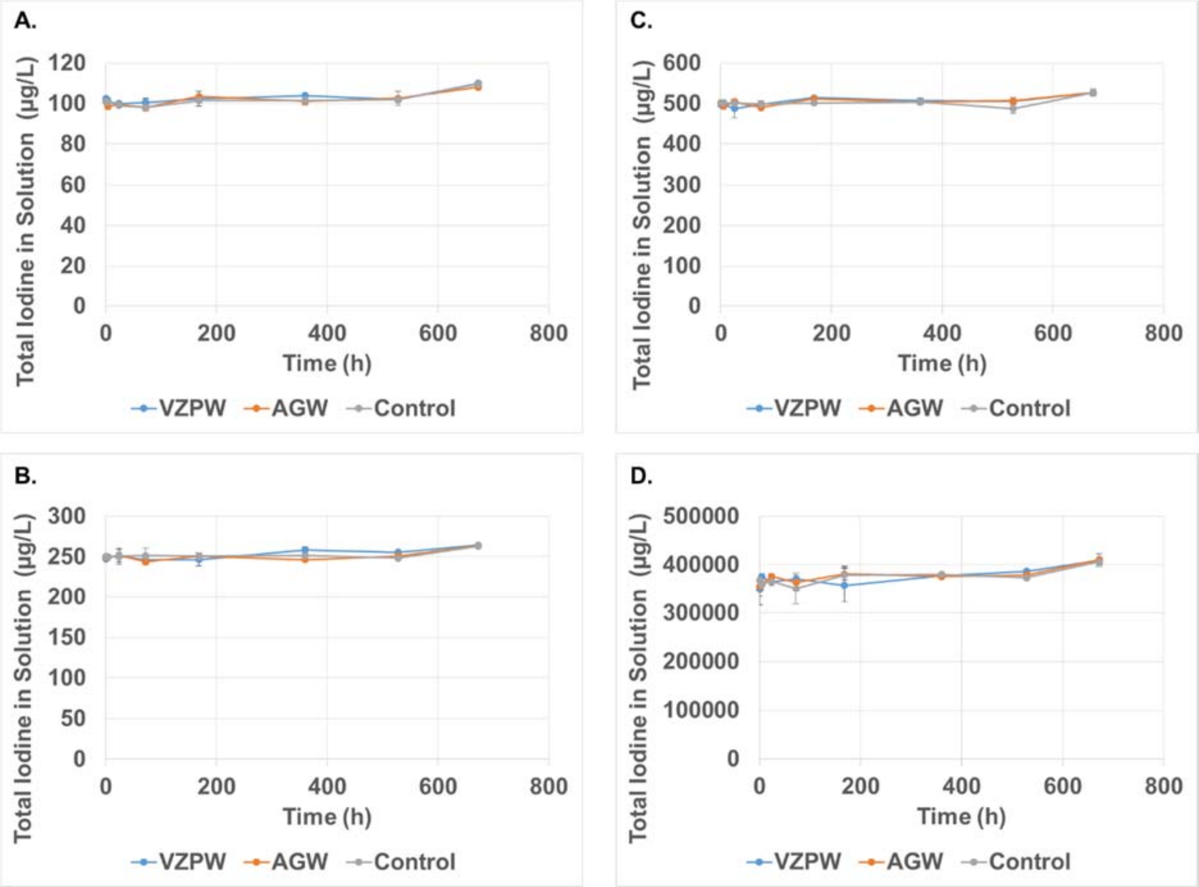

Figure 2.3. Iodine in VZPW and AGW over time. Four concentrations of iodine - 100 µg/L (A), 250 µg/L (B), 500 µg/L (C), and 395784 µg/L (D) - were added to VZPW (blue line) and AGW (orange line) and contained no calcite. Total iodine in solution was measured over a period of 28 days and sampled at 0 h, 4 h, 24 h, 3 d, 7 d, 15 d, 22 d, and 28 d. Gray lines represent iodine concentrations over time in DDI. Samples were performed in duplicate. Error bars represent the standard deviation of replicates for each time point.

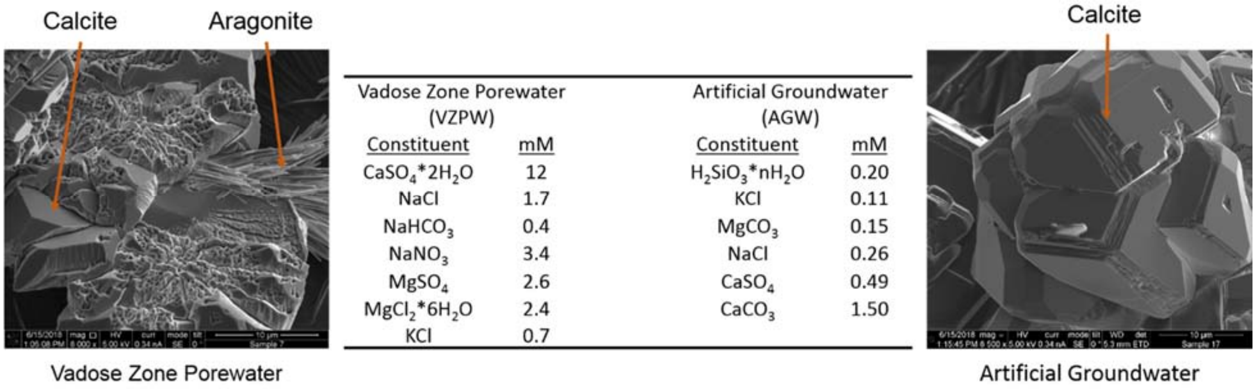

Vadose Zone Porewater (VZPW) Constituent	mM	Artificial Groundwater (AGW) Constituent	mM
$CaSO_4*2H_2O$	12	$H_2SiO_3*nH_2O$	0.20
NaCl	1.7	KCl	0.11
$NaHCO_3$	0.4	$MgCO_3$	0.15
$NaNO_3$	3.4	NaCl	0.26
$MgSO_4$	2.6	$CaSO_4$	0.49
$MgCl_2*6H_2O$	2.4	$CaCO_3$	1.50
KCl	0.7		

Figure 2.4. SEM image of calcium carbonate minerals after 28 days for 500 µg/L iodine in VZPW and AGW. Two types of calcium carbonate minerals were formed – aragonite (needle-like crystals) and calcite (cubic crystals) - in VZPW, a solution containing higher concentrations of groundwater constituents compared to AGW. Only calcite crystals formed in AGW.

Table 2.5. Chemical composition of AGW, VZPW, and DDI solutions with calcite after 28 days.

	AGW			VZPW			DDI		
Analyte (mg/L)	**100 ppb Spike**	**500 ppb Spike**	**396 ppm Spike**	**100 ppb Spike**	**500 ppb Spike**	**396 ppm Spike**	**100 ppb Spike**	**500 ppb Spike**	**396 ppm Spike**
Aluminum	BDL	BDL	BDL	6 ± 1	5 ± 1	4 ± 1	BDL	BDL	BDL
Calcium	180 ± 25	205 ± 3	270 ± 25	680 ± 26	681 ± 23	682 ± 48	214 ± 6	206 ± 1	276 ± 4
Magnesium	3 ± 0.1	3 ± 0.1	3 ± 0.1	102 ± 5	99 ± 1	98 ± 3	BDL	BDL	BDL
Potassium	BDL	BDL	BDL	31 ± 2	30 ± 1	30 ± 0.1	BDL	BDL	BDL
Silicon	8 ± 0.2	8 ± 0.3	8 ± 0.2	BDL	BDL	BDL	BDL	BDL	BDL
Sodium	6 ± 0.4	5 ± 0.1	75 ± 0.1	125 ± 6	121 ± 0	191 ± 6	BDL	BDL	71 ± 2
Sulfur	12 ± 0.2	12 ± 0.8	15 ± 0.2	449 ± 19	441 ± 4	455 ± 9	BDL	BDL	BDL
Tin	BDL	BDL	BDL	3 ± 0.2	2 ± 0.3	3 ± 0.1	BDL	BDL	BDL

2.2.3 Iodate Co-Precipitation with Nano-Calcite

Nano calcite was synthesized for 4 and 24 hours with 100 and 500 µg/L iodate spikes. According to SEM results, calcite formed two types of particles: Type 1 was a single well-formed calcite crystal and Type 2, which tended to be the rest of the particles, were small nanoparticles around 40 nm in size (Figure 2.5). Results from the Parr reactor experiments showed that after 4 h, ~ 79% and 76% iodate was removed from the 100 and 500 µg/L treatments, respectively. However, results also indicated that an increase in synthesis time (i.e. 24 h) increased the amount of iodate removed, where 83% and 78% of iodate was removed from the 100 and 500 µg/L treatments, respectively (Figure 2.6).

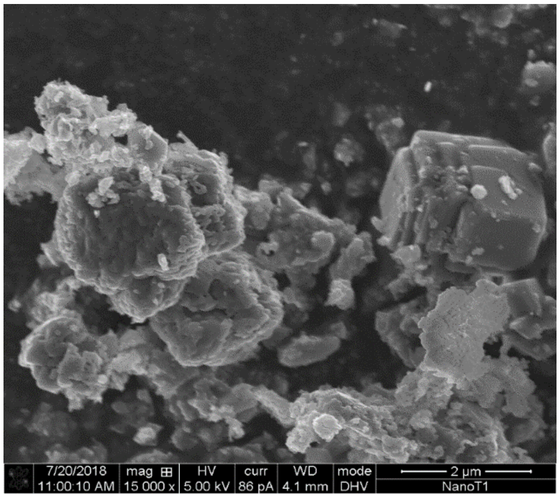

Figure 2.5. Nano calcite with 500 µg/L spike of Iodate after 4 hours. Two different types of calcite minerals formed after being synthesized for 4 h with 500 µg/L sodium iodate. Type 1 consists of large well-formed calcite cubes that look like single crystals (i.e. flat particles and not composed of aggregates). Type II consists of small size nanosize calcite particles (rest of particles) that are likely aggregates of small nanocrystals (~40 nm).

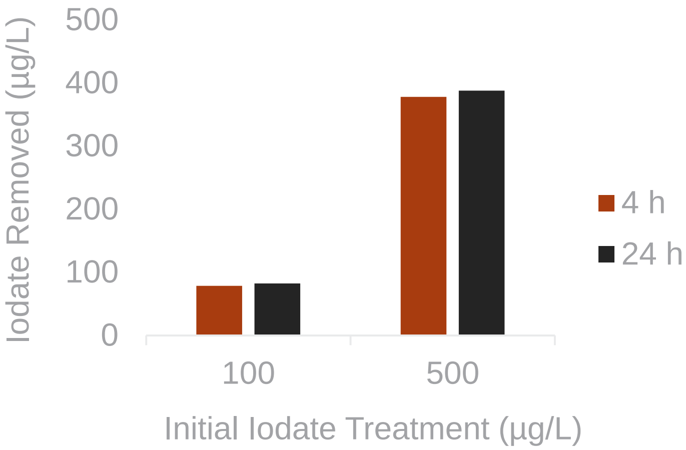

Figure 2.6. Iodate removal in nanocalcite after 4 and 24 h. Red and black bars represent iodate removed in nanocalcite after 4 h and 24 hour respectively for both 100 and 500 µg/L treatments. Experiments were not duplicated and therefore values do not have error bars.

3.0 Incorporation into Apatite/Carbonated Apatite

This laboratory study focused on evaluating (1) the effect of different geochemical conditions on iodate uptake by apatite with an attempt to replicate conditions in a previous study (Campayo et al. 2011) that showed 7% iodate incorporation into solid apatite from a pH 10 to 12 solution, and then with conditions that progressively approached Hanford groundwater conditions, and (2) use of a carbonate-substituted apatite material under conditions informed by results of item 1. Assessment of potential field application will also need to consider the I-127 present in the groundwater in addition to I-129. Experiments were initially conducted in batch tests where apatite forming chemicals were added in the presence of iodate and iodide. Measurements quantified the loss of iodate or iodide from solution over time (i.e., before and after precipitation), the amount of adsorbed iodine species, and iodine species incorporated (by acid dissolution of the precipitated apatite). The baseline apatite treatment was 4 mM phosphate, 6.67 mM Ca, 1.33 mM iodate (i.e., I/P aqueous ratio of 0.33), and pH 11 in oxic AGW. Apatite treatments included variation in (a) pH 11, 9.0, 7.5, (b) iodate concentration from 13 mM (2330 mg/L) to 0.00133 mM (233 ug/L), (c) I/P ratio from 33 to 0.0033, and d) addition of carbonate (CO_3/PO_4 ratio = 0.4). A limited number of treatments also included iodide, carbonated apatite.

The phosphate sources used in these experiments were orthophosphate and a polyphosphate mixture. Orthophosphate (i.e., Na-phosphate) and $CaCl_2$ at pH 7.5 results in immediate precipitation of amorphous Ca-phosphate, with the slow crystallization over weeks to months (Sumner 2000). A Ca-citrate-phosphate solution which relies upon citrate complexing with Ca to prevent immediate precipitation was not used because the reducing conditions created reduces iodate. It should be noted that phosphate precipitation does utilize H^+, so the pH can decrease. At field scale with high sediment/water ratios where minerals buffer pH change, the pH decrease is small (i.e., 7.5 to 7.3), but in a batch system with no sediment and no other aqueous species to buffer the pH, the pH change can be large (i.e., pH 11 initially and pH 6 after precipitation). A polyphosphate solution (i.e., 33% Na-orthophosphate, 33% Na-pyrophosphate, 33% Na-tripolyphosphate) also does not immediately precipitate in the presence of $CaCl_2$. The slow hydrolysis of the polyphosphates into orthophosphate delays Ca-phosphate precipitation for tens of hours (Wellman et al. 2006). A similar decrease in pH from 7.5 to 7.1 was observed at field scale and simulated (Metha et al. 2017).

It is hypothesized that rapid precipitation of amorphous Ca-phosphate may incorporate a greater amount of iodate, then during the subsequent crystallization into hydroxyapatite, less iodate may be incorporated. Experiments with rapid Ca-phosphate precipitation used $CaCl_2$ and Na-phosphate at pH 7.5 to 13. Experiments with slow precipitation of apatite used the polyphosphate mixture described above may incorporate less iodate into the more crystalline apatite precipitate. The advantage of this solution over Ca-citrate-PO_4 is that the polyphosphate solution does not change the redox conditions during precipitation, so iodate isn't reduced to iodide and can incorporate into the apatite. Experiments were not conducted with a Ca-citrate-phosphate solution as the citrate biodegradation results in a sufficient reducing environment created that iodate can be reduced to iodide (based on previous year's preliminary experiments).

3.1 Experimental Methods

3.1.1 Batch Iodate Uptake Experiments with Variable Iodate Concentrations

A series of batch experiments was conducted where iodate concentrations were varied while keeping the pH and iodine/phosphorous ratios constant with Na phosphate, as indicated in Table 3.1. Additional selected experiments were conducted with iodide (not iodate). The batch experiments consisted of 35 mL of the listed solution (made with AGW, Table 2.2) in a 40 mL Teflon centrifuge tube, with 3.0 mL samples taken at multiple time periods ranging from 0.1 to 1000 h. Samples were filtered with a 0.1-micron filter before iodine species analysis. Analysis was conducted by ion chromatography or ICP-MS.

Table 3.1. Iodate and phosphate concentrations, iodine/phosphorus ratios and pH used for variable iodate batch experiments.

Iodate (mg/L) (mM)	PO_4 (mM)	I/P (M/M)	pH
3400 13.3	40.0	0.333	11.0
340 1.33	4.0	0.333	11.0
34 0.133	0.40	0.333	11.0
0.34 0.0133	0.04	0.333	11.0
x n	3n	0.333	11.0

n = selected experiments may be conducted at additional concentrations

3.1.2 Variable Initial pH

A series of batch experiments was conducted in which the pH was varied and the iodate concentration and I/P ratios were kept constant with Na phosphate. The parameters used in these experiments are listed in Table 3.2.

Table 3.2. Iodate and phosphate concentrations, iodine/phosphorus ratios, and pH used for variable pH batch experiments.

Iodate (mg/L) (mM)	PO_4 (mM)	I/P (M/M)	pH
340 1.33	4.0	0.333	11.0
340 1.33	4.0	0.333	9.0
340 1.33	4.0	0.333	7.5
340 1.33	4.0	0.333	m

m = selected experiments may be conducted at additional pH values

3.1.3 Variable Iodine/Phosphate Molar Ratio

A series of batch experiments were conducted in which the I/P ratio was varied and the iodate concentration and pH were held constant with Na phosphate. The parameters used in these experiments are listed in Table 3.3.

Table 3.3. Iodate and phosphate concentrations, iodine/phosphorus ratios and pH used for variable I/P ratio batch experiments.

Iodate (mg/L) (mM)	PO4 (mM)	I/P (M/M)	pH
340 1.33	0.04	33.3	11.0
340 1.33	0.4	3.33	11.0
340 1.33	4.0	0.333	11.0
34 0.133	4.0	0.033	11.0
3.4 0.0133	4.0	0.0033	11.0
p p	4.0	p	11.0

p = selected experiments may be conducted at additional I/P ratios

3.1.4 Carbonated Apatite and Iodate Uptake

A series of batch experiments was conducted with variable carbonate addition (to precipitate a carbonated apatite, while keeping the iodate concentration, I/P ratio, and pH constant with Na phosphate). The parameters used in these experiments are listed in Table 3.4.

Table 3.4. Iodate and phosphate concentrations, iodine/phosphorus ratios and pH used for variable carbonate addition batch experiments.

Iodate (mg/L) (mM)	PO_4 (mM)	I/P (M/M)	CO_3 (mM)	pH
340 1.33	4.0	0.33	0.0	11.0
340 1.33	4.0	0.33	2.2	11.0
0.34 0.0013	0.004	0.33	0.0	11.0
0.34 0.0013	0.004	0.33	0.0022	11.0
340 1.33	4.0	0.33	q	11.0

q = selected experiments may be conducted at additional CO3 concentrations

3.1.5 Use of Polyphosphate

A series of batch experiments was conducted using a mixture of polyphosphates. The polyphosphate reagents are an equimolar mixture of orthophosphate (Na_2HPO_4), pyrophosphate ($Na_4P_2O_7$) and tripolyphosphate ($Na_4P_3O_{10}$), which hydrolyzes slowly over time into orthophosphate. Selected batch experiments with the polyphosphate mixture were conducted while varying the iodate and phosphate concentrations, following methods similar to those in Section 3.1.1. Selected batch experiments with the polyphosphate mixture were also conducted while varying the pH following procedures similar to those described in the previous section. Selected batch experiments with the polyphosphate mixture were conducted while varying the iodine/phosphate ratio, following the methods previously described. Selected batch experiments with the polyphosphate mixture were conducted while varying the addition of carbonate.

3.1.6 Solid Phase-Associated Iodine by Liquid Extraction and Solid Phase Analysis

After liquid sampling from the various batch experiments was completed, additional analyses were conducted on the apatite precipitates to evaluate (a) adsorbed iodate, (b) incorporated iodate, and (c) precipitate phase (to determine if different from non-iodate apatite). After the last liquid samples in the batch experiments were taken, liquid extractions were conducted on the solids to measure adsorbed and incorporated iodine. If sufficient iodate was incorporated into precipitated, selected samples would undergo solid phase analysis by X-ray diffraction (XRD) or other methods. No precipitates contained sufficient iodate mass to be able to evaluate iodate-substituted apatite. The adsorbed iodide and iodate was determined by extraction with a 0.5 mol/L Mg-nitrate solution. The iodide or iodate that was incorporated into apatite was determined by extraction with a weak acid (0.5M HCl). When the weak acid extraction is conducted after the adsorbed extraction, then the remaining iodine mass measured in this extraction is all incorporated.

Long-term stability of iodate-substituted apatite was initially planned in batch experiments at different pH and through long-term leaching. None of the 40 iodate/apatite experiments produced sufficient iodate in precipitates, so long-term stability experiments were not conducted.

3.2 Results

A total of 40 batch experiments were conducted in a wide variety of geochemical conditions to evaluate iodate and iodide substitution into apatite (or Ca-PO_4) precipitates (Table 3.5).

Table 3.5. Phosphate experiments to evaluate iodate and iodide uptake.

	Iodate	Iodide	PO_4	CO_3	I/P	Initial	% aq.	%	TIME	Uptake Ratio	IO_3 loading	Uptake Rate
#	(ug/L)	(ug/L)	(mM)	(mM)	(mol/mol)	pH	uptake	incorp.	(h)*	(mol P/mol I)	(mg/g	(µmol IO_3 h^{-1} $mol^{-1}_{apatite}$)
D32	3.40E5	0	4.0	0	0.33	11.0	20	1.8	350	1.52E+01	8.35	3.88E+01
D33	3.00E4	0	0.4	0	0.33	11.0	4	0.9	350	7.58E+01	1.67	8.21E+00
D34	3400	0	4.0E-02	0	0.33	11.0			350			
D35	340	0	4.0E-03	0	0.33	11.0	25		350	1.21E+01	10.4	2.78E+02
D36	3.40E5	0	4.0	0	0.33	9.0	5.0	1.4	350	6.06E+01	2.09	1.19E+01
D37	3.40E5	0	4.0	0	0.33	7.5	0.0	0.57	350			
D47	3.40E5	0	4.0	0	0.33	7.5	4.0		350	7.58E+01	1.67	8.23E+00
D39	3.40E54	0	4.0	0	3.3E-02	11.0	12.0	6.4	350	2.53E+02	0.50	2.16E+00
D40	3400	0	4.0	0	3.3E-03	11.0		2.1	350			
D41	3400	0	4.0	0	3.3E-04	7.5	5.0	0	350	6.06E+04	2.1E-3	9.72E-01
D44	3.40E5	0	4.0	2.2	0.33	11.0	13	1.4	350	2.33E+01	5.43	3.78E+01
D45	300	0	4.0E-03	2.2E-03	0.33	11.0	0		30			
D46	300	0	4.0E-03	2.2E-03	0.33	7.5	24		100	1.26E+01	10.0	2.50E+02
D42	0	3.82E5	4.0	0	0.33	7.5	0	0	350			
D43	0	980	4.0E-03	0	0.33	7.5	0		350			
D50	1.8E+06	0	40**	0	0.33	11.0	0		1500			
D51	3.02E5	0	4.0**	0	0.33	11.0	0		1500			
D52	3.02E5	0	4.0**	0	0.33	11.0	0		1500			
D53	2.96E5	0	4.0**	0	0.33	9.0	0		1500			
D54	2.78E5	0	4.0**	0	0.33	7.5	0		1500			
D55	2.3E+06	0	40**	0	3.3E-02	11.0	29		1500	1.04E+02	1.21	1.09E-01
D56	3.60E5	0	0.4**	0	3.3	11.0	0		1500			
D57	3.60E5	0	0.04**	0	33.2	11.0	0		1500			
D58	0	2.95E5	4.0**	0	0.33	11.0	35		1500	8.66E+00	14.6	1.69E-02
D59	0	3.41E4	4.0**	0	3.3E-02	11.0	0		1500			
E64	180	0	4.0	0	3.6E-04	11.0	67		336	4.15E+03	3.05E-2	1.26E-01
E65	78	0	4.0	0	1.5E-04	11.0	69		336	9.66E+03	1.31E-2	5.43E-02
E66	21	0	4.0	0	3.0E-05	11.0	33		336	1.01E+05	1.25E-3	5.58E-03
E67	204	0	4.0	0	3.6E-04	12.0	67		336	4.15E+03	3.05E-2	1.26E-01
E68	227	0	4.0	0	3.6E-04	13.0	46		336	6.04E+03	2.09E-2	8.63E-02
E69	190	0	40.0	0	9.1E-05	11.0	65		336	1.69E+04	7.48E-3	1.22E-02
E70	38	0	40.0	0	7.5E-06	11.0	15		336	8.89E+05	1.42E-4	4.84E-04
E71	180	0	4.0	0	3.6E-04	11.0	73		336	3.81E+03	3.32E-2	1.36E-01
E72	341	0	4.0	0	3.6E-04	11.0	0		294			
E73	254	0	4.0	0	3.6E-04	11.0	19		294	1.46E+04	8.65E-3	4.17E-02
E74	254	0	4.0	0	3.6E-04	11.0	17		294	1.63E+04	7.74E-3	3.66E-02
E75	508	0	4.0	0	3.6E-04	12.0	9		294	3.09E+04	4.10E-3	3.57E-02
E76	508	0	4.0	0	3.6E-04	13.0	8		294	3.47E+04	3.64E-3	3.23E-02
E77	254	0	16.0	0	9.1E-05	11.0	0		294			
E78	254	0	16.0	0	9.1E-05	11.0	27		294	4.07E+04	3.11E-3	1.49E-02
E79	341	0	4.0	0	3.6E-04	11.0	26		294	1.07E+04	1.18E-2	7.57E-02

* Final exp. time of measured uptake

** Equal molar mixture of ortho-, pyro-, and tripolyphosphate

3.2.1 Initial pH and Iodate Uptake

In phosphate experiments with different initial pH levels, there was some iodate uptake with an initial pH 11, 12, and 13, and no iodate or iodide uptake with an initial pH of 7.5 or 9.0 (Figure 3.1). In most experiments, there was no iodate uptake (Figure 3.1b). In some experiments, as much as 70% of the iodate was removed from solution at short times, likely into the initial amorphous precipitate, and less iodate uptake at later times when the precipitate crystallized into apatite. The calculated moles of iodate per mole of phosphate precipitated was calculated (Table 3.1) and the fraction adsorbed and incorporated iodate was measured in some precipitates. There was a fair degree of variability between experiments with the $CaCl_2$ and Na-PO_4 solutions, likely caused by slight differences between the amorphous and semi-crystalline precipitates formed. There was no uptake from the polyphosphate solutions (Figure 3.1b). At a much higher phosphate to iodate ratio (Figure 3.1c), there was more fraction iodate uptake. The pH of solutions decreased significantly, typically to pH 6 after precipitation. Adjusting the pH to the initial higher pH after every sample decreased iodate uptake (Figure 3.1d), perhaps because iodate is outcompeted by OH^- in the hydroxyapatite ($Ca_{10}(PO_4)_6(OH)_2$) at higher OH^- concentrations.

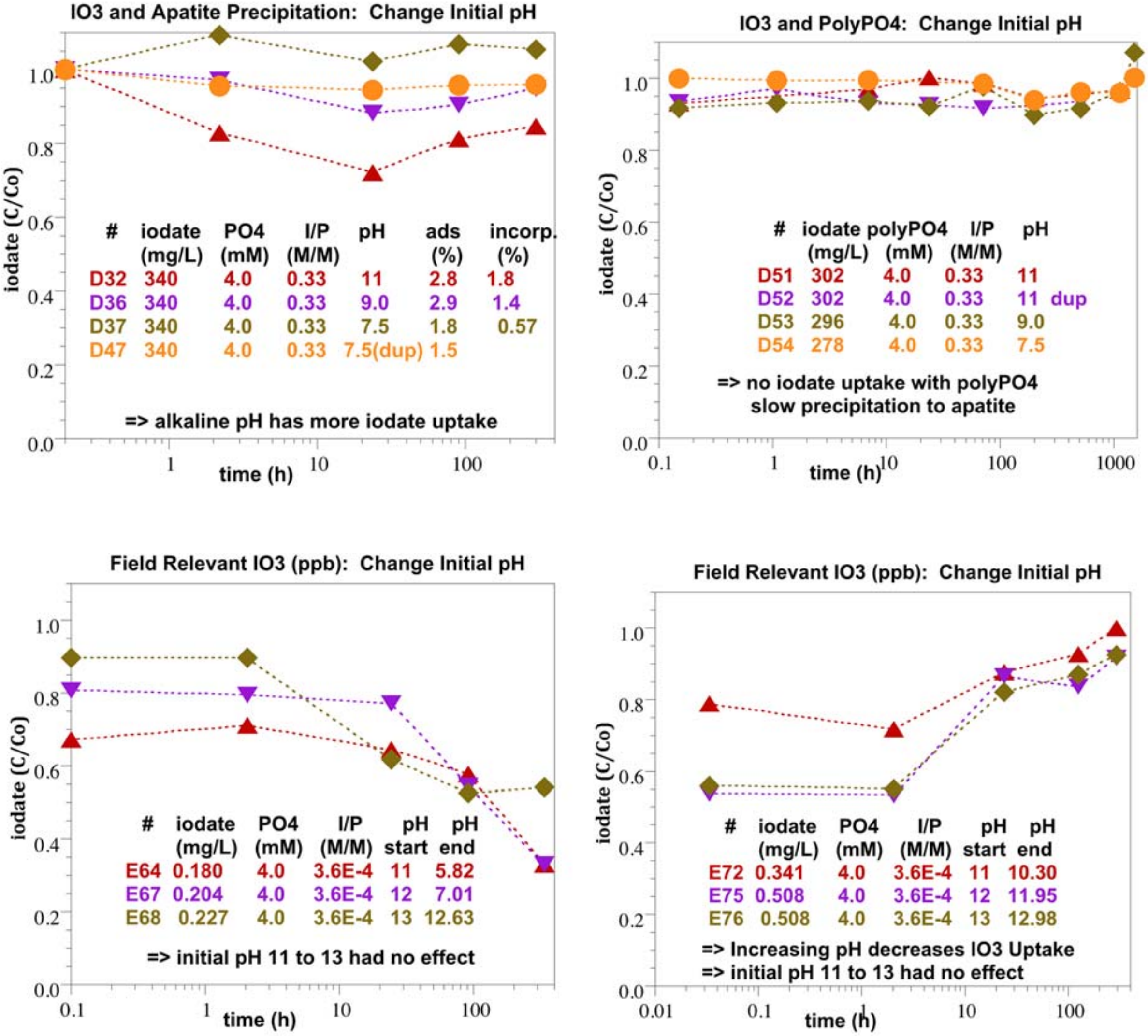

Figure 3.1. Apatite precipitation experiments conducted at different pH with a) $CaCl_2$ and Na-PO_4 solution, b) polyphosphate solution, c) $CaCl_2$ and $NaPO_4$ at low iodate concentration, and d) $CaCl_2$ and $NaPO_4$ at low iodate concentration readjusting pH to initial pH.

3.2.2 Iodate/Phosphate Ratio and Iodate Uptake

In phosphate precipitation experiments varying the molar ratio of iodate to phosphate, results generally show high excess phosphate results in greater iodate uptake (Figure 3.2). Experiments with the greatest iodate uptake from field-relevant iodate concentrations (i.e., < 200 ug/L) (Table 3.1, 67-73% uptake of aqueous iodate, E64, E65, E67, E71) had P/I molar ratios of 4100 to16900. This is equivalent to an iodate loading in the apatite of 11 to 30 ug/g (Table 3.1). Experiments with much higher iodate concentration had significantly greater iodate loadings (as high as 10,000 µg/g). However, in none of the 40 experiments conducted was all of the iodate removed from solution (to detection limits of ~1 µg/g), even with a starting concentration of 21 µg/L (E66, Table 3.1). Therefore, the use of apatite at field scale for decreasing iodate concentrations to < 1 µg/L is highly unlikely.

Experiments in which the pH was readjusted to the initial alkaline pH resulted in a decrease in iodate uptake (Figure 3.2d) compared to experiments in which the final pH was not adjusted (Figure 3.2c).

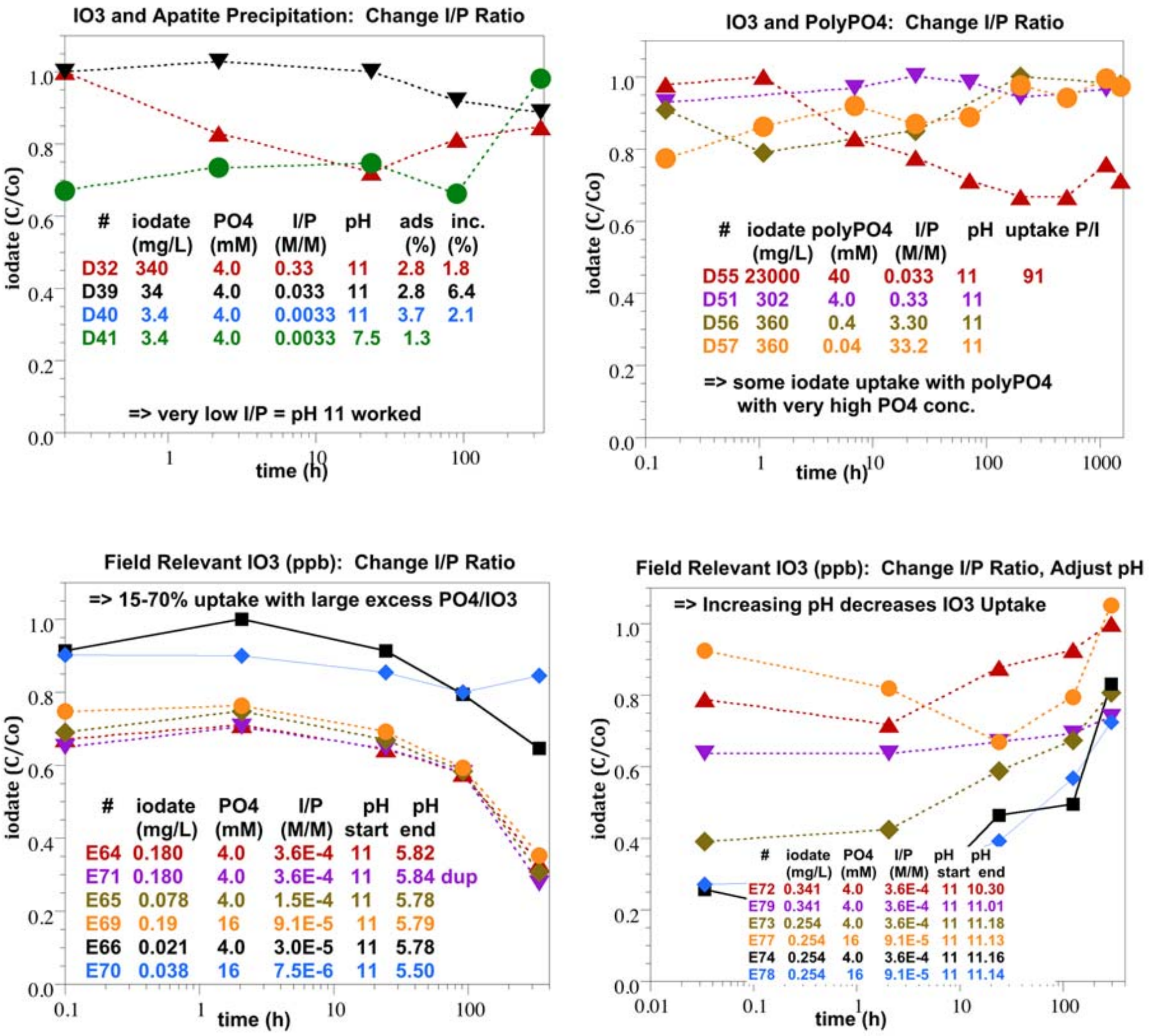

Figure 3.2. Apatite precipitation experiments conducted at different I/P ratio with a) $CaCl_2$ and Na-PO_4 solution, b) polyphosphate solution, c) $CaCl_2$ and $NaPO_4$ at low iodate concentration, and d) $CaCl_2$ and $NaPO_4$ at low iodate concentration readjusting pH to initial pH.

3.2.3 Iodate Concentration and Uptake

Experiments conducted with a range of iodate concentration, maintaining a I/P ratio of 0.33 (Campayo et al. 2011) showed little uptake (Figure 3.3). In most experiments, there was greater uptake at short times (< 100 h), but iodate uptake decreased at later times. This may have been caused by initial iodate uptake in the amorphous Ca-phosphate precipitate, but upon subsequent crystallization to apatite, there was less (or none) iodate incorporation. In addition, none of the experiments exhibited significant iodate sorption.

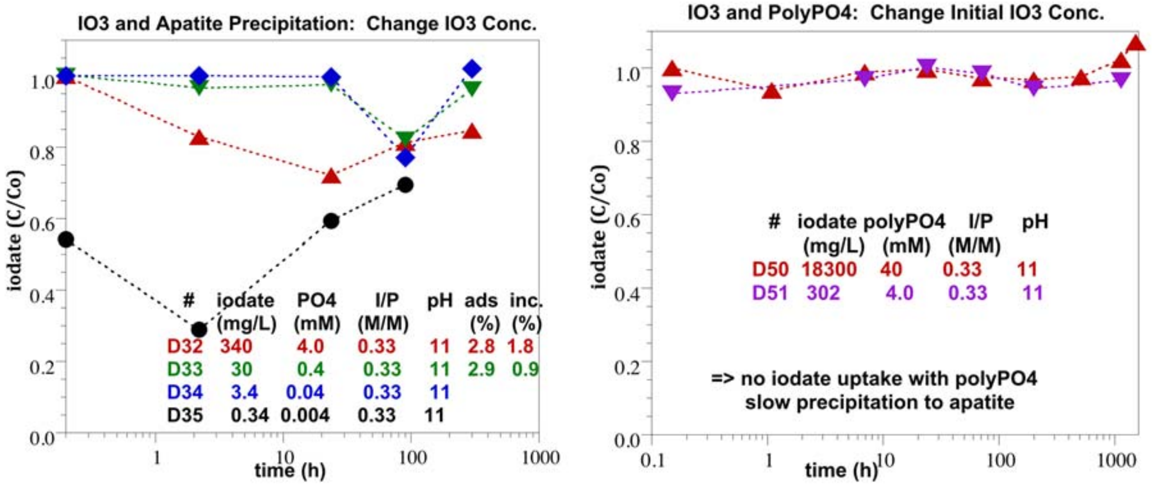

Figure 3.3. Apatite precipitation experiments conducted at different iodate concentration and constant I/P ratio of 0.33 with a) CaCl2 and Na-PO4 solution, and b) polyphosphate solution.

3.2.4 Carbonated Apatite and Iodate Uptake

Phosphate precipitation experiments conducted with a high carbonate content in the apatite (i.e., the solution contained 33% carbonate and 67% phosphate) resulted in the same or less iodate uptake (Figure 3.4) at pH 11 and 7.5.

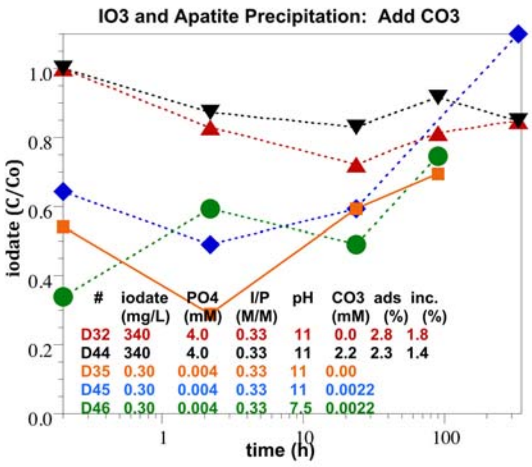

Figure 3.4. Iodate uptake in a solution precipitating carbonate-substituted apatite.

3.2.5 Iodine Uptake

There was no iodide uptake in precipitation experiments conducted with Na-phosphate or polyphosphate solutions (Figure 3.5).

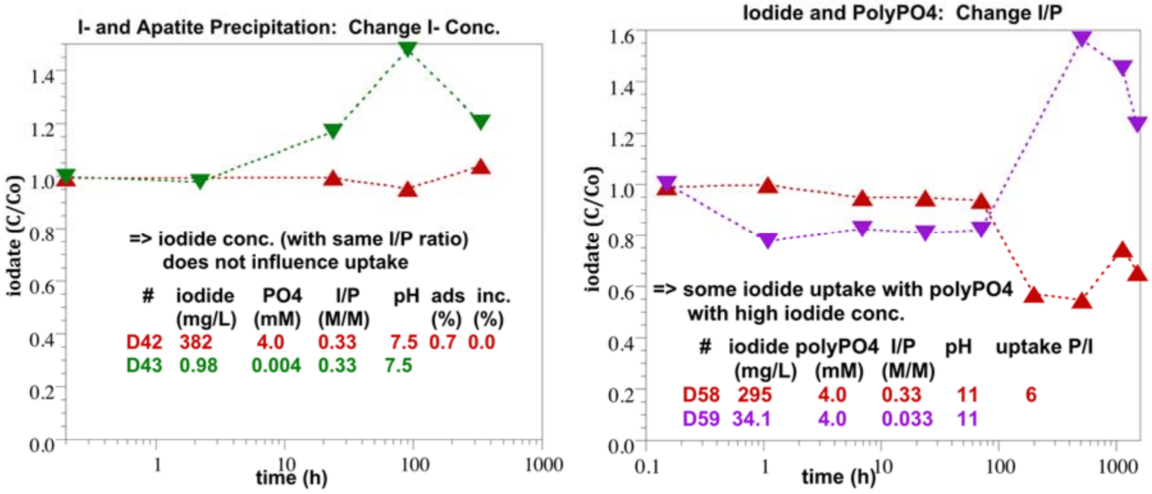

Figure 3.5. Iodide uptake during Ca-phosphate precipitation from a) orthophosphate solutions, and b) polyphosphate solutions.

3.2.6 Apatite in 1-D Columns and Iodate Uptake

In an earlier study, Ca-citrate-phosphate solution was injected into a iodide/iodate-contaminated sediment column to evaluate the change in iodine concentration that would result if iodate was uptaken in the precipitating apatite. In contrast to batch experiments, these 1-D sediment columns additionally have a high pH buffering capacity, and the Ca-citrate-PO4 solution will create a reducing environment. A sediment sample sequential extraction showed a total of 0.9 ug/g iodine, with 5.5% aqueous and adsorbed. About 85% of the iodine was present as iodide and 15% as iodate. Addition of just AGW into the sediment column as a control showed removal of 0.035 µg/g iodine or 3.9% of the mass (Figure 3.6, black diamonds). Injection of 40 mM phosphate in a Ca-citrate-phosphate solution did not decrease iodate, and in fact increased the total aqueous iodine to 0.067 µg/g (Figure 3.6a) or 7.4% of the total iodine in the sediment. This was because (a) most of the iodine present in the sediment was iodide, and (b) reducing conditions created by citrate biodegradation reduced any iodate to iodide, which adsorbs to sediment less than iodate. In a second column, the same iodine-contaminated sediment was added, but additionally with 150 µg/L iodide and 150 µg/L iodate (for a total of 0.96 µg/g iodine). Iodine mass was again increased by the addition of the Ca-citrate-phosphate solution (0.075 µg/g or 7.8%, Figure 3.6b). Clearly, Ca-citrate-phosphate addition to iodine-contaminated sediment was not effective for iodate immobilization. For comparison, a pH 9.3 carbonate solution added to the same sediment extracted about the same iodine as water, suggesting iodine mass is not incorporated into carbonates.

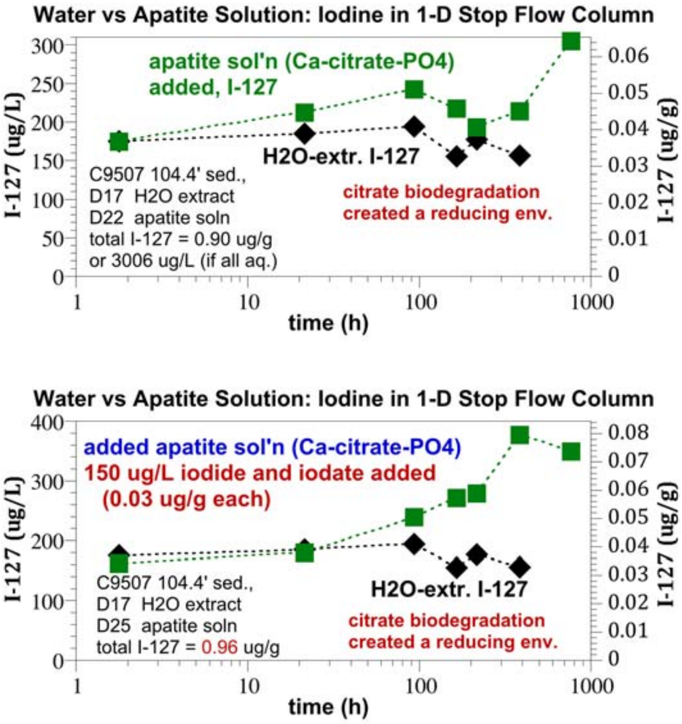

Figure 3.6. Measured total aqueous iodine as a result of phosphate addition to iodine contaminated sediment with Ca-citrate.

4.0 Enhanced Sorption by Organic Carbon

A series of batch adsorption/desorption experiments was conducted to determine the effectiveness of several organic materials for sequestering iodate and iodide from groundwater. Organic materials that were evaluated in this study were chitin, lignin, and humic acid (HA) sorbed to a representative Hanford sediment. In the case of humic/fulvic acids sorbed to Hanford sediment, both as is and sterilized sediments were evaluated to determine potential impacts of microbial activity. Selected samples were analyzed for iodine speciation to determine if any changes in iodine speciation occurred during the course of the experiments.

4.1 Experimental Methods

The organic materials used were chitin (from shrimp shells, practical grade, powder, Sigma-Aldrich), lignin, alkali (Sigma-Aldrich), and Hanford sediment amended with humic acid sodium salt (technical grade, Sigma-Aldrich). Each batch adsorption/desorption experiment was conducted in a 50-mL polypropylene centrifuge tube at room temperature (~22°C) in duplicate. Equilibration times of 1, 3, 7, and 28 days were used for the adsorption experiments, and 28 days for the desorption experiments. The experiments were performed at an organic material-to-solution ratio of 0.2 g organic material to 40 mL synthetic groundwater. A duplicate set of the humic acid experiments was conducted in which the groundwater was amended with 2% glutaraldehyde to evaluate the potential impact of microbial growth. Separate experiments for each sorbent were conducted at initial iodide and iodate concentrations of approximately 75 mg/L. All experiments were conducted in duplicate and a set of control samples containing the solution but no sorbents were also conducted in duplicate for each equilibration time.

The recipe used to make the AGW was shown previously in Table 2.2. In the case of the HA experiments, approximately 10 g of Hanford sediment from borehole C9567 (depth interval 283.0 to 283.5 feet) was treated with a solution of 0.2 g humic acid sodium salt dissolved in 40 mL of the synthetic groundwater. The solution was allowed to contact the sediment for 24 hours on an orbital shaking table. After this initial contact with the humic acid sodium salt solution, the solution was decanted and 40 mL fresh groundwater was equilibrated for 24 hours and then decanted (then repeated). After this, 40 mL of groundwater containing approximately 75 mg/L of iodide or iodate was added to start the adsorption phase of the experiment. A separate set of humic acid adsorption/desorption experiments were conducted in which the groundwater was amended with 2% glutaraldahyde to sterilize the sediments. Total organic carbon (TOC) was measured on the humic acid treated sediments after the 1,3, and 7-day equilibration periods. TOC for the 28-day equilibration period was not measured to allow these experiments to be used to determine desorption K_d values. Both TOC and total inorganic carbon measured on the untreated Hanford sediments was below the detection limit.

4.2 Results

4.2.1 Adsorption K_d Values

The measured adsorption K_d values for iodate and iodide on chitin and lignin are shown in Table 4.1 as a function of contact time. Very little if any sorption of iodate onto either chitin or lignin occurred, with average values and standard deviations of 3.2 ± 4.0 and 4.8 ± 4.8 mL/g, respectively. It appears that slightly greater adsorption (higher K_d values) may have occurred at longer contact times, but this is difficult to discern due to the high relative uncertainty. Similar results were observed for iodide sorption onto lignin, with an average and standard deviation of 3.6 ± 3.5 mL/g. In contrast to these results, significant sorption of iodide onto chitin occurred, with an average and standard deviation of 74.9 ± 4.3 mL/g. Shigeno et al. (1980) reported adsorption of iodine onto chitosan is caused by charge—transfer complexes between amino groups of chitosan and iodine molecules. A similar mechanism may apply to chitin. Overall, these results suggest that adsorption of iodate and iodide onto chitin and lignin reaches equilibrium relatively quickly (possibly less than 1 day). Although, the moderately high sorption of iodide onto chitin is a favorable result, the fact that iodate is the dominant species in Hanford groundwater means that chitin is not likely (under typical Hanford groundwater conditions) to be a useful material for iodine remediation at Hanford. However, it could potentially be an effective sorbent when used in combination with reducing conditions.

Table 4.1. Iodate and iodide K_d (mL/gm) values measured on the chitin and lignin.

Contact Time (days)	Iodate		Iodide	
	Chitin	Lignin	Chitin	Lignin
1	2.8	6.3	80.6	6.4
1	0.3	4.1	76.8	1.2
3	-2.0	-2.1	73.3	4.6
3	1.5	-2.1	81.1	2.5
7	5.8	6.8	70.2	3.6
7	0.3	7.4	70.7	6.6
28	9.4	11.8	74.5	-3.3
28	7.5	6.4	71.9	7.3
Average and Std. Dev.	3.2 ± 4.0	4.8 ± 4.8	74.9 ± 4.3	3.6 ± 3.5

The measured adsorption K_d values for iodate onto a represent Hanford sediment, humic acid treated sediments, and sterilized HA treated sediments as a function of contact time are shown in Table 4.2. In addition, K_d values calculated on a TOC weight basis rather than the weight of the sediments are also provided. Sorption of iodate was quite low for both treated and untreated sediments. The K_d values for humic acid treated sediments (K_d = 0.58 ± 0.27 mL/g) was actually less than for the untreated sediments (K_d = 1.13 ± 0.06 mL/g). This could be the result of competitive effects of the humic acid anions for sorption sites on the sediment that would have been available for iodate; however, the overall effect is fairly small. The sterilized humic acid treated sediments actually had higher adsorption (K_d = 1.84 ± 0.50 mL/gm) than that of both the sediment alone and the humic acid treated sediment. It is hypothesized that sorption of glutaraldehyde to the sediment (a neutrally charged molecule) may be responsible for this slight enhancement of iodate adsorption to the sterilized sediment. A small increase in iodate adsorption with time may have occurred with the H treated sediments (both sterilized and non-sterilized). This was most noticeable for the sterilized HA treated sediments.

Table 4.2. Iodate K_d values (mL/g) measured on sediment and humic acid (HA) treated sediments.

Contact Time (days)	Sediment Only	HA Treated Sediment	Sterilized HA Treated Sediment	TOC Weight Basis	Sterilized TOC Weight Basis
1	1.13	0.40	1.12	591	481
1	1.10	0.39	1.37	250	619
3	1.06	0.53	1.74	421	347
3	1.17	0.76	1.72	1030	439
7	1.08	0.16	1.74	201	379
7	1.17	0.60	1.99	303	972
28	1.06	0.96	2.48	-	-
28	1.24	0.83	2.55	-	-
Average and Std. Dev.	1.13 ± 0.06	0.58 ± 0.27	1.84 ± 0.50	466 ± 284	539 ± 212

Iodate K_d values determined on a TOC weight basis were considerably higher than on a sediment weight basis, ranging from 250 mL/g to 1030 mL/g. In addition, the K_d values determined on a TOC weight basis were highly variable. The amount of TOC measured in the sediments (Table 4.3) was also highly variable, but does not appear to be correlated with the K_d values determined on a TOC weight basis as one might expect. The TOC values measured on the sediment were small relative to what was added (200 mg), indicating that 11% or less of the HA added actually adsorbed to the sediment.

Table 4.3. TOC content of sediment after HA treatment (mg) measured on sediment and humic acid treated sediments.

	Iodate		Iodide	
Contact Time (days)	HA Treated Sediment	Sterilized HA Treated Sediment	HA Treated Sediment	Sterilized HA Treated Sediment
1	6.73	23.2	7.97	18.6
1	15.6	22.1	9.77	23.1
3	12.7	50.2	22.4	23.8
3	7.39	39.2	18.2	22.1
7	7.85	46.0	18.0	29.7
7	19.8	20.5	4.89	26.7
Average and Std. Dev.	11.7 ± 4.8	33.5 ± 12.1	13.5 ± 6.3	24.0 ± 3.5

The measured adsorption K_d values for iodide on a representative Hanford sediment, humic acid treated sediments, and sterilized humic acid treated sediments as a function of contact time are shown in Table 4.4. In addition to K_d values calculated based on the weight of sediment, K_d values calculated on a TOC weight basis rather than the weight of the sediments are provided in Table 4.4. Sorption of iodine was quite low for both treated and untreated sediments and was significantly less than those for iodate for the sediment only and the sterilized humic acid treated sediments. The K_d values for humic acid treated sediments ($K_d = 0.46 \pm 0.05$ mL/g) were slightly more than for the untreated sediments ($K_d = 0.34 \pm 0.05$ mL/g). The sterilized humic acid treated sediments had higher adsorption ($K_d = 0.54 \pm 0.12$ mL/g) than that of both the sediment alone and the humic acid treated sediment, but the differences were very small. In addition, sorption of iodide may have increased slightly with time for the sterilized humic acid treated sediments.

Table 4.4. Iodide K_d values (mL/g) measured on sediment and humic acid treated sediments.

Contact Time (days)	Sediment Only	HA Treated Sediment	Sterilized HA Treated Sediment	TOC Weight Basis	Sterilized TOC Weight Basis
1	0.35	0.51	0.38	648	206
1	0.30	0.53	0.47	548	205
3	0.30	0.41	0.47	181	198
3	0.32	0.38	0.39	209	177
7	0.34	0.47	0.60	259	200
7	0.37	0.43	0.65	872	246
28	0.33	0.46	0.66	-	-
28	0.44	0.50	0.68	-	-
Average and Std. Dev.	0.34 ± 0.05	0.46 ± 0.05	0.54 ± 0.12	453 ± 256	205 ± 20.5

As with iodate, iodide K_d values determined on a TOC weight basis were considerably higher than on a sediment weight basis, ranging from 181 mL/g to 872 mL/g. In addition, the K_d values determined on a TOC weight basis were highly variable. The amount of TOC measured in the sediments (Table 4.3) was also highly variable, but does not appear to be correlated with the K_d values determined on a TOC weight basis as one might expect.

4.2.2 Desorption K_d Values

For the case of iodide desorption from chitin (28 days), approximately 52% of the adsorbed iodide desorbed. This resulted in an average desorption K_d value of 190 ± 3 mL/g. Iodate desorption from chitin, as well as both iodide and iodate desorption values, is not reported because their relative high variability renders it useless. The high variability is due to the fact that very little iodine was sorbed and the K_d values are calculated from the difference between small numbers (amount of iodine sorbed and the amount desorbed) with relatively high uncertainty.

The duplicate 28-day desorption K_d values measured on the untreated sediment, HA treated sediments, and sterilized HA treated sediments are shown in Table 4.5. The desorption K_d values on the untreated sediments for both iodate and iodide were similar to those determined for the adsorption K_d values determined at 28 days (Table 4.2 and Table 4.3), indicating that sorption of iodate and iodide is reversible for untreated sediments. The desorption K_d values for the HA treated sediments for both iodate and iodide were significantly higher than those determined for adsorption (Table 4.2 and Table 4.3), indicating that sorption of iodate and iodide onto HA treated sediments is not completely reversible at 28 days. For the sterilized HA treated sediments, the desorption K_d values for iodate are only slightly higher than those determined for adsorption (Table 4.2), indicating that sorption of iodate onto sterilized HA treated sediments is close to reversible at 28 days. The desorption K_d values for iodide sterilized HA treated sediments are only significantly higher than those determined for adsorption (Table 4.3), indicating that sorption of iodide onto sterilized HA treated sediments is not completely reversible at 28 days.

Table 4.5. Desorption K_d values (mL/g) measured on sediment and humic acid (HA) treated sediments (28 day desorption period).

Sediment Only	HA Treated Sediment	Sterilized HA Treated Sediment	Sediment Only	HA Treated Sediment	Sterilized HA Treated Sediment
Iodate			Iodide		
1.08	3.68	2.80	0.39	2.66	2.77
1.48	2.63	3.52	1.30	2.56	3.32

4.2.3 Iodine Speciation after the Adsorption Experiments

Total iodine and iodine speciation results for the various adsorption experiments at the 28-day contact time are shown in Table 4.6. In general, the final speciation of iodine is consistent with the iodine species that was added at the start of the experiments. A notable exception is for the lignin adsorption experiments in which iodine was added as iodate. For these experiments, it appears that the added iodate was completely reduced to iodide by the lignin during the course of the experiment. The reason for this has not been determined.

Table 4.6. Total measured iodine and speciation results in adsorption experiments after 28 days contact.

Experiment	Total Measured Iodine (µg/L)		Iodate (µg/L, as I)	Iodide (µg/L)
	Added as Iodate	Added as Iodide		
Chitin-1	70.3	-	73.2	ND
Chitin-2	70.9	-	72.4	ND
Lignin-1	69.4	-	ND	68.7
Lignin-2	71.3	-	ND	74.6
Blank	73.5	-	77.5	ND
Blank	73.9	-	80.4	ND
Chitin-1	-	54.1	ND	46.8
Chitin-2	-	55.0	ND	52.9
Lignin-1	-	75.6	ND	70.9
Lignin-2	-	71.7	ND	57.8
Blank	-	74.3	ND	61.1
Blank	-	74.5	ND	85.4
HA-1	59.2	-	51.9	ND
HA-2	60.8	-	58.5	ND
HA-S-1	55.1	-	47.3	ND
HA-S-2	54.6	-	48.3	ND
Sediment-1	58.0	-	53.3	ND
Sediment-2	56.0	-	44.2	ND
HA-1	-	66.6	ND	59.9
HA-2	-	66.0	ND	57.1
HA-S-1	-	65.5	ND	56.3
HA-S-2	-	65.2	ND	53.5
Sediment-1	-	68.6	ND	59.6
Sediment-2	-	66.8	ND	53.9

ND – not detected

5.0 Co-Precipitation with Iron Oxides

Laboratory studies of batch adsorption/desorption of iodate, column reactive barrier adsorption/desorption of iodate and co-precipitation of iodate and iodide with 2-line-ferrihydrite (HFO), and in situ formation of HFO in column experiments were conducted to evaluate the potential of these approaches for in situ remediation of iodine.

5.1 Experimental Methods

5.1.1 Iron Oxide Preparation

Batch sorption/desorption of iodate (IO_3^-) was conducted on iron oxides at neutral pH prepared in DDI, artificial Hanford groundwater (AGW), and Hanford sediment with AGW (SAGW). HFO in DDI was synthesized by adding ferric nitrate [8.0089 g of $Fe(NO_3)_3 \cdot 9H_2O$] to 100 mL DDI in a polyethylene bottle at room temperature, followed by addition of approximately 59 mL 1 M NaOH dropwise while stirring until a pH of approximately 7 to 7.5 was achieved. The precipitated HFO was washed five times using approximately 100 mL DDI followed by centrifugation. The final HFO slurry was filtered using a 0.45 µm vacuum filter and air-dried at room temperature. The air-dried bulk solid HFO was ground to powder using a mortar and pestle.

Goethite in DDI was synthesized by adding ferric nitrate [8.0089 g of $Fe(NO_3)_3 \cdot 9H_2O$] to 100 mL DDI water in a polyethylene bottle at room temperature, followed by addition of approximately 1 M NaOH dropwise while stirring until a pH of approximately 12 was achieved. The slurry was stirred for 30 min, followed by heating at 70°C for 60 h, which allows the initial HFO precipitate to age to goethite. The same washing, filtering, and drying procedures used for HFO were applied to the goethite precipitates.

Methods to prepare HFO and goethite in AGW were the same as those used to prepare the materials in DDI. The recipe used to make the AGW was the same as that listed in Table 2.2. Preparation of HFO with AGW involving sediment was done using two methods. In the first method, ferric nitrate [16 g of $Fe(NO_3)_3 \cdot 9H_2O$] was dissolved into 200 mL AGW in a polyethylene bottle, followed by addition of 7 g sediments [Hanford fine sand (HF)]. Then, approximately 118 mL of 1 M NaOH was added dropwise while stirring the slurry until a pH of 7 to 7.5 was achieved. Approximately 4 g of HFO was produced, which was precipitated in the sediment matrix.

In the second method, instead of 1M NaOH, calcite-dominated rock collected from the Hanford Cold Creek Unit was pulverized and added to neutralize the solution pH. In this case, ferric nitrate [4 g of $Fe(NO_3)_3 \cdot 9H_2O$] was dissolved into 50 mL AGW in a polyethylene bottle, followed by addition of 2 g of the rock powder. The solution was gently mixed on an orbital shaker for 20 days while the slurry pH was monitored until the pH reached approximately 7 to 8.

Preparation of goethite in AGW with sediment was performed as follows. Ferric nitrate [16 g of $Fe(NO_3)_3 \cdot 9H_2O$] was dissolved into 200 mL AGW in a polyethylene bottle, followed by addition of 7 g sediment (HF). The pH of the slurry was increased to ~pH 12 by adding 1 M NaOH dropwise. The slurry was then stirred for 30 min, followed by heating at 70°C for 60 h.

In this work, the above laboratory-synthesized HFO and goethite were named as DDI-HFO, DDI-goethite, AGW-HFO, AGW-goethite, SAGW-HFO, and SAGW-goethite, corresponding to the solution matrix of DDI, AGW, and AGW with sediments, respectively. Figure 5.1 shows the iron oxides prepared in polyethylene vessels. The HFO precipitated through pH buffering by calcite dissolution was named as calcite-HFO. In addition, in the AGW and SAGW systems, the 1M NaOH solution used was prepared by dissolving 10M NaOH (initially prepared in DDI) into AGW solutions in order to minimize any ionic strength effects in AGW due to large volumes of NaOH addition.

Each of the iron oxide minerals were characterized using XRD, SEM, and N_2-BET, for mineralogy, particle morphology and size, as well as specific surface area (SSA).

Figure 5.1. Iron oxides [HFO (left) and goethite (middle)] preparation in polyethylene vessels; the conversion of AGW-HFO to AGW-goethite (right) was visible by color changing, where no obvious color changed in the SAGW systems, indicating the conversion of HFO to goethite was strongly retarded when sediment was included.

5.1.2 Iodate Sorption/Desorption on Iron Oxides

Batch sorption/desorption experiments were conducted using iodate concentrations of 10, 50 and 200 ppb with solid to solution ratios of 2 g/L (for HFO) or 10 g/L (for goethite) in 50 mL centrifuge tubes. These experiments were run in triplicate. In addition to the sorption test samples, duplicate controls consisting of 25 mL of the iodate spiked solutions with no sorbent were also run. After assembly, the samples were gently mixed on a shaker table for 7 and 30 days. After the 7- or 30-day contact period, the pH of the samples was measured and then the tubes were centrifuged at 3,500 rpm for 30 minutes. Supernatant was then collected and filtered (0.20 µm) for total iodine analysis by ICP-MS. Selected samples were also analyzed for iodine speciation.

After the adsorption phase of the experiments was complete, the quantity of residual solution in the centrifuge tube was determined and fresh iodate-free AGW solution was added and recorded. After the respective 7- or 30-day contact period, the pH of the samples were measured and then the tubes were centrifuged at 3,500 rpm for 30 minutes. Supernatant was then collected and filtered (0.20 µm) for total iodine analysis by ICP-MS. Selected samples were analyzed for iodine speciation (ICP-MS) and for iron concentrations [inductively coupled plasma – optical emission spectroscopy (ICP-OES)]. The sorption K_d was calculated based on the iodine mass balance in the batch reactor.

In order to investigate the sorption of iodine on iron oxides using microscopy techniques, two extra sets of sorption experiments with higher iodate concentrations [1.0×10^{-2} and 5.76×10^{-4} M (=100 ppm)] in the AGW/DDI solution matrix were conducted. The sorption contact time was 7 days, and sorption was confirmed by the decrease in solution iodine concentrations (data not shown). At the end of the experiments, the solids were air-dried and analyzed by X-ray photoelectron spectroscopy (XPS).

5.1.3 Iodate Column (Reactive Barrier) Sorption/Desorption Experiments

Column iodate adsorption/desorption experiments were conducted with HFO and goethite synthesized with AGW (AGW-HFO and AGW-goethite). The columns were packed with silica sand (0.21 to

0.30 mm) mixed with ~1% to 6% iron oxides in the center of the column with pure silica sand (~1 cm thickness) at both ends of the columns. Filters were also emplaced at each end of the columns (5 µm pore sized PEEK frit and 15 to 45 µm pore-sized poly-filter at the inlet and outlet of the column, respectively). A control column with only silica sand was run in parallel. The columns were composed of PEEK with inside diameters of 0.76 cm and lengths of 10 cm. Prior to running the sorption/desorption experiments, the columns were conditioned by pumping AGW through the columns at a constant flow rate with a residence time of approximately 1 to 2 hours to remove any fine particles for column stabilization. Figure 5.2 is a schematic of the column packing structure.

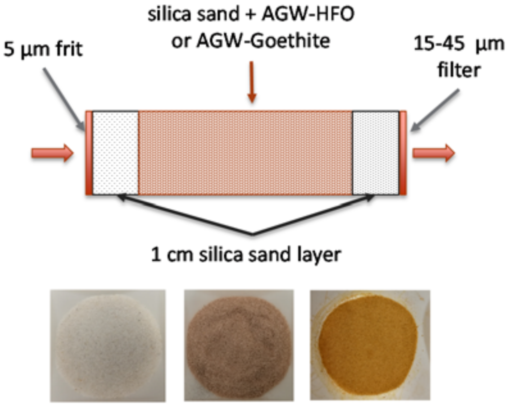

Figure 5.2. Sorption/desorption reactive barrier column packing with an 8 cm-length layer of silica sand mixture either containing 1.0% AGW-HFO or ~ 5.5% AGW-Goethite. The three images (left to right) are of the materials of the control silica sand, silica sand + AGW-HFO, and silica sand + AGW-Goethite, respectively.

The adsorption phase of the experiments was conducted by injecting iodate-spiked AGW solution (50 ppb) into the bottom of the column (positioned vertically) at a constant flow rate with an approximate residence time of 1.6 hours. Samples were collected at the outlet of the column in sufficient number and frequency to measure the changes in iodate concentrations until breakthrough. After breakthrough, desorption was initiated by injecting iodate-free AGW at the same constant flow rate as applied during the sorption phase of the experiment.

The effluent samples were collected automatically using a programmable fraction collector. The sampling intervals (10 minutes to 2 hours) were pre-determined based on the K_d results in the batch adsorption experiments. Two stop-flow events were performed during both the sorption and desorption phase of the experiments. The duration of the stop flow events was 48 hours. Bromide tracer tests were conducted after the sorption/desorption column tests. Selected effluent samples were analyzed for iodate and iodine speciation.

5.1.4 Iodate and Iodide Co-Precipitation with HFO

Co-precipitation of iodate/iodide with HFO in DDI, AGW, and AGW with sediment (SAGW) systems was performed using methods similar to those described in Section 5.1.1 for HFO synthesis. However, in this case, the DDI and AGW solutions were first spiked with iodate or iodide at three concentrations (5, 50, and 200 ppb). The co-precipitation experiments were conducted in duplicate in 125 mL polyethylene bottles. Within an hour of precipitation of the iron oxides, the reaction vials were centrifuged at 3500 rpm for 25 minutes. The solution supernatant was filtered through a 0.20 µm filter for iodate or iodide analysis using ICP-MS. The final pH of the solution slurry was measured, and then the solid precipitates were washed 3 to 5 times with approximately 100 mL DDI water, air-dried, and ground for weight measurements and for solid characterization analysis.

5.1.5 Long-Term Sorption of Iodate/iodide on Iron Oxides

This work is an extension of sorption experiments initiated in FY17 (Strickland et al. 2017a), where batch sorption experiments for iodate and iodide on HFO, goethite, magnetite, and hematite were conducted in duplicate in 50 mL centrifuge tubes at room temperature under neutral pH (~ pH 7.4) conditions. The batch experiments were carried out with a solid to solution ratio of 2.0 g/L for HFO and 10.0 g/L for magnetite, hematite, and goethite. A 48-hour contact time between the iron oxide samples with a Hanford synthetic ground water (similar to AGW) was applied to reach sorption equilibrium based on the kinetic study results. At the end of the reaction time (48 hours), the batch reactors were centrifuged at 3,500 rpm for 20 minutes to separate the sorbent particles from the supernatant. About 3 mL supernatant solution was sampled from each reactor using a pipette, followed by filtration through a 0.2 µm filter. The remaining supernatant (~ 22 mL) and the iron oxides in the tubes were re-mixed with a vortex mixer and the reaction was allowed to continue for up to 200 days. The weight of the reactor tube was recorded for determining the remaining solution volume and the remaining iodate mass in the reactor after the 48-hour sampling event. The reactors were shaken by hand once per month during the entire test period. On day 200, the batch reactors were centrifuged at 3,500 rpm for 20 minutes and about 3 mL of supernatant solution was collected and filtered (0.2 µm) for iodate concentration measurement by ICP-MS and the final solution slurry pH was measured. The solids from certain selected reactor tubes were collected and air-dried for XRD analysis to characterize any potential iron oxide mineral transformation during the long-term reaction period.

5.2 Results

5.2.1 Solid Characterization on Synthesized Iron Oxides

The detailed XRD analysis results and SEM images of the synthesized iron oxides under different conditions are shown in Figure 5.3 and Figure 5.4. For ferrihydrite, its powder XRD pattern contains only two or six scattering bands in its most disordered state. The observed two broad XRD patterns of the both synthesized HFO in DDI water (DDI-HFO) or in the AGW system (AGW-HFO) in the present study were typical for 2-line ferrihydrite, which agrees with its bulk material morphology in the SEM image (Figure 5.4). The synthesized DDI-goethite and AGW-goethite showed well-crystalized, needle-shaped micrometer-sized minerals that matched well with their JADE XRD reference peak. For the SAGW-HFO, synthesized using the first method with NaOH addition, where 7 g of HF was added in the solution system, the dominant minerals observed in the collected bulk solids were HF minerals quartz, feldspar, and mica, etc. However, the XRD analysis on the dark brown particles, which were handpicked out of the collected bulk solids, clearly showed the presence of HFO. This implies that the HFO generated in the SAGW system was likely physically mixed with the sediment minerals. A similar mineral mixing pattern was observed in the SAGW-goethite synthesis system, but without goethite present. Instead of the expected SAGW-goethite, materials similar to SAGW-HFO was observed (Figure 5.3), even after heat-treatment (70°C) for 60 hours. This is because silicate retards the conversion of ferrihydrite to goethite (Schwertmann and Cornell 2000). In the SAGW-goethite synthesis system, Si dissolution from the Hanford sediment minerals, such as quartz and feldspar, can be expected in the strongly alkaline media (pH ~12).

Figure 5.5 shows the XRD spectra and an SEM image of the calcite-HFO prepared using the second method) (without NaOH addition). The XRD pattern clearly shows that the solids were dominated by

2-line ferrihydrite, with quartz and calcite also present. The SEM image shows the bulk fine particle morphology is similar to the images of the DDI- or AGW-HFO (Figure 5.4). The pH evolution of the synthesis solution through the self-buffering process by calcite-dissolution is shown in Figure 5.6. It illustrates the solution pH approached pH 7 after a reaction period of 20 days.

The SSAs measured by N_2-BET for each synthesized iron oxide are listed in Table 5.1. As expected, high specific surface areas were observed in DDI- and AGW-HFO products (~336 to 337 m^2/g). These values agree well with literature values (Schwertmann and Cornell 2000). Calcite-HFO shows a somewhat lower SSA (~216 m^2/g), which could be due to the presence of quartz in the final product. Interestingly, SAGW-HFO shows an SSA of ~75 m^2/g. Assuming that no significant interactions between the synthesis solutions and sediments occurred, 2 g of HFO could be expected in the SAGW-HFO experiment (Schwertmann and Cornell 2000). Ignoring the much less SSA contributions from the added 7 g HF sediments, the HFO contributed a surface area of ~339 m^2/g [75.4 m^2/g x (2 g HFO + 7 g HF)/2 g HFO], almost the same SSA as the DDI- and AGW-HFO. This agrees with the XRD findings, where the produced HFO was physically mixed with the sediments. Geochemical modeling should be conducted in the future to confirm these assumptions. Compared to HFO, lower SSA values were observed in the DDI- and AGW-goethite samples (~62 to 63 m^2/g), which is still much higher than that of normal Hanford sediments. Similar SSA values for SAGW-goethite (~78 m^2/g) and SAGW-HFO (~75 m^2/g) were found in these experiments, which confirms that no significant goethite conversion occurred from HFO due to the dissolved silica retardation effects.

Table 5.1. Specific surface area (SSA) of the synthesized iron oxides determined by N_2-BET method.

Sample	DDI-HFO	AGE-HFO	SAGW-HFO	DDI-goethite	AGW-goethite	SAGW-goethite	Calcite-HFO
SSA (m^2/g)	337.56	336.49	75.43	61.75	62.81	78.12	216.20

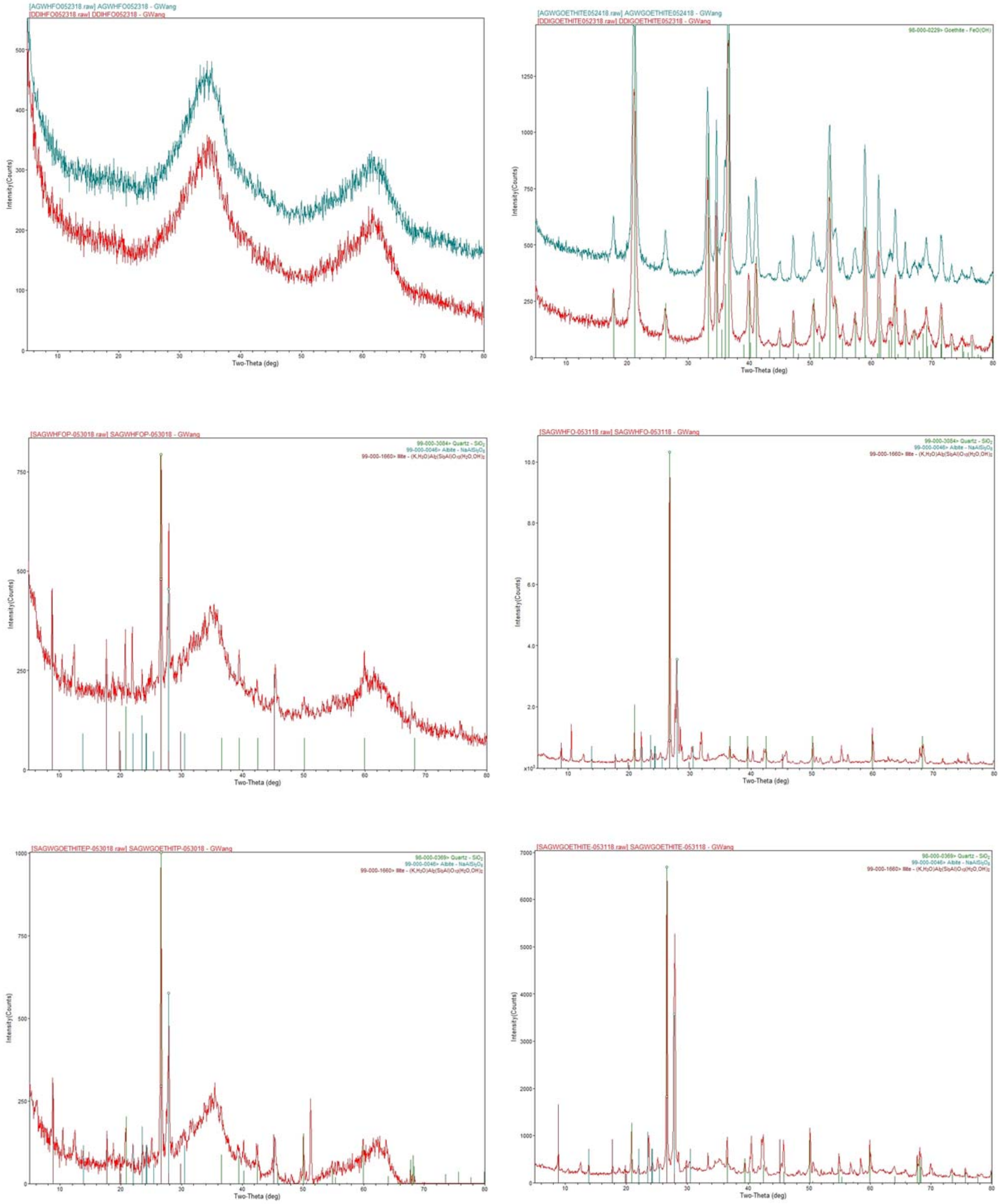

Figure 5.3. XRD analysis showing the typical 2-line-ferrihydrite or goethite patterns for each iron oxides synthesized in the present study.

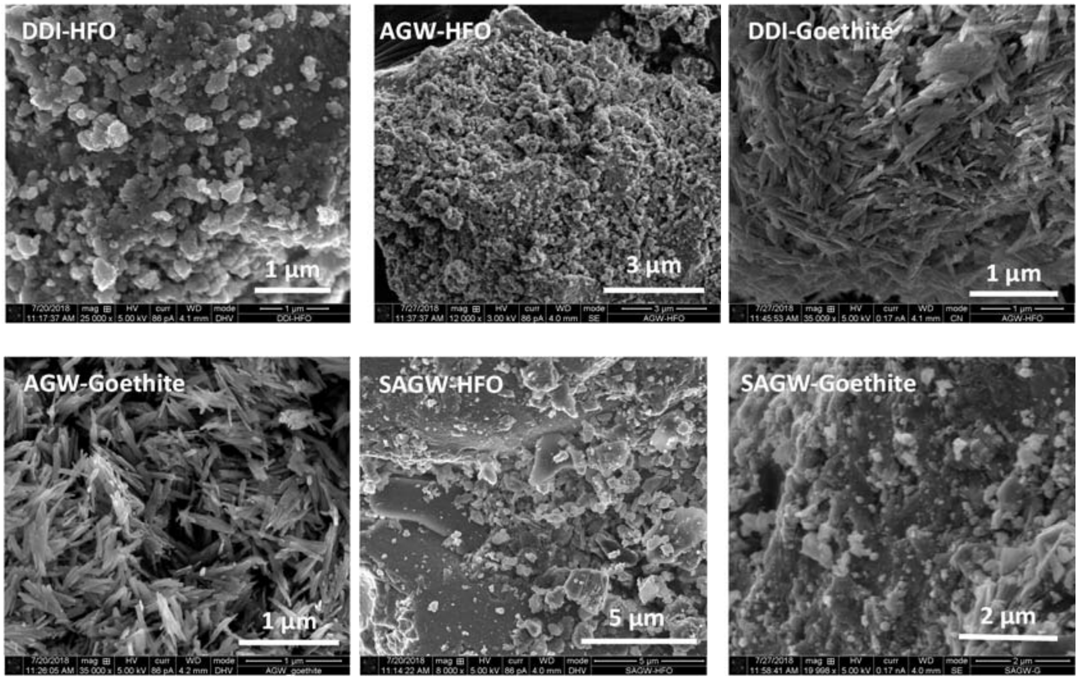

Figure 5.4. The SEM analysis showing the typical 2-line-ferrihydrite or goethite crystal morphology for each iron oxides synthesized in the present study.

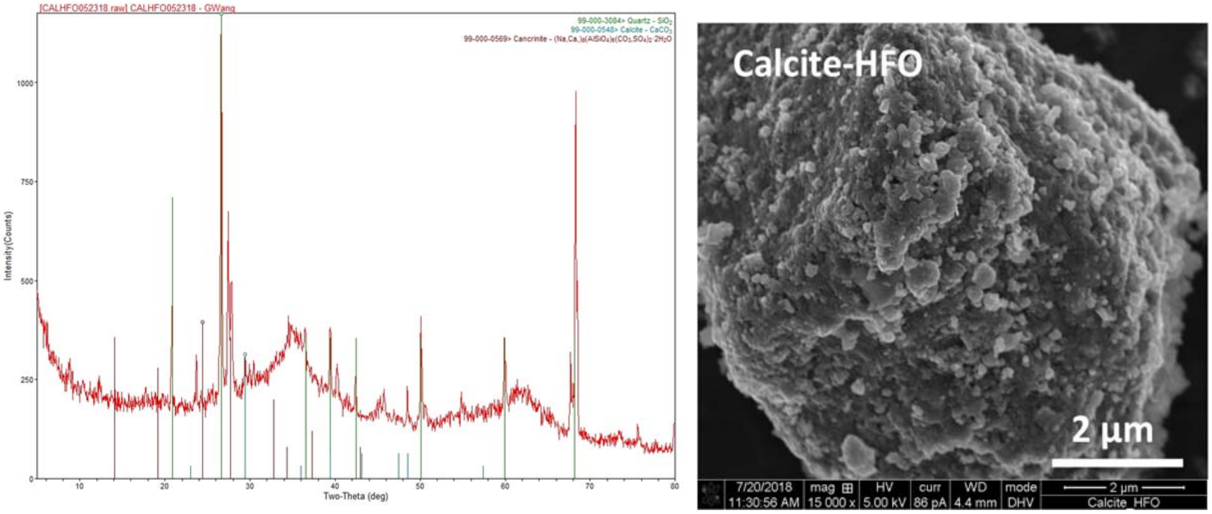

Figure 5.5. XRD analysis showing the 2-line ferrihydrite containing certain amount of quartz and tiny calcite in the calcite-HFO. The SEM images showing a similar mineral morphology as in DDI- or AGW-HFO products (Figure 5.4).

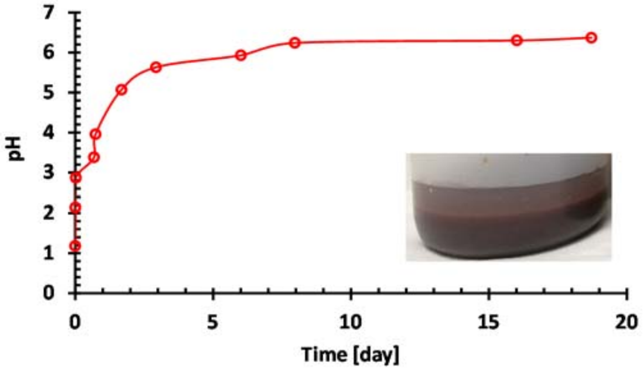

Figure 5.6. Evolution of solution pH with time in the calcite-HFO precipitation system [4 g $Fe(NO_3)_3 \cdot 9H_2O$ + 50 mL DDI + 2 g calcite rock powder], resulting in calcite-HFO precipitations through solution pH self-buffering.

5.2.2 Sorption/Desorption of Iodate on Iron Oxides

The sorption of iodate (IO_3^-) on the synthesized DDI-, AGW-, and SAGW-HFO or goethite at room temperature for 7 and 30 days at three different concentrations at neutral pH (pH ~7.3) are plotted in Figure 5.7. A linear regression of the data indicated R^2 values of 0.94 to 1.00, demonstrating near linear sorption onto these synthesized iron oxide materials. Among the tested samples, the sorption coefficients (K_d) were found to be in the order of DDI-HFO (goethite) > AGW-HFO (goethite) > SAGW-HFO (goethite) (Figure 5.7 and Table 5.2). Between the DDI- and AGW- samples (either HFO or goethite), considering their similar SSA values (~336 or ~62 m^2/g for –HFO and –goethite, respectively) and the same experimental conditions, the significantly lower sorption for AGW- samples may be the result of differences in the sorbent properties. For AGW- samples, which were synthesized in the artificial ground water, cation (Ca, Mg etc.)–substitution or other anion-incorporation into HFO or goethite may have occurred, which could affect the material's affinity for iodine. Previous sorption experiments conducted in FY17 (Strickland et al. 2017a) showed that higher solution ionic strength resulted in lower sorption capacity of iodine on iron oxide minerals. The SAGW-HFO and SAGW-goethite showed much lower sorption compared to that of the iron oxides synthesized without sediments. The lower sorption on SAGW-HFO or –goethite can be explained by the sorbent's much lower SSA (~75 to 78 m^2/g). The dissolution of sediment minerals in the SAGW system may also have resulted in sorption decreases through higher solution ionic strength effects or because of the more complex aqueous composition. Consistent with their differences in SSA, HFO showed a far higher sorption affinity for IO_3^- than did goethite, indicating the strong control of surface area on iodate adsorption.

The calculated sorption K_d values for each synthesized sample with 7-days reaction time are listed in Table 5.2. In general, high K_d values were observed on the HFO samples synthesized in the DDI and AGW systems (3253.4 to 5712.2 L/kg after 7-days reaction), followed by the goethite (164.8 to 436.9 L/kg), and then the HFO and goethite samples synthesized in the systems involving sediments (149.5 to 312.4 L/kg). Higher sorption K_d values for SAGW samples could be expected if the observed K_d values were normalized by the iron oxide mass in the iron oxide-sediment mixtures. Similar to the SSA normalization method described in 5.2.1, iron oxide mass normalized K_d values of 672.8 to 1405.8 L/kg [(149.5 or 312.4) x (2 g HFO + 7 g HF)/2 g HFO] can be estimated. The iron oxide mass-normalized K_d values are listed in parentheses in Table 5.2. Sorption experiments with the dark brown HFO particles separated from the precipitate-sediment mixtures should be conducted in the future to determine iodate affinity on SAGW-HFO precipitates. A lower K_d compared to the normalized K_d value might be possible because more element-substituted HFO precipitates may have formed due to the presence of the sediment, resulting in lower sorption.

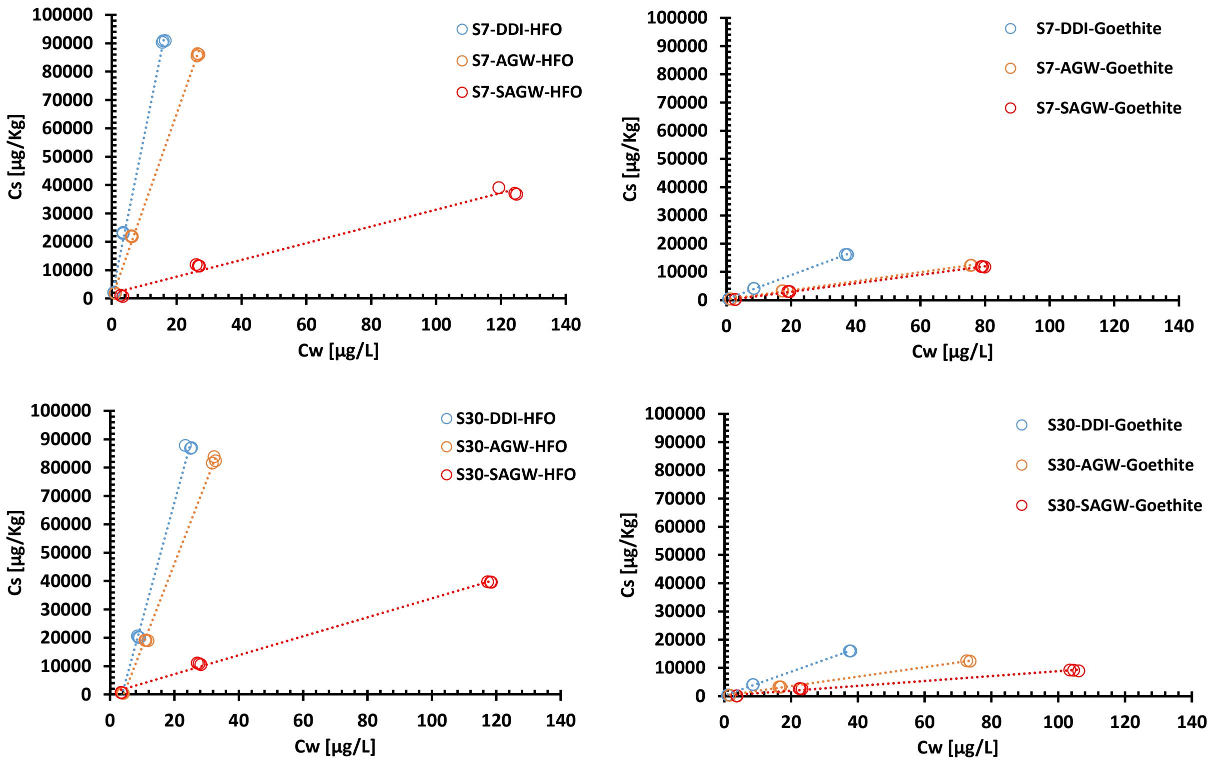

Figure 5.7. Linear iodate sorption on the synthesized iron oxides at room temperature for 7- and 30-days.

Table 5.2. Calculated sorption and desorption K_ds on the synthesized -HFO and -goethite samples at neutral pH in Hanford artificial ground water (AGW) for 7-day and 30-day reaction times.

Samples	Linear Regression Parameters*	Sorption after 7-day Reaction (L/kg)	Desorption after 7-day Reaction (L/kg)	Sorption after 30-day Reaction (L/kg)	Desorption after 30-day Reaction (L/kg)
DDI-HFO	K_d	5712.2	3633.5	3329.2	2618.3
	R^2	1.00	0.99	0.94	0.97
AGW-HFO	K_d	3253.4	2958.3	2430.4	2403.7
	R^2	1.00	1.00	0.95	0.97
SAGW-HFO	K_d	312.4	411.9	339.7	383.2
		(1405.8)	(1853.6)	(1528.7)	(1724.4)
	R^2	0.98	0.99	1.00	1.00
DDI-goethite	K_d	436.9	401.7	427.7	374.2
	R^2	1.00	1.00	1.00	1.00
AGW-goethite	K_d	164.8	199.3	172.2	192.1
	R^2	1.00	1.00	1.00	1.00
SAGW-goethite	K_d	149.5	174.7	89.0	115.0
		(672.8)	(786.2)	(400.5)	(517.5)
	R^2	1.00	1.00	0.99	0.99

The comparison of iodate sorption between the contact times of 7 days and 30 days are plotted in Figure 5.8. For both DDI-goethite and AGW-goethite, the data for both periods nearly overlap, indicating that sorption equilibrium was reached within 7 days. Of particular interest for both DDI- and AGW-HFO was the significantly lower sorption (~25% to 42%) observed for the 30-day reaction period compared to the 7-day reaction period. This decrease in K_d with increasing reaction time was not observed on the SAGW-HFO sample. The reasons for these observations are not currently apparent. Re-dissolution of the precipitated HFO solids into the batch sorption system was eliminated as a possible cause by the solution analysis, which showed no detectable Fe by the ICP-OES (data not shown).

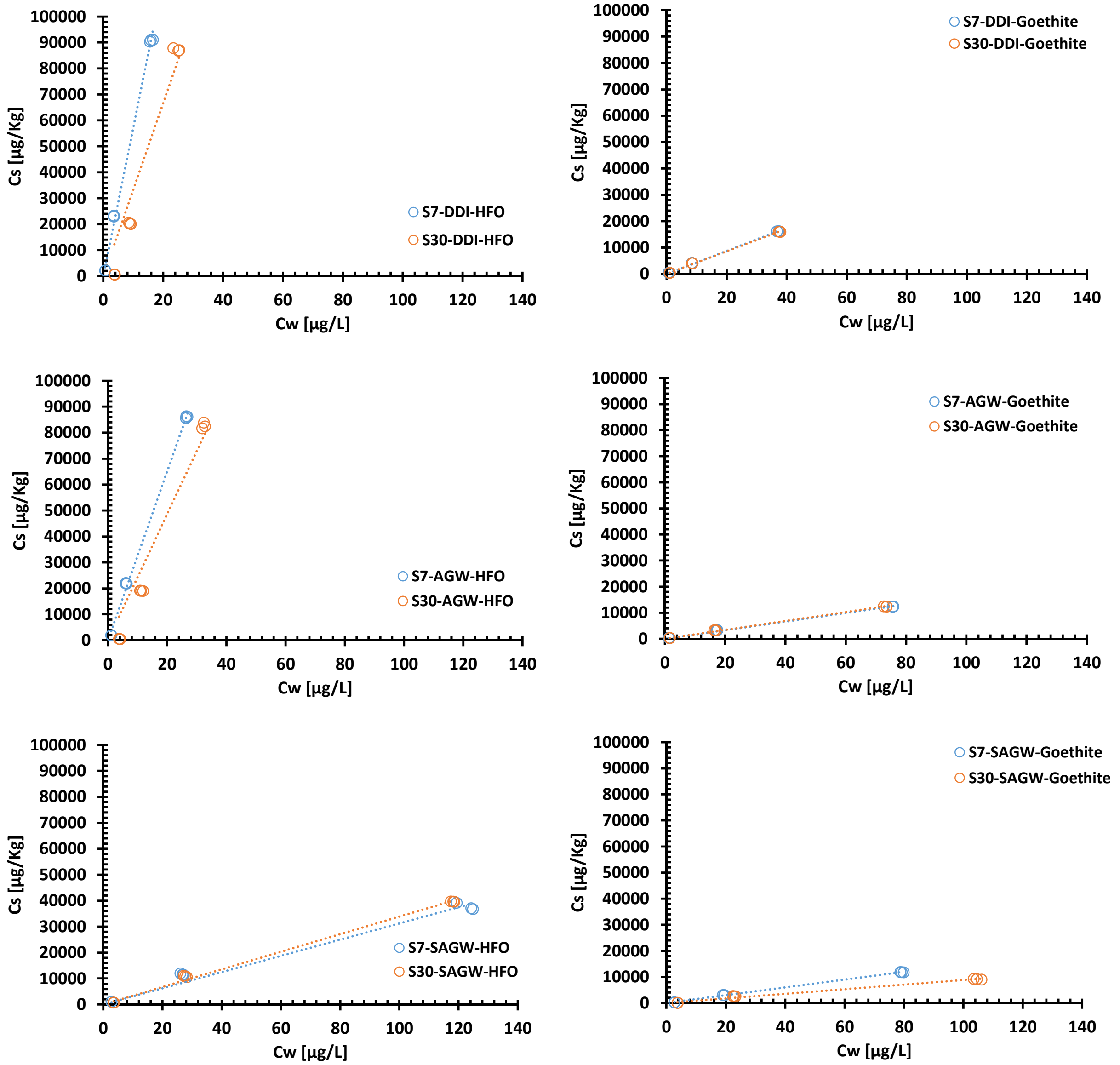

Figure 5.8. Comparison of iodate sorption on the synthesized iron oxides between the reaction time of 7 and 30 days.

The results for iodine desorption (for both 7 days and 30 days) are illustrated in Figure 5.9 and Figure 5.10, with the calculated desorption K_d values listed in Table 5.2. In general, the measured sorption and desorption K_d values were quite comparable, with a variation of ± 1% to 30%, indicating reversible sorption/desorption of iodine for the iron oxides tested in this study. However, different sorption/desorption behavior occurred among the different samples. For example, compared to sorption, samples of DDI-HFO showed lower desorption K_d values of ~ -36% and ~ -21% for 7-day and 30-day reaction times, respectively. Whereas the samples in SAGW-HFO and SAGW-goethite showed an increased desorption K_d (~ +13% to 32%) for both reaction times. Considering the observed nearly identical sorption K_d values on the sample SAGW-HFO between 7- and 30-day reaction times (discussed above), it appears that sorption of iodine on SAGW-HFO was readily reversible in the synthesized AGW conditions.

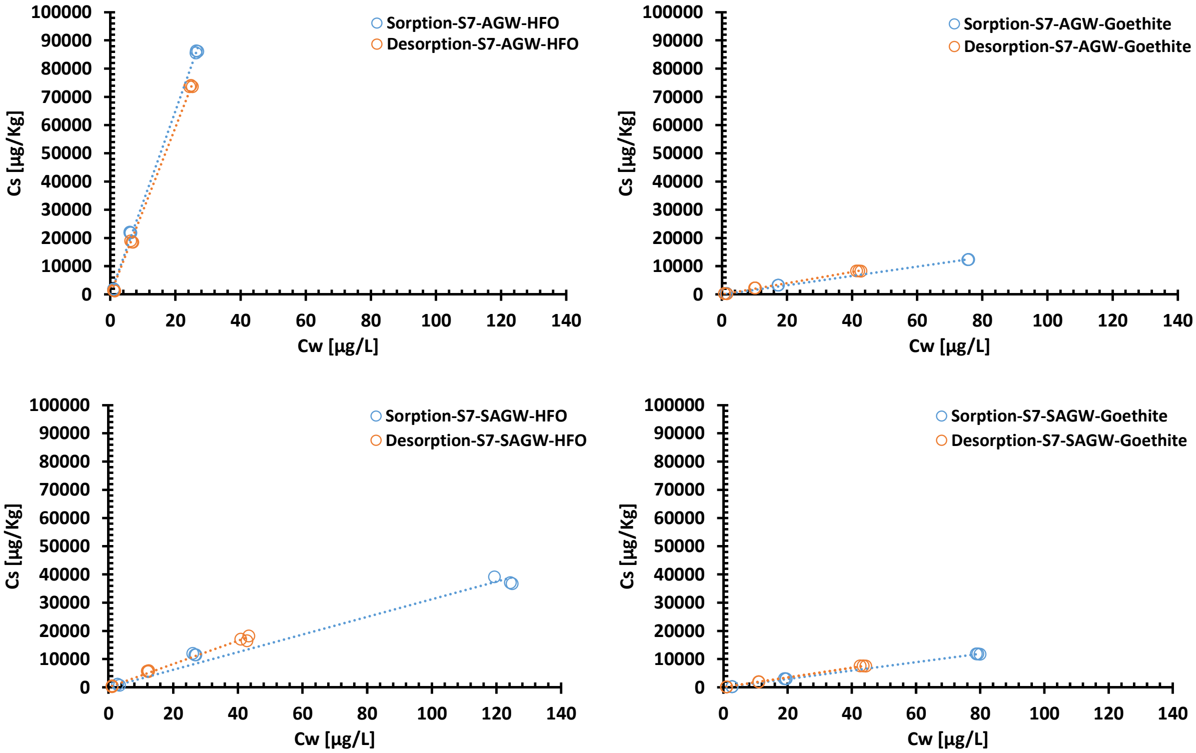

Figure 5.9. Sorption and desorption of iodate on the synthesized iron oxides at room temperature for 7 days.

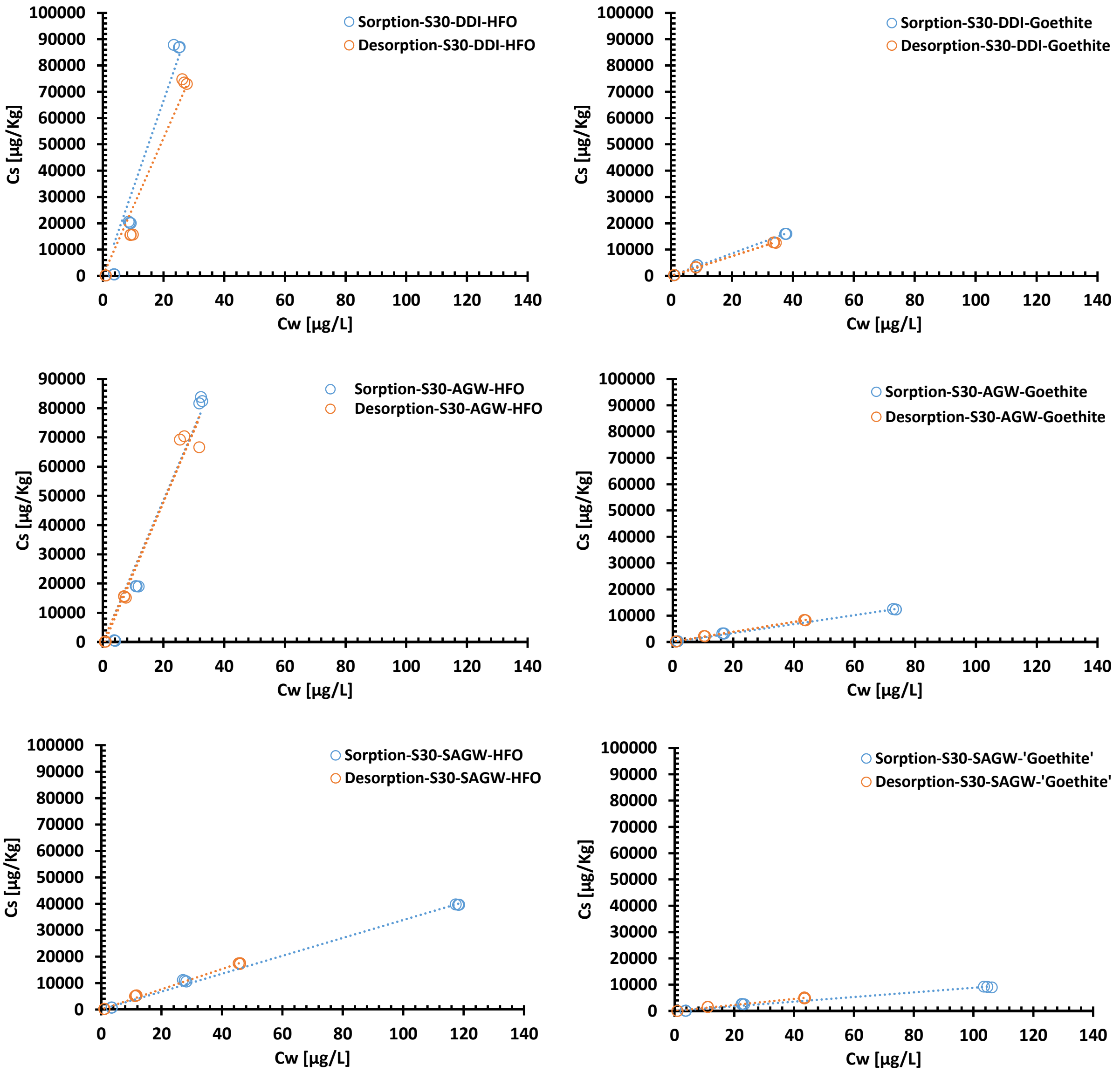

Figure 5.10. Sorption and desorption of iodate on the synthesized iron oxides at room temperature for 30 days.

5.2.3 Sorption/Desorption Reactive Barrier Column

The measured concentrations of total iodine in the effluents of columns packed with AGW-HFO, AGW-goethite, and silica sand are shown in Figure 5.11. As expected, the iodine breakthrough from the control silica sand column occurred after ~1 pore volume (PV), indicating conservative iodine flow without detectable iodine-silica sand interactions. In contrast, the iodate transport was significantly retarded in the AGW-goethite and is due to sorption processes. The iodine breakthrough time at $C/C^0 = 0.5$ occurred after ~27 and ~59 PV in AGW-goethite and AGW-HFO columns, respectively, resulting in retardation factors of about 27 and 59 under the current column packing and flow conditions.

If the iron oxide content of the AGW-HFO column (~1.0%) were more similar to that of the AGW-goethite column (~5.5%), then much later iodine breakthrough would be expected. The large iodine retardation differences between the two packed iron oxides is consistent with the batch sorption experimental results, in which a much higher sorption K_d value was observed for AGW-HFO (4936 L/kg) compared to AGW-goethite (260 L/kg) at an initial iodine concentration of 50 ppb.

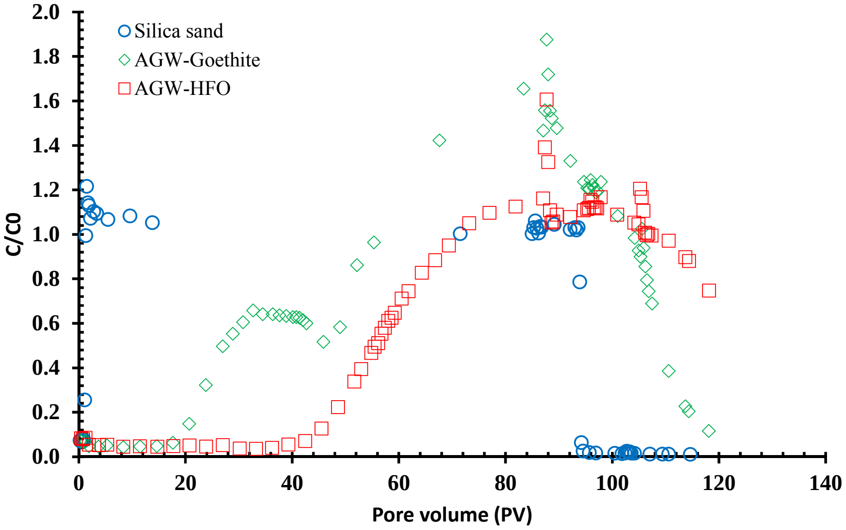

Figure 5.11. Breakthrough curves of the total iodine in the reactive barrier flow-through column experiments [AGW-HFO, AGW-goethite, and the (control) silica sand].

The measured iodine concentrations, selected sample pH, as well as the sorption/desorption stop-flow events are illustrated in Figure 5.12. The effluent samples from the AGW-HFO or AGW-goethite columns were also filtered with a 0.2 µm filter for iodine concentration measurements to check for potential release of iron oxide particles that could result in particle-facilitated iodine transport in the experimental setup. For the AGW-HFO and AGW-goethite columns, the nearly identical iodine concentration values between the 0.2 µm-filtered and non-filtered effluent samples indicated that no > 0.2 µm-sized colloid-facilitated iodine transport occurred. For both columns, the 48-hour stop-flow event during the sorption phase resulted in a significant increase in iodine concentrations in the effluent. Similar to the iodine behavior in the 48-hour desorption stop-flow events, iodine concentration increases during the stop-flow event of the sorption phase indicate release of iodine from the initial sorbed phase back into solution.

This phenomenon is consistent with the iodine breakthrough curves before the sorption stop-flow and before the desorption phase of the experiment, where for both AGW-HFO and AGW-goethite columns, the relative effluent iodine concentrations (C/C^0) > 1.0 were observed, up to 1.16 and 1.88 for AGW-HFO and AGW-goethite, respectively. The reason for this is not yet clear. Any pH effect can be ruled out by the pH monitoring results, which indicated nearly constant pH values (pH 7.16 to pH 7.45) during the entire sorption/desorption test. One possible explanation for the unexpectedly high C/C^0 values in the effluent could be that the initial sorbed iodine released back in the solutions at a later time, overlapping with the freshly injected iodine solution. This phenomenon could potentially be the result of a change in iodine speciation during the course of the experiment. After the initial iodate sorption to the AGW-HFO or AGW-goethite surfaces, part of the iodate may have been reduced to iodide, which then was released due to its much low sorption K_d.

This hypothesis is supported by the XPS characterization results (discussed in Section 5.2.6), in which iodide was observed on the iron oxide surfaces after reaction with iodate solutions. This finding appears to be consistent with some of the batch results presented in Section 5.2.2, where decreased sorption K_d on DDI-HFO and AGW-HFO samples was found for the sorption duration (7 days to 30 days). Iodine speciation measurements on some selected column effluent samples are currently ongoing to validate this hypothesis. The redox mechanisms responsible for this phenomenon is not fully understood; however, microbial reduction is a possibility.

The redox assumption above is based on the premise that the packed silica sand, AGW-HFO or AGW-goethite are initially free of iodine. Table 5.3 lists the flow-through solution volumes during the sorption/desorption processes and the calculated total iodine mass. Within ICP-MS analytical errors, good mass recoveries from the control silica sand column (104.3%) and AGW-goethite column (98.7%) were observed. The mass recovery of ~ 67.9% from the AGW-HFO column indicates that some iodine (~ 32%) was still sorbed to the solid after flushing with ~ 20 PV AGW. Nevertheless, the mass recovery, especially for AGW-goethite, which showed much higher C/C^0 values, confirmed that the packed column samples were iodine-free.

Table 5.3. Flow-through solution volumes during the sorption/desorption processes and the calculated total iodine mass.

Samples	Iodate AGW Solution Injected during Sorption (PV)	Total Iodate Mass Injected during Sorption (µg)	Calculated Effluent Iodine Mass during Sorption (µg)	AGW Desorption Volume (PV)	Calculated Effluent Iodine Mass during Desorption (µg)	Mass Recovery (%)
AGW-HFO	95.35	6.71	3.12	20.32	1.44	67.91
AGW-goethite	95.33	6.71	5.48	22.77	1.11	98.2
Silica sand	92.72	7.03	7.17	21.90	0.17	104.3

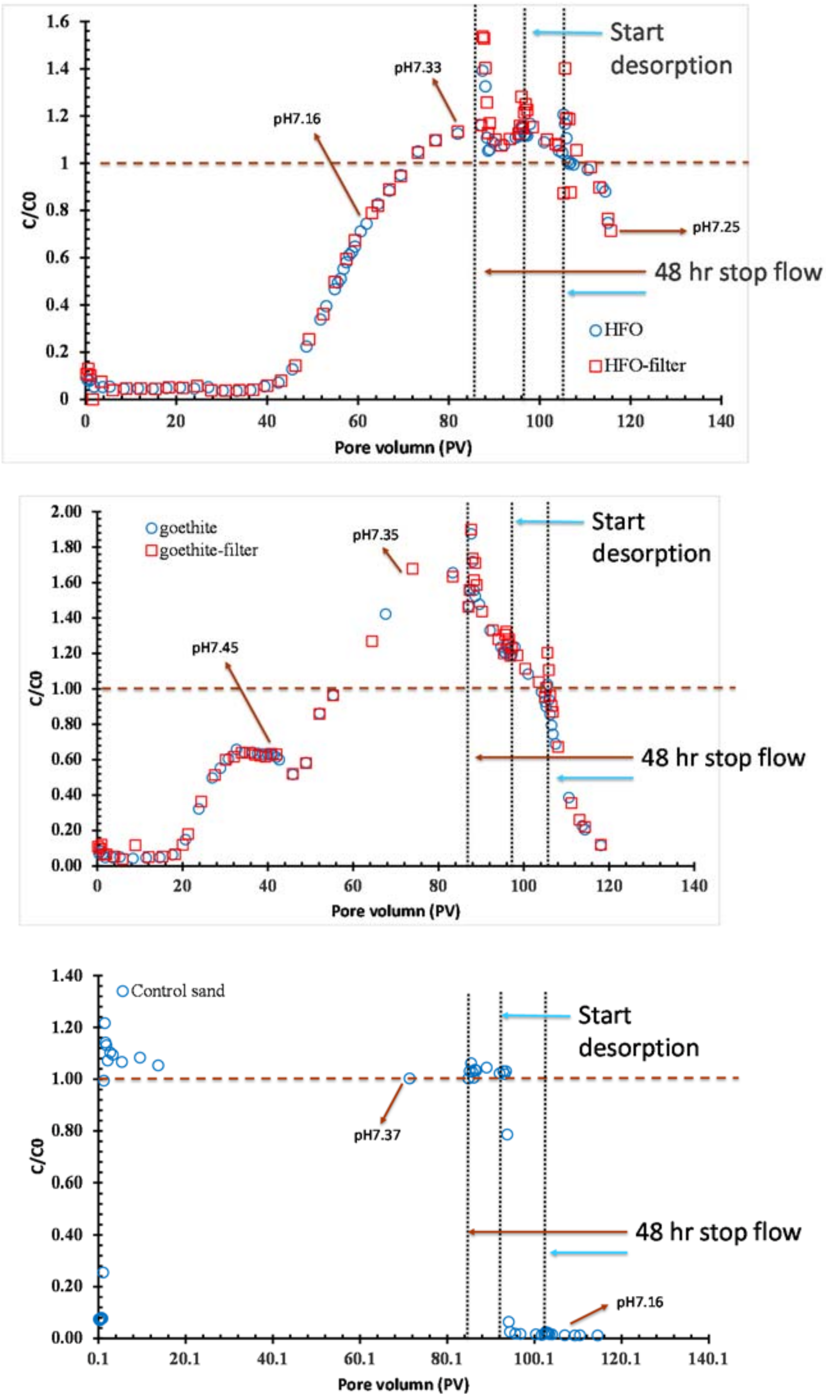

Figure 5.12. The breakthrough curves of iodine in the reactive barrier column packed with the synthesized iron oxides (AGW-HFO, AGW-goethite, and silica sand). The brown dashed lines indicate where the effluent iodine concentrations (C) is equal to the injected iodine concentration (C^0). The empty blue circle and red square represent unfiltered effluent samples and filtered (0.2 µm) effluent samples. The vertical black dashed lines and related arrows illustrate the locations stop flow events. Selected effluent pH values are shown.

5.2.4 Long-Term Iodate Sorption on Iron Oxides

The 200-day and 2-day sorption results for iodate (IO_3^-) on HFO, goethite, magnetite, and hematite at initial concentrations ranging from 5 to 200 ppb and neutral pH (~pH 7.3) are shown in Figure 5.13. Linear regressions of the data produced R^2 values of 0.96 to 1.00, indicating near linear sorption on these iron oxide materials. The zero-intercept linear regression fitted K_d values are listed in Table 5.4. Similar to the 2-day reaction results (Strickland et al. 2017a), Table 5.4 shows that the HFO showed the highest sorption capacity (1210 L/kg), followed by goethite (125 L/kg), magnetite (30.3/kg), and hematite (12.5 L/kg). In general, compared to the 2-day reaction, an increase of sorption K_d (~ +27% to 48%) was observed when the reaction time approached 200 days. The limited K_d increase may have resulted from sorption kinetics or from changes in the solid:solution ratio [in the 2-day reaction, the solid/solution ratio increased from 2.0 to 2.2 for HFO and 10.0 to 10.9 for the other iron oxide samples, because 3 mL of supernatant was removed for sampling in 2-day experiments (see Section 5.1.5)].

No significant mineral transformation of the synthesized HFO was observed after the 200-day reaction period. The XRD patterns of the HFO (synthesized in FY17; containing ~20% hematite) before and after 200-day reaction periods (Figure 5.13) showed a small goethite peak (~ 21 deg) generated after the reaction. The 200-day reaction HFO sample was further heat-treated at 70°C for a week. The XRD results still showed a very limited transformation to goethite (Figure 5.14). These findings imply that the synthesized HFO is relatively stable within the experimental conditions and duration of the study.

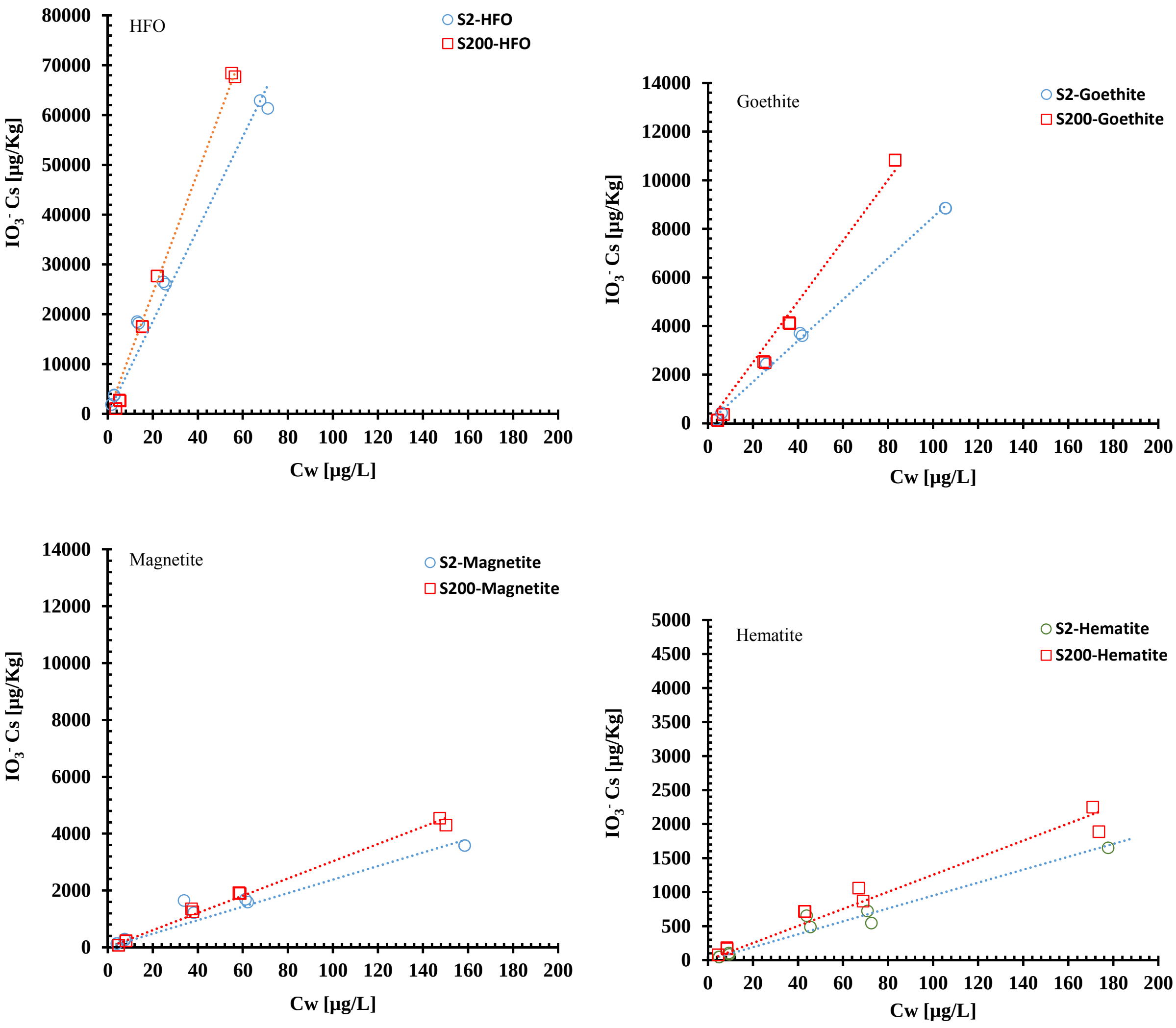

Figure 5.13. Long-term (200 days) extended iodate sorption experiments with HFO, goethite, magnetite, and hematite. The 2-day reaction results are also shown for comparison purpose.

Table 5.4. Calculated sorption K_d in the extended long-term (200 days) sorption experiments, and comparison with the 2-day sorption results.

Samples	Linear Regression Parameters* (ppb)	K_d after 2-day Reaction (L/kg)	K_d after 200-day Reaction (L/kg)	K_d Differences between 2- and 200-day Reaction Time (%)
HFO	K_d	927.5	1212.5	30.7
	R^2	0.98	0.99	
Goethite	K_d	84.9	125.2	47.5
	R^2	1.00	0.98	
Magnetite	K_d	23.8	30.3	27.3
	R^2	0.94	0.99	
Hematite	K_d	9.5	12.5	31.6
	R^2	0.96	0.96	

*Zero intercept linear regression model.

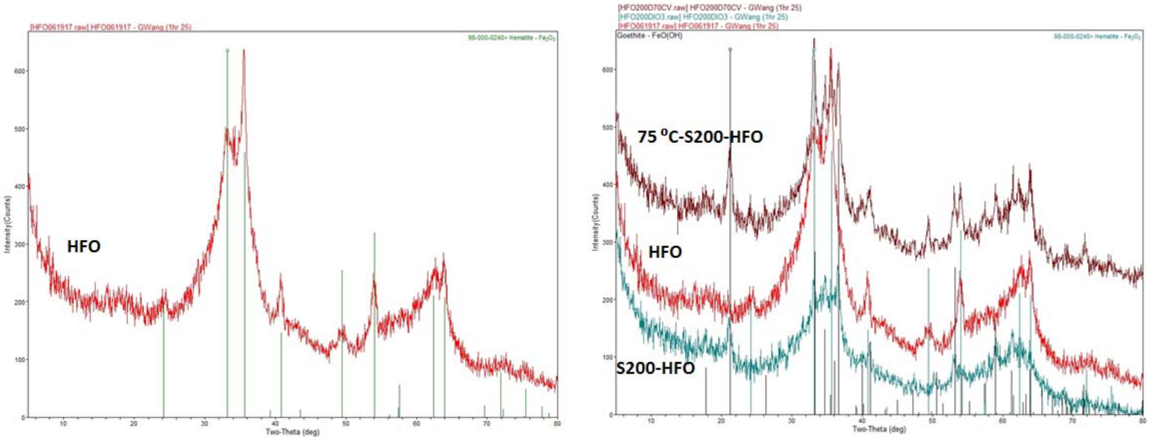

Figure 5.14. XRD analysis on the synthesized HFO (FY17; containing ~20% hematite) before (HFO) and after the 200-day reaction (S200-HFO), as well as a sample further heat-treatment at 70°C for a week (75°C-S200-HFO).

5.2.5 Iodine Uptake during HFO Precipitation (Co-precipitation)

Results of iodate and iodide removal efficiency through co-precipitation with HFO in the three different solution systems of DDI, AGW, and SAGW are shown in Figure 5.15. Greater than 90% of the iodate was removed from solution through co-precipitation with DDI-HFO, AGW-HFO, and SAGW-HFO for initial concentrations ranging from 5 to 200 ppb (except SAGW-HFO at 5 ppb, which showed an average value of 68.3%). For iodide, lower removal efficiencies (20% to 70%) were observed among all the tested systems. The iodate and iodide co-precipitation efficiencies were also presented in terms of iodine loading (mg/kg), in which the solid mass used in the iodine loading calculation referred to the collected, air-dried solid precipitate weights. Figure 5.16 and Table 5.5 show the co-precipitated loadings for iodate and iodide with different initial iodine concentrations in the three tested systems. In general, much higher co-precipitation of iodate (~0.21 to 7.97 mg/kg) was found than for iodide (0.04 to 4.35 L/kg). Although lower than that of iodate, the iodide loadings are still much higher than for sorption on natural sediments, which implies a potential iodide sequestration approach. For either iodate or iodide, similar iodine loading values were observed at eZach concentration level (except "iodide-SAGW-200 ppb" batch) for each of the three testing conditions (DDI, AGW, and SAGW). These findings are different from the batch sorption experiment results (where a sorption K_d of DDI- > AGW- > SAGW- was observed), which might reflect a different iodine-iron oxide association mechanism.

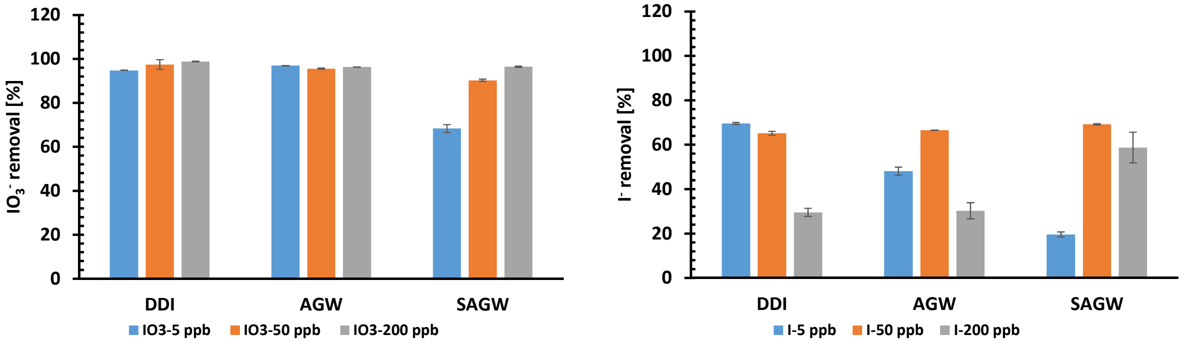

Figure 5.15. Removal efficiency of iodate and iodide through HFO co-precipitation in three different solution systems (DDI, AGW, an SAGW) under a concentration range of 5 to 200 ppb.

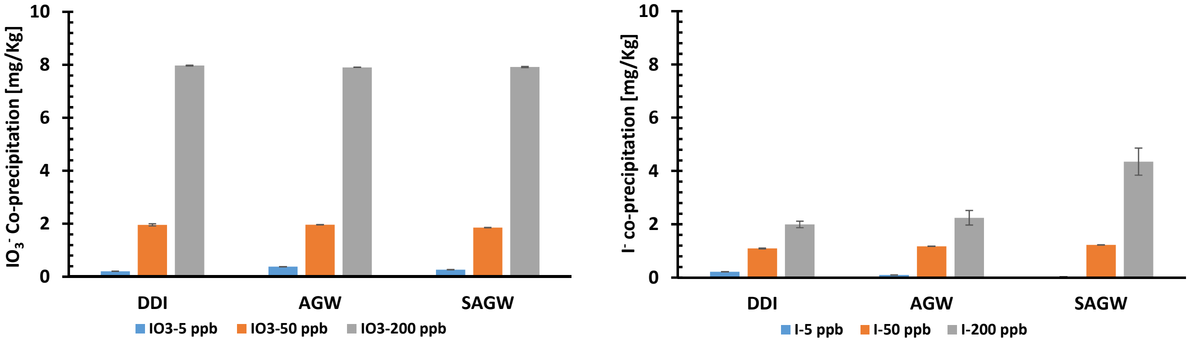

Figure 5.16. Calculated loadings of iodate and iodide (mg/kg) through HFO co-precipitation in three different solution systems (DDI, AGW, an SAGW) under a concentration range of 5 to 200 ppb.

Table 5.5. Calculated loadings of iodate and iodide through HFO co-precipitation in three different solution systems (DDI, AGW, and SAGW) under three initial concentrations of 5, 50, and 200 ppb.

Initial Iodine Concentrations	DDI-IO_3^- Loading (mg/kg)	AGW-IO_3^- Loading (mg/kg)	SAGW-IO_3^- Loading (mg/kg)	DDI-I^- Loading (mg/kg)	AGW-I^- Loading (mg/kg)	SAGW-I^- Loading (mg/kg)
5 ppb	0.21 ± 0.00	0.39 ± 0.00	0.27 ± 0.01	0.22 ± 0.00	0.10 ± 0.00	0.04 ± 0.00
50 ppb	1.96 ± 0.04	1.97 ± 0.00	1.86 ± 0.01	1.10 ± 0.01	1.18 ± 0.00	1.23 ± 0.00
200 ppb	7.97 ± 0.01	7.91 ± 0.00	7.92 ± 0.02	1.99 ± 0.12	2.24 ± 0.27	4.35 ± 0.51

5.2.6 XPS Analysis on Iodine Sorption

XPS is a versatile surface analysis technique that can be used for compositional and chemical state analysis. To enhance understanding of iodate sorption on iron oxide surfaces, XPS spectra were collected on four selected samples: DDI-HFO, DDI-goethite, magnetite, and hematite. The iron oxide samples were reacted with iodate-spiked AGW solutions with initial concentrations of 1.0×10^{-2} and 5.76×10^{-4} M (100 ppm).

A full-range XPS spectra was conducted for each sample. An example spectra (AGW-goethite after reaction with 1.0×10^{-2} M iodate solution in AGW system) is shown in Figure 5.17. It clearly revealed the presence of iodine on the goethite, and I 3d peaks were clearly identified in the survey scan spectrum after iodate adsorption.

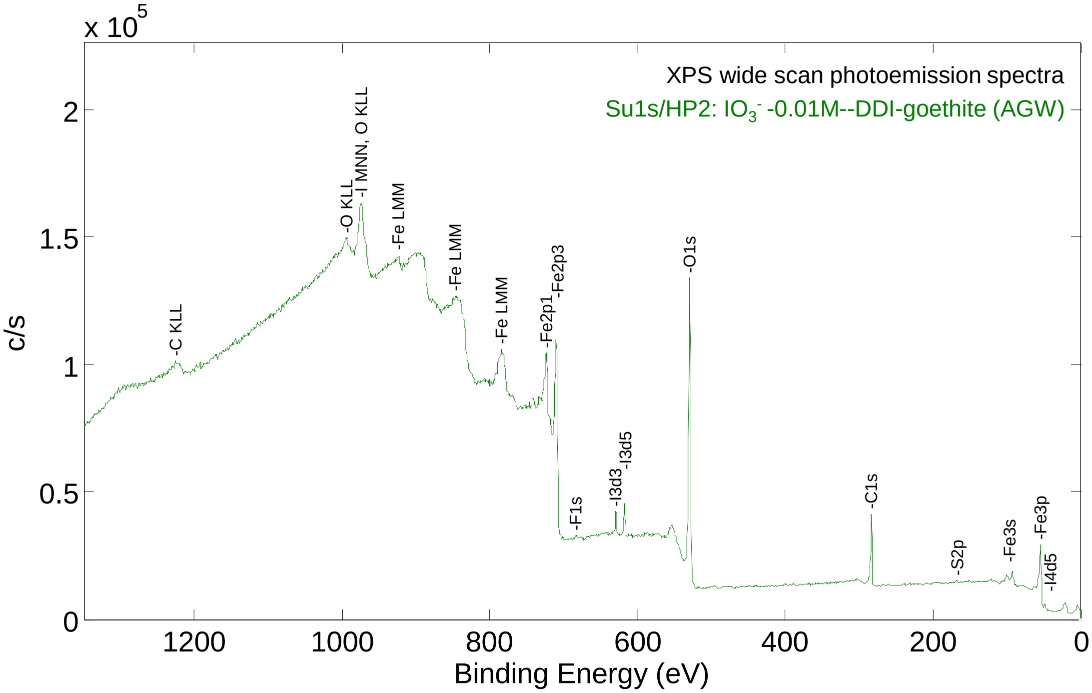

Figure 5.17. Full-range XPS spectra of AGW-goethite after iodate sorption in 0.01 M iodate AGW solution.

To determine the chemical environment of iodine, high resolution XPS spectra of the I 3d peaks of the samples before and after 7-days reaction with 1.0×10^{-2} or 5.76×10^{-4} M iodate (IO_3^-) AGW solutions were collected and are shown in Figure 5.18. Two major peaks located at 624.1 eV and 635.2 eV appear to result from the I 3d spin-orbital doublet (I $3d_{5/2}$ and I $3d_{3/2}$, respectively) with a splitting of 11.1 eV. These two peaks were expected and are assigned to iodate based on literature values (Li et al. 2016). According to previous work (Du et al. 2004; Li et al. 2016), the peak of I $3d_{5/2}$ at the binding energy of 624.1 eV might be associated with the formation of iron iodate because of the strong interaction between iodate and surface iron atoms. Unexpectedly, Figure 5.18 also has two major peaks at the binding energy of 619.2 eV and 630.5 eV, which are consistent with iodide (I^-) signals (Li et al. 2016). It is not clear what the chemical bonding was between iodide and the iron oxide surfaces. In addition, no significantly detectable sorption of iodide on iron oxides can be reported in our FY17 scoping batch experiments (Strickland et al. 2017a). High resolution XPS spectra of the I 3d peaks on the control samples (the samples reacted with AGW without iodine) were also collected, indicating no iodate or iodide contamination in the samples (Figure 5.18).

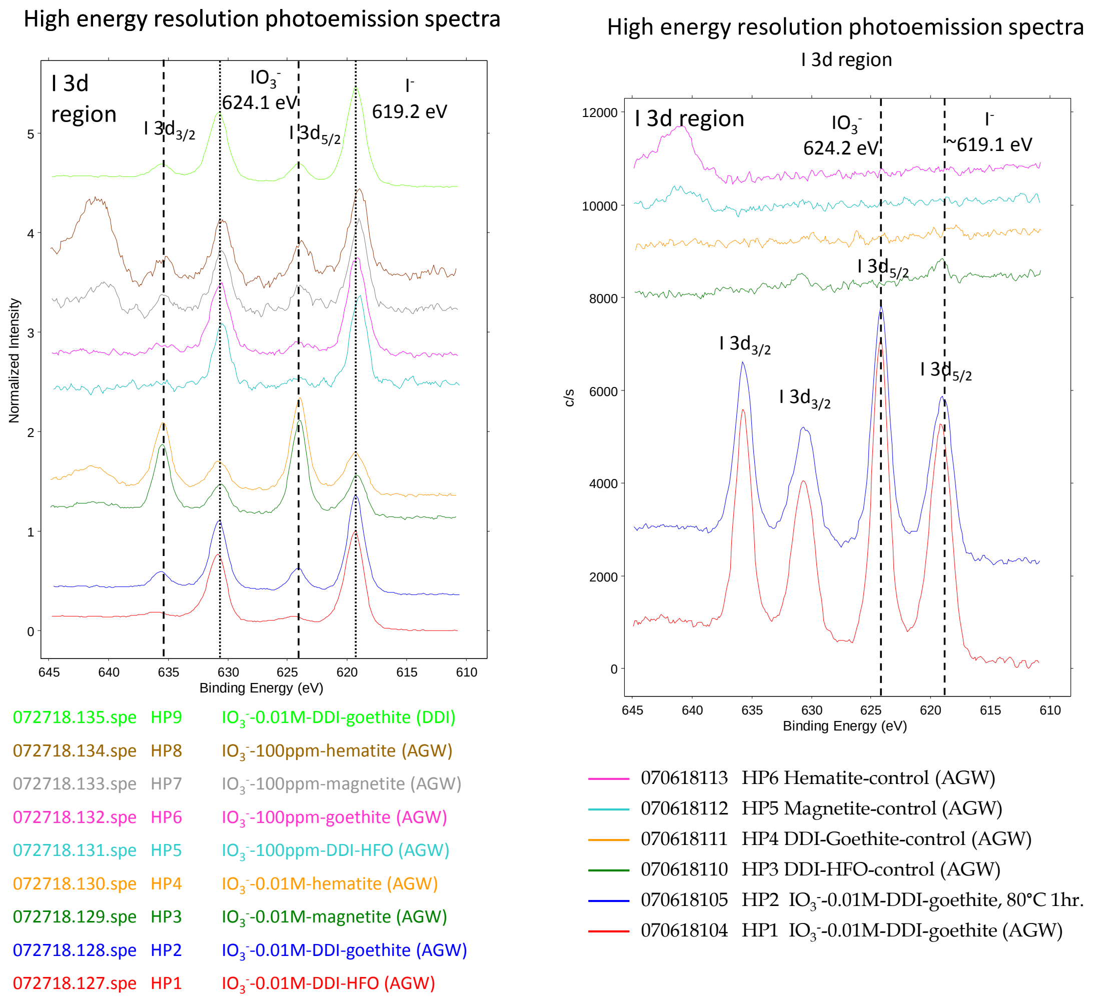

Figure 5.18. High resolution XPS spectra of the I 3d peaks on the samples reacted with AGW solutions of 100 ppm or 0.01 M iodate (left), as well as the XPS spectra on the control samples (right). The sample label "IO$_3^-$-0.01M-DDI-goethite, 80°C 1hr" represented the 1.0E-02 M IO$_3^-$ reacted DDI-goethite sample was further heat-treated at 80°C for 1 hour.

To understand the presence of iodide, one can consider the possibility that the added iodate was reduced to iodide on the iron oxides in the AGW system (reduction potential of the IO$_3^-$/I$^-$: 1.085 V for acid solution and 0.26 V for alkaline solution). This scenario does not appear to be likely because the iron oxides were synthesized with ferric iron (except magnetite) and is supported by the Fe XPS spectra (Figure 5.19) where no clear indication of Fe^{2+} was found. In order to evaluate any redox artifacts resulting from the XPS beam, multiple sequential XPS beam scans were conducted to monitor any potential changes in the IO$_3^-$: I$^-$ peak ratio (Figure 5.20). No clear indication of peak ratio changes were found in sample DDI-HFO and hematite, whereas a limited IO$_3^-$/I$^-$ decrease was observed in magnetite and DDI-goethite. The results indicate that the XPS X-ray beam might result in limited reduction of iodate, depending on the sample; however, it is not possible to quantify the magnitude of iodate reduction that occurred during the first beam exposure.

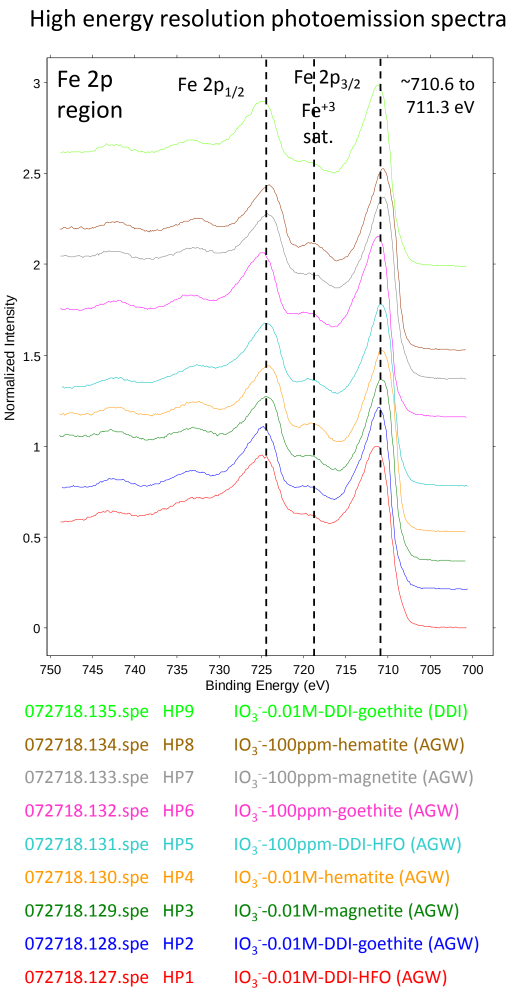

Figure 5.19. High resolution XPS spectra of the Fe 2p peaks on the samples reacted with AGW solutions of 100 ppm or 0.01 M iodate. Two major peaks at 710.6-711.3 eV and ~724.6 eV were assigned to Fe^{3+}, while the Fe $2p_{3/2}$ peak has associated satellite peaks at ~718.5 eV (Yamashita and Hayes 2008).

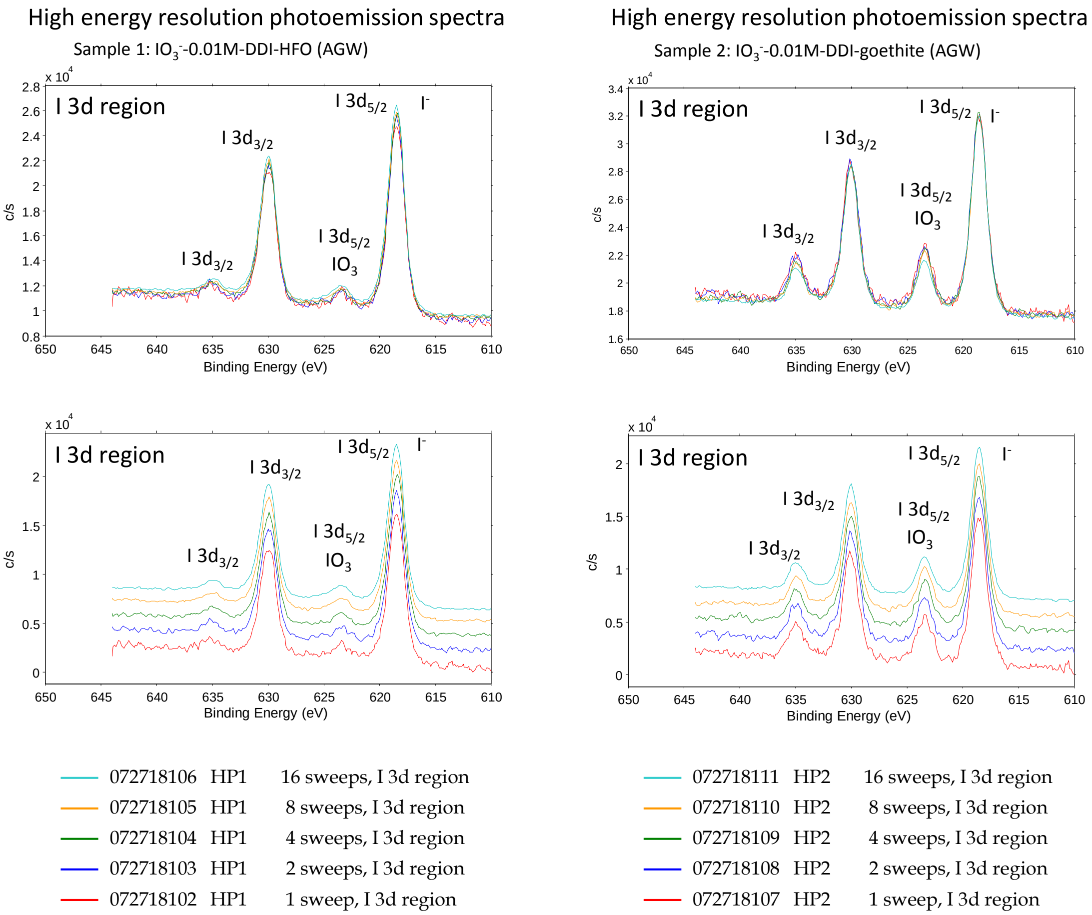

Figure 5.20. Multiple sequential scans for high resolution XPS spectra of the I 3d peaks on selected samples (DDI-HFO, DDI-goethite, reacted with AGW solutions of 0.01 M iodate) for potential iodate reduction monitoring caused by XPS beam energy.

6.0 Dithionite-Enhanced Iodine Mobility

The purpose of investigating dithionite for remediation of iodine in Hanford sediments is to remove aqueous iodide and iodate as well as some iodate incorporated into iron oxides. It is hypothesized that iodine-contaminated Hanford sediments have a higher proportion of iodine in Fe oxides than in calcite. Dithionite treatment of sediments dissolves some ferric oxides (20% to 40%), and reduces ferric species to ferrous, which precipitate as multiple ferrous phases. The dithionite also reduces aqueous iodate and iodate removed from the dissolved ferric oxides. Because iodine is actually made more mobile, this reduction technology is designed to be used to enhance the P&T system by removing more iodine from the sediments more quickly compared with just pumping groundwater. As a laboratory study of the potential use of a technology for iodine remediation, the specific objectives are:

- Na-dithionite solution type (i.e., bicarbonate and citrate) and iodine removal efficiency from sediments
- Na-dithionite concentration and iodine removal efficiency from sediments
- identify the surface phase(s) that are dissolving and releasing iodine
- long-term leaching of iodine from sediments after dithionite treatment
- evaluate the applicable of dithionite treatment to sediments from different waste sites that may contain different co-contaminants and have iodine incorporated into different solid

Although the technology evaluations in this report are focused on iodate immobilization, enhanced mobilization may be appropriate for enhancing capture with a groundwater P&T system. Sequential liquid extractions conducted on vadose zone sediments beneath the B, T, and S complexes showed that 2% to 15% of the total I-127 mass was aqueous and adsorbed, with the remainder in unidentified precipitates (Truex et al. 2017: Szecsody et al. 2017). Whereas groundwater is predominantly iodate, identification of the iodine species in the vadose zone cores showed that 5 of 8 cores were iodide dominated, 2 of 8 cores were iodate dominated, and 1 core had equal iodide and iodate mass. While these results show that the vadose zone sediments and pore water are iodide-dominated, iodine species measurements in groundwater are nearly all iodate, although there are only a limited number of measurements. A vertical profile in groundwater at depths ranging from at the water table to 34 ft below the water table (Lee et al. 2017), iodide was 55% of the mass at the water table, but iodate dominated all deeper locations.

Because iodide and iodate exhibit low sorption, leaching of iodine-contaminated sediments should release iodide first (K_d 0.07 mL/g to 0.1, Rf in Hanford sediments 1.3 to 1.5; Truex et al. 2016), then iodate (K_d 0.3 mL/g to 1.2, Rf in Hanford sediments 2.4 to 6.2), so by 10 pore volumes, adsorbed iodide and iodate should be released from sediments. A comparison of iodine leaching behavior from 11 sediments from B, T, and S complexes, however, indicated that while the highest iodine concentrations were released within the first few pore volumes, the amount of iodine mass leached by 10 pore volumes represented only 54.7 ± 14.2% of the total iodine mass released from the sediment over 100 pore volumes. Therefore, while aqueous and adsorbed iodate/iodide is the most mobile mass (and needs to be remediated), this represents only 55% of the readily mobilized mass in the Hanford subsurface (Figure 6.1). Clearly, solid phases are being dissolved, releasing additional iodine species.

It has been hypothesized that iodine is incorporated in calcite, Fe-oxides, and possibly other precipitates. Slow dissolution of these phases can release iodine species to groundwater, even under natural conditions. For example, calcite in natural Hanford subsurface is in equilibrium with the aqueous calcium, magnesium, and carbonate aqueous species, but there is still continuous calcite dissolution and re-precipitation with no net dissolution or precipitation. During this exchange process, iodate can be released to aqueous solution. Calcite, amorphous Fe oxides such as ferrihydrite, and crystalline oxides such as goethite, have moderate solubility, as opposed to very low solubility (stable) minerals such as quartz or apatite. In addition, waste operations can accelerate dissolution of some of these phases. In the Hanford 100K Area, P&T operations withdraw pH 7.5 water but reinject pH 5.5 to 6.2 water, which is causing some dissolution of calcite near injection wells and downgradient calcite precipitation once the pH has been neutralized. During this process, C-14 and Sr-90 incorporated in the calcite has been released to aqueous solution. If in iodate-laden sediments, the injection of acidic water dissolving calcite and some Fe-oxides would release significantly greater iodate into groundwater than the natural groundwater.

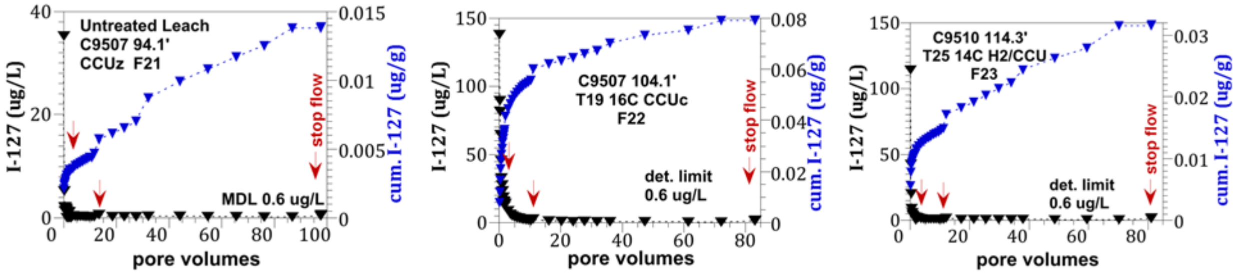

Figure 6.1. Iodine-contaminated Hanford vadose zone sediments showing AGW leaching of: a) C9507 94.1' sediment, b) 9507 1104.1' sediment, and c) C9510 114.3' sediment.

Sodium dithionite ($Na_2S_2O_4$, sodium hydrosulfite) is a strong aqueous reductant that is used for industrial dyeing, pulp processing, water treatment, and cleaning in a wide variety of industries. In geosciences, it is used for enhanced oil recovery, as crystalline ferric iron extraction process (DCB extraction), and for creation of a subsurface reduced permeable reactive barrier (Fruchter et al. 1998). Sodium dithionite by itself will react with ferric oxides in sediment:

$$S_2O_4^{2-} + 4Fe^{3+} + 2H_2O <=> 4Fe^{2+} + 4H^+ + 2SO_3^{2-}$$

dissolving and reducing the ferric phases to multiple ferrous phases including (a) adsorbed Fe^{2+}, (b) FeS, (c) $FeCO_3$ (Szecsody et al. 2004), and (d) structural Fe(II) in 2:1 clays (Stucki et al. 1984). The produced sulfite will oxidize to sulfate. It should be noted that one mole of dithionite reduces four moles of iron and produces four moles of H^+, so the system (with no pH buffer) will become as acidic as pH 2.3, which results in mainly aqueous ferrous iron (along with dissolving other minerals; Szecsody et al. 2004). The addition of four moles of K_2CO_3 pH buffer at pH 12 with each mole of Na-dithionite results in an initial pH of 12, but after reaction with sediments a pH of 8 to 9. This mixture of Na-dithionite and K_2CO_3 pH buffer has been successfully deployed at the Hanford 100D Area for chromate reduction and in a limited number of other field sites for chromate, TCE (Vermeul et al. 2002), and RDX remediation (Szecsody et al. 2001). Because the goal of the dithionite-K_2CO_3 treatment is to create solid ferrous phases (for a permeable reactive barrier), the pH needs to be neutral to alkaline (as ferrous iron desorbs under acidic conditions). A mixture of Na-dithionite, potassium carbonate, and sodium citrate (i.e., DCB extraction) has been used for decades for characterization of the total amount of amorphous and crystalline ferric oxide in sediments (Heron et al. 1994), Chao and Zhou et al. 1983). In contrast, the DCB extraction is designed to dissolve ferric oxides, reduce the iron, but maintain the ferrous iron in aqueous solution by complexation with citrate so that the total amount of ferrous iron can be measured.

For this study, Na-dithionite (with one or more additional chemicals) treatment of sediments is for (a) reduction of aqueous and adsorbed iodate as iodide species exhibit less sorption, and (b) dissolution of amorphous and crystalline ferric oxides that contain iodate/iodide, and keep iodide (the product) aqueous. The efficiency of three different Na-dithionite solutions (i.e., Na-dithionite by itself, Na-dithionite and

K_2CO_3, and DCB) are compared in terms of the efficiency for iodine removal from field-contaminated sediments.

6.1 Experimental Methods

Batch experiments to identify appropriate concentration ranges of dithionite to release and maintain iodine mobility by converting iodate to iodide and by dissolving iron oxides on sediment surfaces, releasing iodine species to aqueous solution, were conducted. The experiments were designed to bound the appropriate concentration ranges and evaluate potential analytical interferences with iodine quantification.

6.1.1 Na-Dithionite Solution Chemistry and Concentration

Batch experiments are conducted to evaluate the efficiency of iodine removal from sediment using (a) 0.1 mol/L Na-dithionite, (b) 0.1 mol/L Na-dithionite and 0.4 mol/L K_2CO_3, and (c) 0.1 mol/L Na-dithionite and 0.4 mol/L K_2CO_3 and 0.6 mol/L Na-citrate. The batch experiments consisted of 3.0 g of sediment with 30 mL of the extraction solution in a 45 mL Teflon centrifuge tube for 200 h. In addition, a fourth experiment is conducted in which the 0.1 mol/L Na-dithionite and 0.4 mol/L K_2CO_3 solution is reacted with the sediment for 3 days, then a new 0.1 mol/L Na-dithionite and 0.4 mol/L K_2CO_3 added each three days (repeated four times) to evaluate repeated treatment efficiency. The concentration of iodine (I-127) is measured in all four vials.

A series of batch experiments was conducted to evaluate the efficacy of variations of buffered Na-dithionite extractant solution (0.01 mol/L Na-dithionite, 0.04 mol/L K_2CO_3, and 0.004 $KHCO_3$) for removal of iodine from iodine-contaminated sediments. In these experiments, the Na-dithionite concentrations in the final solutions were varied from 0.001 to 0.1 mol/L. The experiments were conducted in an anaerobic chamber to remove the influence of oxygen oxidizing the Na-dithionite solution. Selected experiments were repeated with the same solution, but with oxic water.

The batch experiments consisted of 3.0 to 10.0 g of sediment and 30 mL of the extraction solution in a 45 mL Teflon centrifuge tube. 3.0 mL samples were taken at multiple time periods, ranging from 0.1 to 100 h. Collected samples were filtered with a 0.45-micron filter before iodine species analysis. Analyses were conducted by ion chromatography, liquid scintillation counting or ICP-MS. Multiple iodine-contaminated sediments were used, and sequential liquid extractions were conducted before the leach studies. After the last liquid sample was taken, sequential liquid extractions were conducted to measure adsorbed and incorporated iodine.

6.1.2 Evaluate Solid Phases Mobilized by Na-dithionite

A series of batch experiments was conducted with varying reductant (Na-dithionite) concentration in different Hanford sediments, and the aqueous solutions were analyzed for ions that are from the dissolution of Fe/Mn oxides (Fe, Mn, Ti) and carbonates (Ca, Mg, U by ICP-OES, aqueous carbonate by carbon analyzer). These sediments were also analyzed for iron oxides before and after dithionite treatment using iron extractions and solid phase inorganic carbon (i.e., carbonates).

Sequential extractions were conducted to estimate specific association relationships of contaminants or other components with specific phases. The reagents used and their intended targets were as follows. AGW targeted aqueous contaminants. The extractant 0.5 mol/L HCl targeted the adsorbed fraction, pH 5 acetate targeted some carbonates and amorphous Fe oxides, pH 2.3 acetic acid targeted nearly all carbonates and Fe oxides, 0.1 M ammonium oxalate/oxalic acid targeted any remaining Fe-oxides, and 8 M nitric acid at 95°C targeted some alumosilicates, phosphates, and oxides (defined as the hard to extract contaminant fraction).

The extractions were conducted in 45-mL Teflon centrifuge tubes at a sediment:liquid ratio of 1:2. For each set of 20 samples, a set of six preparation blanks and six blank spikes were performed. The set of six blanks consisted of the six solutions (i.e., extractions 1 through 6). The set of six blank spikes consisted of the six extraction solutions spiked with the contaminant(s) of interest. In addition, one duplicate sediment sample was conducted for each batch of 20 samples.

For the first extraction, 20 mL of AGW was mixed with 10 g of sediment in a 45-mL centrifuge tube (with O-ring seal) for 50 minutes on a slow (6 rpm) rotary mixer. The tube was then centrifuged at 3000 rpm for 10 minutes. Liquid was drawn off the top of the sediment and filtered (0.45 μm nylon/PVDF) for analysis. This process was then repeated for each of the other five extractants.

6.1.3 Evaluate Long-Term Stability of Iodine Remaining in Sediment

A series of batch experiments were conducted with selected sediments that received the dithionite treatment to evaluate the long-term stability of iodine remaining in the sediment after the dithionite extract (and iodine mobilization) was removed. These batch experiments used the sediments extracted in Section 6.1.1, but after the sediments had been washed three times with AGW.

The batch experiments consisted of 3.0 to 10.0 g of cleaned sediment and 35 mL of AGW in a 45 mL Teflon centrifuge tube, with 3.0 mL samples taken at multiple time periods ranging from 0.1 to 1500 h. The samples were filtered with a 0.45-micron filter before iodine species analysis. Iodine species analysis was conducted by ICP-MS. Multiple iodine-contaminated sediments were used, and sequential liquid extractions were conducted before these leach studies. After the last liquid sample was collected, sequential liquid extractions were conducted to measure adsorbed and incorporated iodine.

Column experiments were also conducted to evaluate the rate at which iodine is released from sediments at near field sediment/water ratios using the dithionite solution, and the long-term immobilization of the remaining iodine in the sediment after dithionite-mobilized iodine is removed. These column studies were conducted at different flow rates on selected sediments used in Section 6.1.1. In contrast to the batch leaching experiments (Section 6.1.1), the column leach experiments had a high sediment/water ratio similar to that in the field, which will likely result in greater iodine species interactions with mineral or organic phases in the sediment and slower dissolution of Fe-oxides and iodine release.

In these column experiments, sediment was reacted with the AGW for different time periods as water flowed through the sediment (approximating groundwater flow through contaminated sediment). Each column experiment was unique in terms of the exact flow rate, mass of sediment, size of column, and the change in concentration of contaminant(s) leaching from the sediment.

Moist sediment was packed into a column, ranging in size from 0.77-cm diameter by 10-cm length to 2.6-cm diameter by 100-cm length. The weight of the moist sediment in the column was determined. The moisture content of the moist sediment was determined by weighing 3 to 5 g of moist sediment before and after drying for 48 h at 105°C. The packed column was then water-saturated by injecting AGW into one end of the column until water exited the effluent end of the column. The dry bulk density of the sediment was calculated from the dry sediment weight in the column divided by the column volume. The pore volume, or total water weight in the column, was calculated from the weight of the water in moist sediment plus weight of the water added to saturate the column. The porosity was calculated from the total water weight in the column divided by the column volume.

The injection solution (AGW) was modified to contain 80 mg/L bromide as a conservative tracer. The column experiment consisted of injecting AGW into one end of the column at a constant flow rate to achieve a 1- to 4-hour residence time for a total duration of 10 to 200 pore volumes (depending on the contaminant). Liquid samples were collected in sufficient number and frequency to measure the change in concentration of the contaminant(s), which was typically 30 or more samples. These samples were collected using a timed fraction collector (Isco Foxy 200 or other), which contained either 4.5- or 15-mL falcon tubes to collect effluent samples. More effluent samples were collected in the first two pore volumes, with less frequent sample collection for subsequent pore volumes. Stop-flow events ranging from 10 to 1000 hours with no flow were utilized to provide additional time for contaminants present in one or more surface phases on the sediment surface to partition into the pore water.

6.2 Results

6.2.1 Different Na-Dithionite Solutions and I-127 Removal

Experiments with Na-dithionite with additional chemicals showed that the addition of the K_2CO_3 pH buffer enhanced the I-127 removal from the sediment by 20% (second versus first set of bar graphs, Figure 6.1a), but the addition of Na-citrate decreased the I-127 removal by 7%. Greater time (i.e. reaction time of 1000 h versus 170 h) increased the I-127 removal from the sediment an average of 40%, even though the Na-dithionite itself is no longer reactive after a few days due to dissociation in water to sulfate, although FeS precipitates may have continued to react with Fe oxides. Additional time-dependency of I-127 removal is in the next section. Repeated washing with a fresh Na-dithionite and K_2CO_3 every few days also increased I-127 removal from the sediment 15% compared to the same solution and contact time with no solution replacement (last set of four bar graphs, Figure 6.1a). It should be noted that this is a similar effect to injection of the solution into sediment (i.e., over time, fresh Na-dithionite solution contacts the sediment. Therefore, the recommended treatment is Na-dithionite with K_2CO_3 leaving the solution in situ. Since the ultimate products of Na-dithionite injection are Na^+, SO_4^{2-}, K_+, and CO_3^{2-}, previous field scale injections have had regulatory approval to leave the spent solution in place. Experiments varying the Na-dithionite and K_2CO_3 solution concentration showed that while higher concentrations removed greater I-127 from the sediment, there was a decrease in efficiency at a Na-dithionite concentration > 0.03 mol/L (Figure 6.1b). With a 3x increase in concentration from 0.01 to 0.03 mol/L Na-dithionite, I-127 extracted increased from 0.18 to 0.343 ug/g (90% increase), but the 3x increase from 0.03 to 0.1 mol/L resulted in I-127 increase to 0.455 ug/g (33% increase).

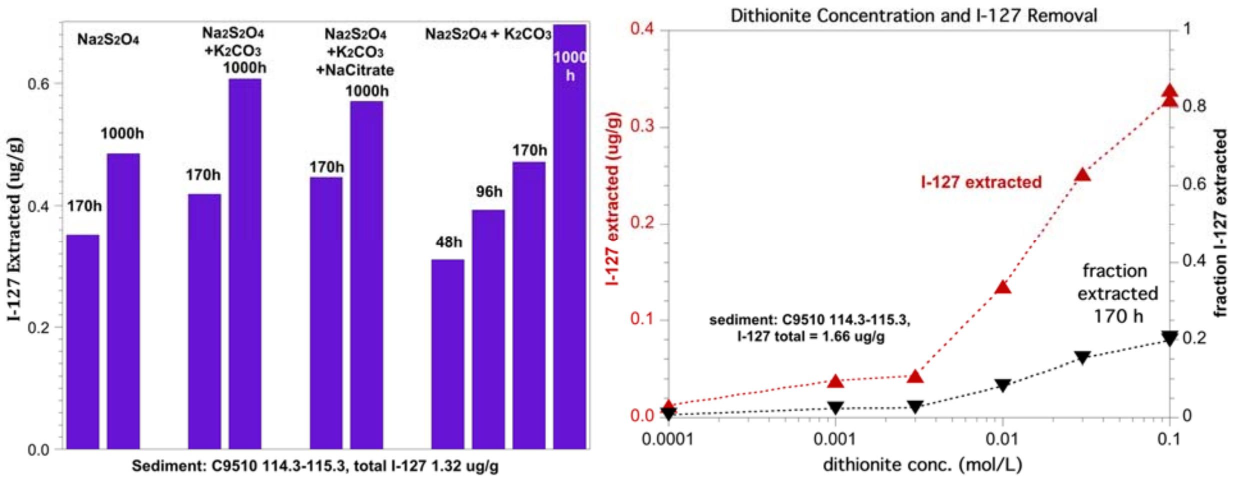

Figure 6.2. Iodine removal from a field-contaminated sediment using a) Na-dithionite solutions of differing composition, and b) differing Na-dithionite concentrations.

A total of 21 different iodine-contaminated vadose zone and groundwater sediments from Hanford 200 area were used in Na-dithionite treatments, as described in the following sections. The I-127 removed by Na-dithionite/K_2CO_3 solution (purple diamonds, Figure 6.2) varied considerably, as the total I-127 in different sediments varied. For sediments that had complete sequential extraction I-127 analysis (9 of 21 sediment), the Na-dithionite treatment of different iodine-contaminated Hanford vadose zone and groundwater sediments removed 61.9 ± 21.2% of the iodine from the sediment, in contrast to the aqueous plus adsorbed fraction of 11.7 ± 14.3% of the iodine in the sediment. The total I-127 in sediments was measured by sequential liquid extractions, although in earlier studies, the most acidic extraction solutions were not measured by ICP-MS (so the total I-127 is inaccurately reported). Total I-127 values reported in Figure 6.2 are accurate, as they account for the total I-127 removed from the sediment by extractions, leaching, and dithionite treatment. Dithionite removed 30 to 80% of the I-127 from the sediment. As shown in a later section, dithionite treatment and leaching removed 22 to 38 times more I-127 compared with untreated leaching, leaving an I-127-depleted sediment.

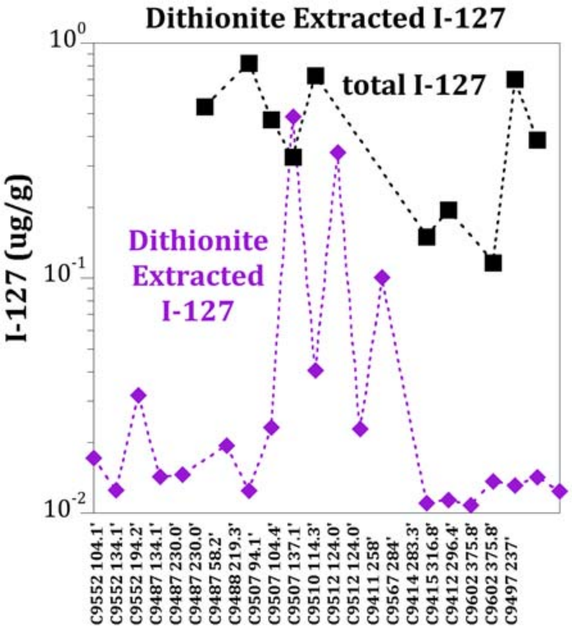

Figure 6.3. Iodine removal from a field-contaminated sediments with Na-dithionite/K_2CO_3 in 170 h.

6.2.2 Contact Time and Iodine Removal with Na-Dithionite

Using a solution of 0.1mol/L Na-dithionite and 0.4 mol/L K_2CO_3 in three different sediments that were iodine-contaminated, the rate of iodine removal was evaluated. Over the first 140 hours, the rate of iodine removal in these three different sediments showed a log-linear relationship (Figure 6.3a). After 144 hours, the Na-dithionite/K_2CO_3 solution was removed to evaluate any additional release of iodine in the sediment. These experiments showed that over the next 1000 hours, there was a slight increase in aqueous iodine (Figure 6.3b), although at a slower rate than in the Na-dithionite/K_2CO_3 solution. This indicates that although the Na-dithionite itself is no longer redox reactive, ferrous iron surface phases (i.e., adsorbed ferrous iron, FeS and $FeCO_3$ precipitates) may be continuing to dissolve Fe oxides, releasing iodine into aqueous solution.

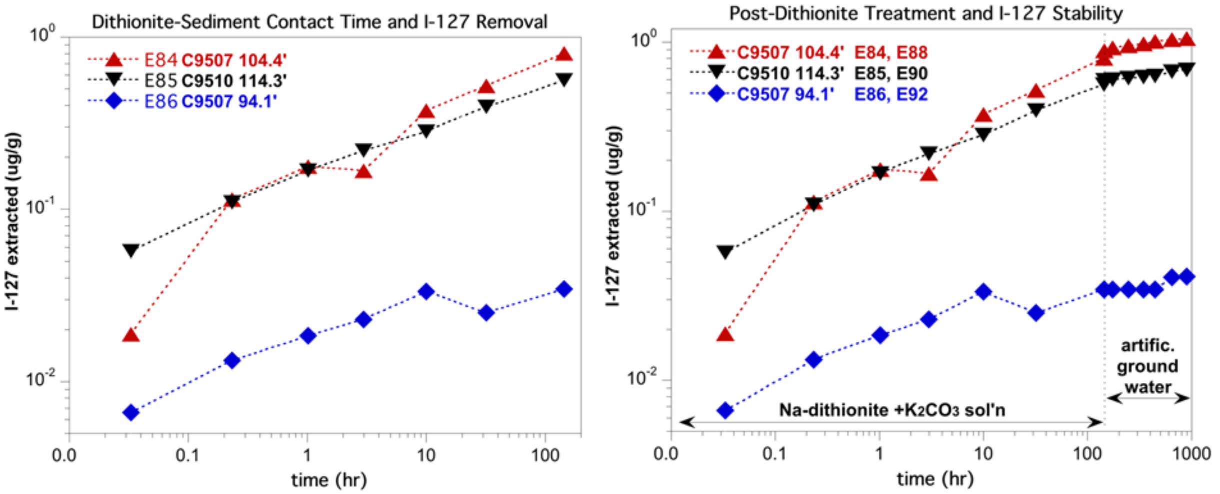

Figure 6.4. Time-dependent release of iodine from sediments with: a) Na-dithionte/K_2CO_3 solution, b) Na-dithionte/K_2CO_3 solution followed by AGW at 144 hours.

Comparison of the iodine release from untreated sediments to dithionite-treated sediments (after dithionite and released iodine has been replaced with AGW) shows that sediments treated with the Na-dithionite/K_2CO_3 solution released iodine at a more rapid rate (Figure 6.5). Again, this result indicates the dithionite treatment produced surface phases that are continuing to dissolve Fe oxides.

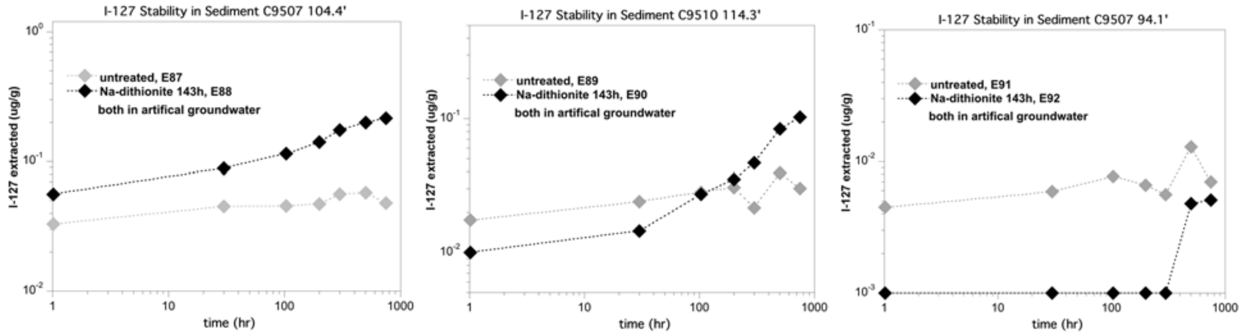

Figure 6.5. Rate of iodine-127 release from three sediments without and with Na-dithionite/K_2CO_3 treatment.

6.2.3 Effect of 1-D Flow in Sediment Columns on Iodine Removal

In order to evaluate the efficiency of Na-dithionite treatment as the solution flows through sediment at field scale (rather than batch experiments shown in the previous section), 1-D sediment columns were used in which a solution of 0.1mol/L Na-dithionite and 0.4 mol/L K_2CO_3 was injected for 170 hours, then AGW was injected into the sediment column for the next 570 hours. Three sediments were used (C9507 104.4', C9510 114.3', C9517 94.1'), which were also dithionite-treated in batch systems (shown in the previous section). Untreated I-127 leach concentrations and cumulative mass are shown on a linear scale (Figure 6.1), and compared to I-127 leach concentrations and cumulative mass for the dithionite-treated sediment (Figure 6.6). Similar behavior was observed in the three sediments included (a) I-127 aqueous concentrations were 1 to 2 orders of magnitude higher with dithionite treatment, (b) I-127 aqueous concentrations decreased 2 to 3 orders of magnitude for untreated and decreased 1 order of magnitude for dithionite treated sediment, (c) the I-127 aqueous concentration for dithionite-treated sediments stayed higher than the untreated sediment for 120-150 pore volumes, and (d) leached mass for dithionite treated sediment was 1 to 2 orders of magnitude higher than untreated sediment.

The higher I-127 leach concentrations for dithionite treatment was expected, as aqueous/adsorbed iodate was reduced and some Fe-oxides were dissolved (see Section 6.2.4.1 for details) releasing some solid phase iodate into solution, which was then reduced. Because the Na-dithionite/K_2CO_3 solution is only redox reactive for a few days (27 h dithionite dissociation half-life), dissolution of ferric oxides presumable occurs only the same time period, releasing I-127 into aqueous solution. Because of that, it was expected that during flow in these 1-D columns, once AGW was injected into the sediment columns (after 5 pore volumes), it was expected that the aqueous I-127 concentrations for the dithionite treated sediments would decrease to below concentrations in the untreated sediments. This was not the case, as aqueous I-127 concentrations in all three sediments stayed 1 to 2 orders of magnitude greater in the dithionite treated sediments compared to untreated sediments even after 150 pore volumes of injected AGW. There are multiple ferrous phases created including adsorbed Fe^{II}, FeS, and $Fe^{II}CO_3$ (described in Section 6.2.4.1), so the reduced sediment could continue to reduce any aqueous or adsorbed iodate, but would not be dissolving additional ferric oxides. The continued elevated I-127 aqueous concentrations in the dithionite-treated sediment, even after the pH has decreased to near groundwater concentration (Figure 6.7) appears to indicate that there is a continued slow reduction of iodate in the reduced sediment. It is likely that adsorbed iodate (which has a retardation factor < 6) would be quickly reduced to iodide and with less sorption remain mainly aqueous, so the mechanism slowly releasing I-127 (iodide) to aqueous solution from the sediment is not well understood.

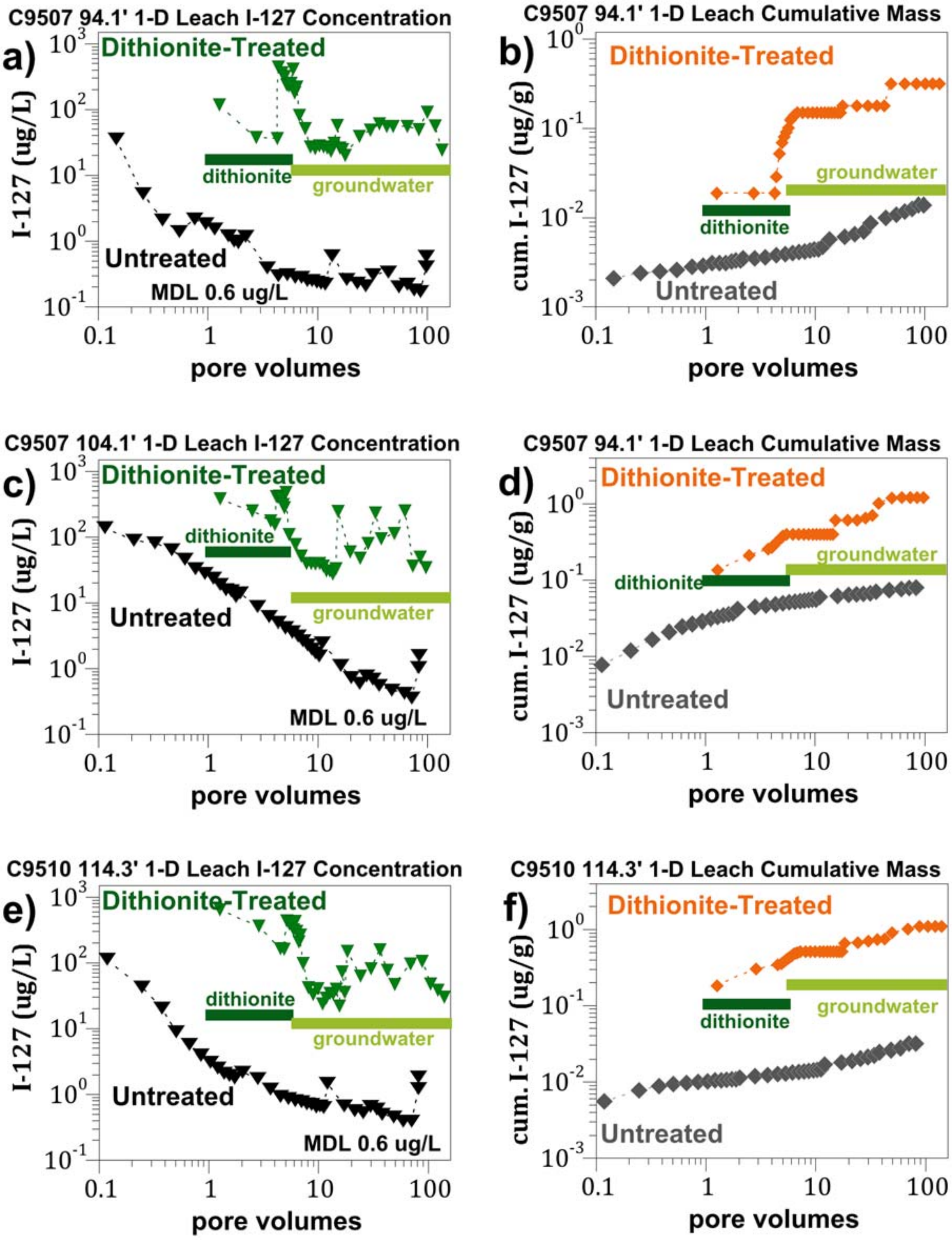

Figure 6.6. Comparison of 1-D leaching behavior for untreated and dithionite-treatment of sediment from: a) C9507 94.1', b) C9507 104.1', and c) C9510 114.3'.

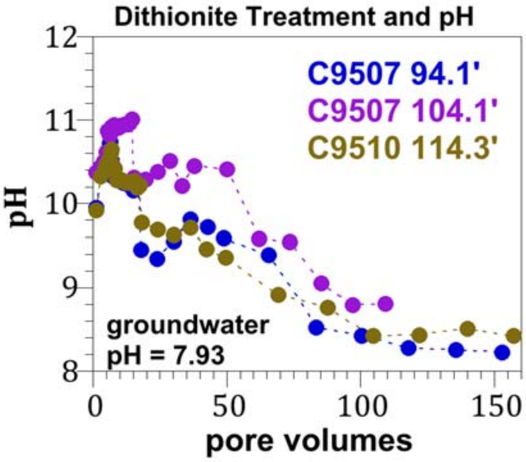

Figure 6.7. Change in pH during leach of dithionite-treated sediments.

For remediation application to enhance iodine recovery during pump and treat, dithionite treatment of sediment has clearly shown that much greater iodine can be removed from the sediment more quickly compared to leaching of just untreated sediment. However, it was expected that after Fe-oxides were dissolved and iodide advected from the sediments, I-127 concentrations in the dithionite-treated sediments would eventually be lower than untreated sediments. Unfortunately, leaching experiments have shown continued elevated iodine concentrations 100 to 150 pore volumes after dithionite treatment (compared to untreated sediments). This observation needs to be investigated further as it may limit dithionite treatment use at field scale. It is possible that once the sediment is subsequently oxidized, the I-127 concentrations would decrease.

6.2.4 Effect of Dithionite Treatment on Sediment Surface Phases

Because the Na-dithionite/K_2CO_3 is well documented to dissolve amorphous and crystalline ferric oxides (Szecsody et al. 2004; Fruchter et al. 1998), sequential iron(II) and (III) extractions were conducted to quantify the extent of changes in the sediment, along with measurements of the aqueous iron (Heron et al. 1994). Inorganic carbon extractions were also conducted to evaluate any potential changes in calcite from the dithionite treatment. In addition, major and trace metals were also analyzed in dithionite-treated sediments to evaluate whether mobilized iodine was related to a different dissolving phase other than ferric oxides.

6.2.4.1 Iron Oxides

Comparing iron oxides before and after dithionite treatment, there was on average a 16% loss in Fe(III) phases, which corresponded to a gain in Fe(II) phases (last two columns in Table 6.1). The total Fe(II+III) remained constant (Figure 6.8a). The Na-dithionite/K_2CO_3 treatment was designed to dissolve Fe(III) oxides and create mainly immobile ferrous iron surface phases (i.e., adsorbed Fe(II), FeS, siderite), and the aqueous ferrous iron that remained in the spent high ionic strength treatment solution averaged 1.9 mg/L (0.065 µmol/g). There was no correlation between the aqueous ferrous iron and mobilized I-127 (Figure 6.8b) because while the mass of iodate in sediments varied two orders of magnitude, the mass of iron dissolved by the dithionite treatment was relatively constant between sediments. In contrast, for a synthetic Fe oxide precipitated from a solution also containing iodate, there should be a constant iodate/Fe ratio as the Fe oxide dissolves.

Table 6.1. Iron characterization of sediments before and after Na-dithionite treatment.

Sediment	Treatment	$Fe^{II}CO_3$, FeS (mg/g)	Other Fe^{II} (mg/g)	Am. + Crys. Fe^{III} (mg/g)	Other Fe^{III} (mg/g)	Total Fe^{III} (mg/g)	Fe^{III} Loss (%)	FeS Gain (mg/g)
C9487 58.2 - 59.2’	None	0.859	1.74	2.15	9.04	13.78		
	Dithionite/CO_3	1.873	1.64	1.57	7.00	12.09	23.3	1.014
C9507 94.1-95.1'	None	0.337	0.652	1.42	9.95	12.36		
	Dithionite/CO_3	1.208	0.993	0.83	9.45	12.48	9.6	0.871
C9507 104.4-105.4'	None	0.000	3.49	0.00	7.32	10.80		
	Dithionite/CO_3	0.000	2.88	0.00	5.42	8.30	25.9	0.000
C9507 137.1-138.1'	None	2.80	3.70	2.89	10.09	19.46		
	Dithionite/CO_3	3.05	2.49	1.630	9.61	16.78	13.4	0.249
C9510 114.3-115.3'	None	0.062	3.06	0.124	11.64	14.89		
	Dithionite/CO_3	0.891	2.23	0.000	8.34	11.46	29.1	0.829
C9510 114.3-115.3' (dup)	None	0.005	2.56	0.000	10.56	13.12		
	Dithionite/CO_3	0.878	1.89	0.000	9.06	11.83	14.2	0.873
C9414 283.3-284.5	None	0.237	1.72	0.746	9.81	12.51		
	Dithionite/CO_3	1.438	1.12	0.287	9.22	12.06	9.9	1.201
C9415 316.8-327.8	None	0.268	1.60	0.961	7.76	10.58		
	Dithionite/CO_3	1.398	1.18	0.262	6.99	9.83	16.8	1.130
C9412 296.4-297.4	None	0.179	2.17	1.12	9.67	13.14		
	Dithionite/CO_3	1.719	1.98	0.348	10.85	14.89	-3.8	1.540
C9602 375.8-376.5	None	0.204	0.429	0.569	6.60	7.80		
	Dithionite/CO_3	0.630	0.406	0.265	5.36	6.66	21.6	0.426

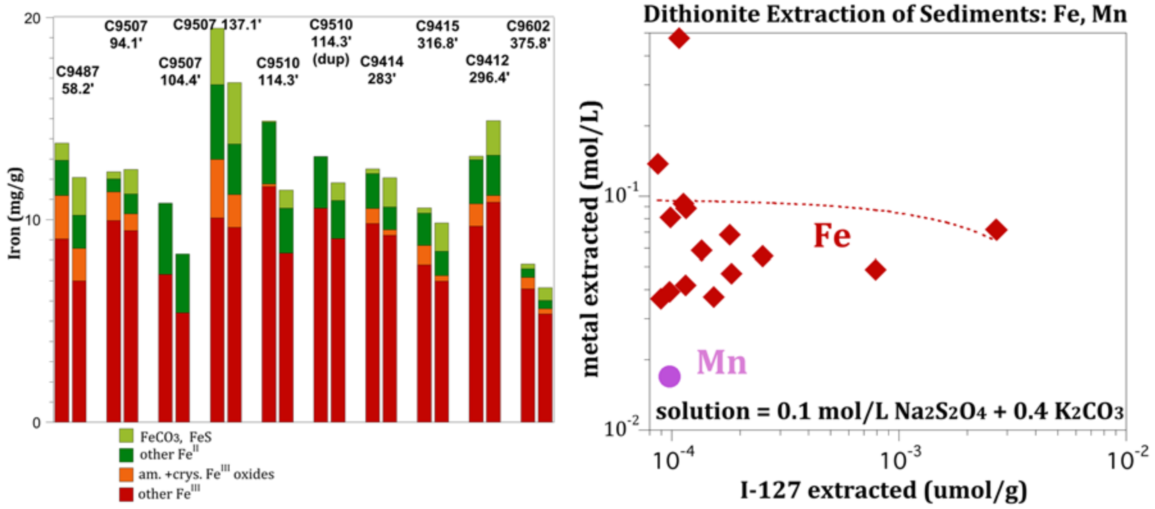

Figure 6.8. Iron oxide characterization of sediments pre- and post- dithionite treatment.

6.2.4.2 Calcite Dissolution and Carbonate Precipitation

The inorganic carbon in sediments was also measured in selected untreated and dithionite-treated samples to evaluate whether calcite is being dissolved. Unfortunately, the Na-dithionite/K_2CO_3 treatment process results in the formation of multiple ferrous iron phases including siderite ($FeCO_3$) along with adsorbed Fe(II) and FeS, utilizing ferrous iron from ferric oxide dissolution and aqueous carbonate. The dithionite-treated sediments on average contained 98% greater solid phase carbonate compared with the same untreated sediment (Table 6.2). Because only two of seven sediments showed a small (3.3% and 3.8%) decrease in total inorganic carbonate and the remainder increases in carbonate precipitates, it is likely that the dithionite treatment does not dissolve calcite.

Table 6.2. Inorganic carbon (IC) analysis on untreated and dithionite-treated sediments.

#	Sediment	Untreated (%IC)	Dith. Treat (%IC)	Increase (%)
E62.6	C9487 58.2 - 59.2’	0.105	0.180	71.9
E62.6 dup	C9487 58.2 - 59.2’	0.113	0.136	20.7
E62.8	C9507 94.1-95.1'	0.284	0.351	23.7
E62.9	C9507 104.4-105.4'	3.034	2.933	-3.3
E62.10	C9507 137.1-138.1'	0.010	0.054	464.6
E62.11	C9510 114.3-115.3'	1.384	1.331	-3.8
E62.21 dup 11	C9510 114.3-115.3'	1.29	1.383	7.4
E62.16	C9414 283.3-284.5'	0.018	0.059	226.2
E62.17	C9415 316.8-327.8'	0.016	0.040	141.8
E62.19	C9412 296.4-297.4'	0.178	0.278	56.2
E62.20	C9602 375.8-376.5'	0.016	0.028	79.0
E62.20 dup	C9602 375.8-376.5'	0.016	0.031	94.4
MCL		0.005	0.005	

Another approach to evaluate whether calcite in the untreated sediment was dissolving is to compare the untreated inorganic carbon (Table 6.2) against the aqueous Ca and Mg in dithionite treated aqueous solution. With the inorganic carbon varying by over two orders of magnitude in different sediments, there was a relatively uniform aqueous concentration of Ca and Mg (Figure 6.9), indicating calcite is likely not being dissolved by the Na-dithionite treatment.

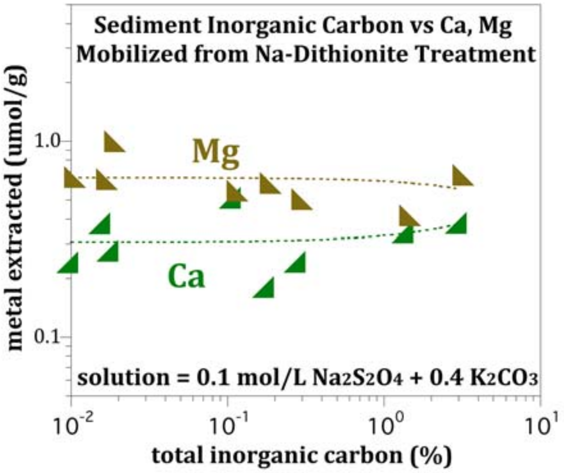

Figure 6.9. Total inorganic carbon in untreated sediments and Ca, Mg mobilized from Na-dithionite treatment.

6.2.4.3 Dissolution of Other Minerals: Metals Mobilization

A number of major and trace metals were analyzed in dithionite-treated sediments to evaluate whether mobilized iodine was related to a different dissolving phase other than ferric oxides. Metals analyzed included Al, Ba, Ca, Fe, Mg, Mn, Mo, K, Si, Na, Sr, Ti, Zr, Bi, Cr, Co, Cu, Ag, P, and Zn. Aqueous concentrations of Mn, Bi, Cr, Co, Cu, and Zn were all below detection limits. The aqueous concentrations of I-127 and 10 metals mobilized in 21 different sediments by dithionite treatment showed no correlation of I-127 mobilized with any other mobilized metal (Figure 6.5). The 0.1 mol/L Na-dithionite and 0.4 mol/L K_2CO_3 solution contained high Al (19.0 mg/L) and P (8.5 mg/L), but low concentrations of I

(< 1.26 ug/L), Ca (< 3.36 mg/L), Mg (< 0.27 mg/L), Fe (< 1.0 mg/L), Mn (< 0.24 mg/L), and Si (< 5.48 mg/L).

The aqueous Si concentrations averaged 9.1 ± 4.1 mg/L (Figure 6.10), so somewhat less than the 15 mg/L in the AGW used, indicating silica was not being dissolved (and may be precipitating). The Al aqueous concentrations averaged 5.0 ± 0.92 mg/L, which was less than the 19 mg/L in the dithionite solution, also suggesting some precipitation. The aqueous P concentrations of 4.1 to 6.3 mg/L was also less than the 8.5 mg/L in the dithionite solution, indicating phosphate precipitation. Both Na (at 0.2 mol/L) and K (at 0.8 mol/L) were present at high concentrations in the Na-dithionite/K_2CO_3 treatment solution. Aqueous concentrations of Mg averaged 9.4 mg/L and Ca averaged 7.4 mg/L, likely from a combination of desorption from ion exchange sites and dissolution of minerals. Sorbed cations on ion exchange sites (2 meq/100g or 20 µmol/g) could account for some of the ion concentrations observed, but should be of similar proportion of the AGW (i.e., 70% Ca, 20% Mg, 8% Na, 2% K). Calcite dissolution was unlikely dissolving and producing the aqueous Ca and Mg as calcite contains 95% Ca and < 5% Mg. The sediment with the highest calcite (Table 6.2, C9507 104', 3.03% inorganic carbon) also did not have any greater aqueous Ca and Mg. A common mineral present in basalt (forsterite, $MgSiO_4$) may be dissolving in the dithionite solution. The lack of a correlation between the mass of I-127 in sediments and any mobilized metal (Figure 6.10) could indicate that there are no other phases (other than Fe oxides and possibly calcite) that are dissolving and contain iodine.

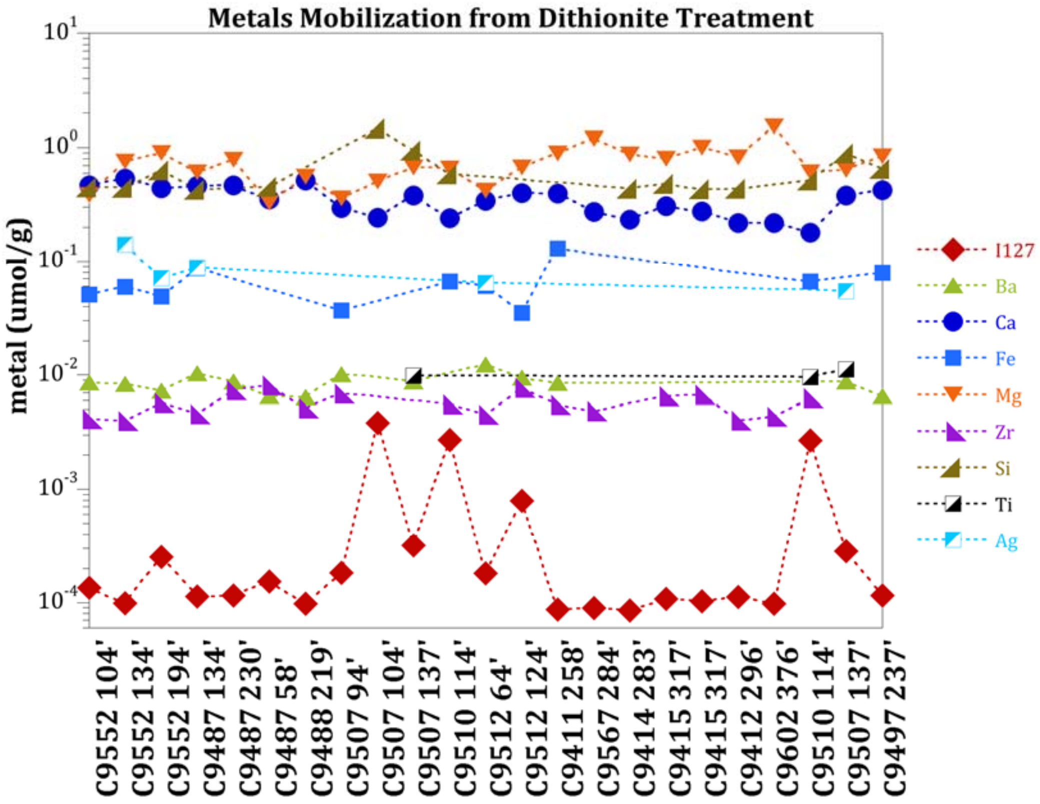

Figure 6.10. I-127 and other metals mobilized by Na-dithionite treatment.

In order to prove that the iodate/iodide from reaction of the dithionite solution with sediments were from sediments and could be analyzed in the high ionic strength solution, a series of dithionite solutions were prepared and analyzed for iodine. The reduced and oxidized Na-dithionite/K_2CO_3 solution analyzed for I-127 showed that there were no iodine impurities in the dithionite or carbonate chemicals (Table 6.3). In addition, when I-127 was added to the high ionic strength Na-dithionite/K_2CO_3 solution, I-127 was accurately measured, so the dithionite (S_2O_4 mass of 128 g/mol) did not interfere with the I-127 mass analysis by ICP-MS. Therefore, I-127 reported in dithionite solution reaction with sediments was from the sediment.

Table 6.3. Dithionite solutions analyzed for I-127.

Solution	Added Iodate (µg/L)	Added Iodide (µg/L)	Measured I-127 (µg/L)
0.06M $Na_2S_2O_4$ + 0.24M K_2CO_3	0.0	0.0	< 1.26
0.06M $Na_2S_2O_4$ + 0.24M K_2CO_3	0.0	0.0	< 1.26
(oxidized)			
0.06M $Na_2S_2O_4$ + 0.24M K_2CO_3	150.0	0.0	135.0
0.06M $Na_2S_2O_4$ + 0.24M K_2CO_3	0.0	150.0	145.0

6.3 Discussion

6.3.1 Mass of Iodine Removal by Na-Dithionite

The Na-dithionite/K_2CO_3 solution mobilized considerable I-127 from 200 Area Hanford subsurface sediments (Table 6.4, Figure 6.11). Batch (i.e., no flow) experiments showed that 170 h of solution treatment (light blue triangles, Figure 6.11) removed an average of 28.7% ± 20.4% of the total I-127 (black squares) associated with the sediment. Additional dithionite-sediment contact time (i.e., 300 h, 1000 h) removed a greater amount of iodine from the sediment (darker blue triangles, Figure 6.11). In 1-D columns where the dithionite solution was injected (170 h) then AGW (575 hours), 61.9% ± 21.2% of the total I-127 was removed from the sediment. The total iodine in the sediment was difficult to measure, as sequential liquid extractions had to be pH neutralized and diluted before I-127 analysis (black squares, Figure 6.11). Early sequential liquid extractions had incomplete I-127 analysis because the most acidic extractions could not be analyzed by ICP-MS (red squares).

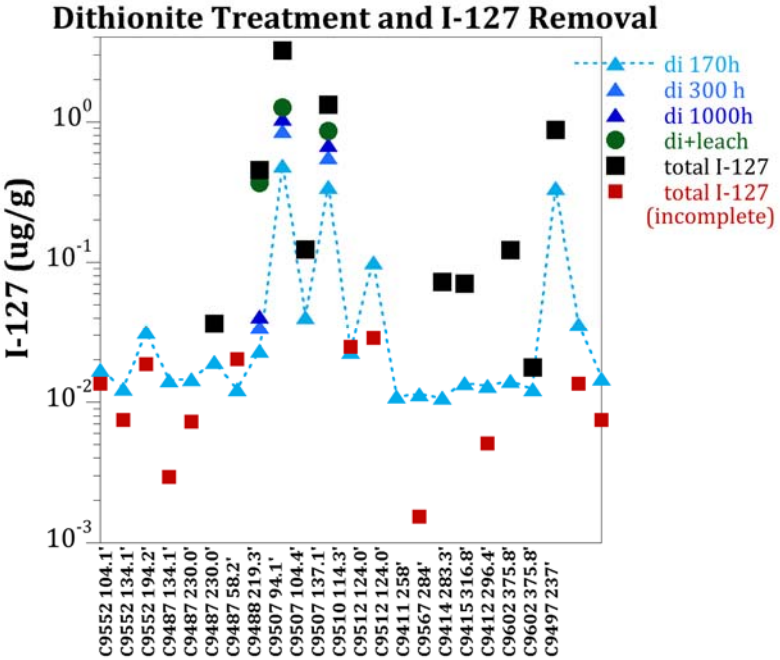

Figure 6.11. Na-dithionite/K_2CO_3 mobilization of I-127 from contaminated field sediments.

Table 6.4. Iodine-127 associated with sediments, characterized by sequential liquid extractions, dithionite treatment, and carbonate treatment.

Sediment Borehole Depth	Untreated Partial Seq. Extr. I-127[1] (ug/g)	Untreated 1000h Co3 I-127[2] (ug/g)	Untreated 100 Pv leach I-127 (ug/g)	Dithionite Treat 170h extr. I-127 (ug/g)	Post Dith. Seq. Extr. I-127[5] (ug/g)	Dithionite Treat 300h extr. I-127 (ug/g)	Dithionite Treat 1000h extr. I-127 (ug/g)	Dithionite 1-D Treat I-127[3] (ug/g)	Post Dith. 1-D Leach extr. I-127[4] (ug/g)	Total I-127[4] (ug/g)
C9552 104.2-105.2’	1.36E-02	4.69E-03	0.00762	1.71E-02						
C9552 134.1-135.1’	7.44E-03	2.63E-03	0.00747	1.25E-02						
C9552 194.2-195.2’	1.87E-02	1.73E-02	0.00817	3.18E-02						
C9487 134.1-135.1’	2.94E-03	3.07E-03	0.00673	1.43E-02						
C9487 230.0-231.0’	7.25E-03	4.04E-03	0.00788	1.46E-02						
C9487 58.2 - 59.2’	5.25E-02	2.81E-03	0.0112	1.94E-02	1.69E-02					3.63E-02
C9488 219.3–220.3’	2.03E-02	4.83E-03	0.00699	1.24E-02						
C9507 94.1-95.1'	2.19E-01	2.30E-02	0.0138	2.32E-02		3.45E-02	4.11E-02	3.67E-01	8.63E-02	4.53E-01
C9507 104.4-105.4'	8.91E-01	1.07E-01	0.0793	4.86E-01		8.61E-01	1.05E+00	1.26E+00	1.97E+00	3.23E+00
C9507 137.1-138.1'	9.72E-02	2.12E-02		4.06E-02	8.36E-02					1.24E-01
C9510 114.3-115.3'	7.34E-01	6.84E-02	0.0317	3.43E-01		5.61E-01	6.87E-01	8.63E-01	4.56E-01	1.32E+00
C9512 64.2-65.2'	2.47E-02	6.07E-03		2.29E-02						
C9512 124-125'	2.86E-02	1.09E-02		1.00E-01						
C9411 258-259'	1.54E-03		0.00587	1.10E-02						
C9567 284-285'	2.45E-03		0.00847	1.14E-02						
C9414 283.3-284.5'	6.36E-03		0.01171	1.08E-02	6.17E-02					7.25E-02
C9415 316.8-327.8'	2.48E-03		0.0253	1.37E-02	5.69E-02					7.06E-02
C9415 316.8-327.8'	2.48E-03			1.31E-02						
C9412 296.4-297.4'	5.08E-03		0.01713	1.42E-02	1.08E-01					1.22E-01
C9602 375.8-376.5'	6.41E-03		0.01311	1.24E-02	5.30E-03					1.77E-02
C9510 114.3-115.3'	7.34E-01	6.84E-02	0.0317	3.39E-01	5.40E-01					8.79E-01
C9507 137.1-138.1'	9.72E-02	2.12E-02	0.0253	3.61E-02						
C9497 237-238'				1.47E-02						

1 Sequential extractions 1-6, but not all extractions were analyzed (i.e., represents partial I-127)
2 pH 9.3 0.1 M Na-CO3 extraction for 1000 h
3 Leached 100 pore volumes after 300 h of dithionite extraction of I-127
4 Total I-127 is dithionite extracted + sequential extraction (after dithionite) + leached (in some cases)
5 Sequential extractions 1-6, pH neutralized before analysis so all six analyzed (i.e., represents total I-127)

6.3.2 Iodine Mass Balance in Sediments Pre- and Post-Dithionite Treatment

Sequential liquid extractions that were conducted after 170 h dithionite treatment provided a measure of the total I-127 remaining in the sediment (Figure 6.12). These extractions showed that the fraction of I-127 removed by the dithionite treatment varied from 20% to 75% (Figure 6.12b). Sequential extractions conducted on sediments prior to dithionite treatment did not provide a complete measurement of the I-127 in sediments, as acetate and oxalic acid extractions were not analyzed in all cases, and the nitric acid extraction was not analyzed (Figure 6.13, Table 6.4). These extractions are, however, useful for identification of the first three mobile phases in the sediments. For the three sediments that were dithionite treated in 1-D columns for 743 h (which removed significant I-127 from the sediment), a comparison of pre- and post-treatment sequential extractions does show that the oxalic acid extraction (which dissolves Fe oxides) decreased significantly. Because the 8M nitric acid extraction was not analyzed for I-127 in pretreatment extractions, it is difficult to evaluate the full mass balance.

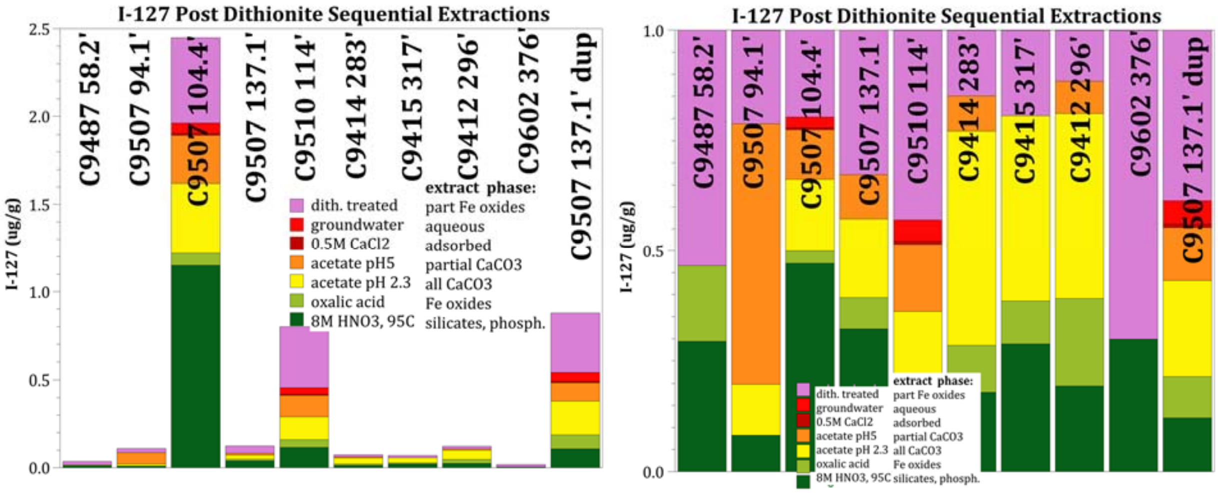

Figure 6.12. I-127 in field-contaminated sediments removed by dithionite/K_2CO_3 treatment then sequential liquid extractions, as shown by a) I-127 concentration (µg/g) and b) I-127 fraction of total.

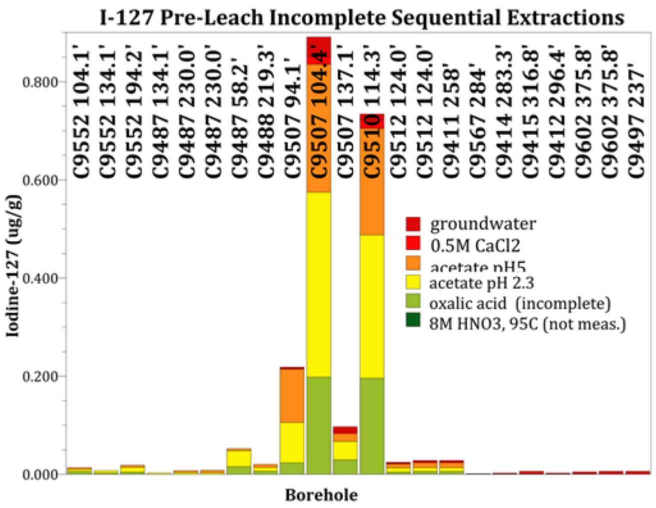

Figure 6.13. Untreated sediment sequential liquid extractions for I-127.

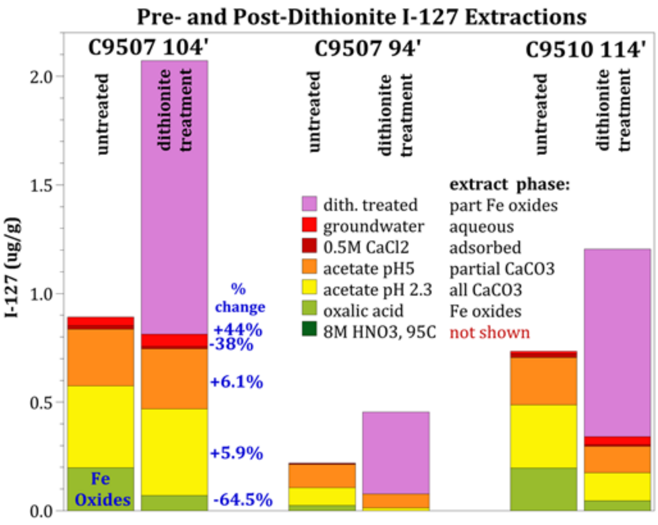

Figure 6.14. Comparison of pre- and post-dithionite treatment sequential liquid I-127 extractions.

Because most of the sequential liquid extractions are acidic, alkaline extractions were also conducted in an effort to evaluate the total iodine in the sediments. This pH 9.3 Na-carbonate extraction (1000 h), unfortunately, removed an average of 6.4% of the total I-127 in the sediment. This 1000-hour carbonate extraction has been previously used to exchange aqueous carbonate in calcite to extract some of the uranium, which substitutes into the calcite structure. For I-127, this may indicate the fraction in carbonates is small. In the sequential liquid extractions, the pH 5 Na-acetate extraction is also designed to dissolve a small fraction of carbonates. It should also be noted that multiple surface phases likely dissolve in the different extraction solutions, and amorphous ferrihydrite may partially dissolve in the pH 5 solution. Untreated sediment extractions indicate this pH 5 Na-acetate extraction removed 27.5% of the I-127 in the sediment and post-dithionite treated extractions indicate that this pH 5 Na-acetate extraction removed 16.8% of the I-127 from the sediment. Because the dithionite treatment dissolves (by reductive dissolution) about a third of Fe oxides (a higher fraction of amorphous and less crystalline; Section 6.3.4.1), it is hypothesized that most Fe-oxides that contained I-127 were dissolved by the dithionite treatment and the pH 5 Na-acetate post dithionite treatment represents a portion of I-127 in calcite (i.e., 17%).

Another measure of “labile” iodine is the mass of iodine released after 100 pore volumes of groundwater leaching (although this is somewhat arbitrary). For uranium, this leached mass roughly equal to sequential extractions 1 (aqueous) + extraction 2 (adsorbed) + half of extraction 3 and 4 (presumed carbonates). For iodine, this sum of sequential extractions removed 18.4% of the iodine from sediments, whereas the 100 pore volume leach removed an average of 20.3% of the total iodine.

6.3.3 Rate of Iodine Release from Sediments

Untreated release I-127 into aqueous solution and dithionite-treated sediments release a significantly greater mass, likely due to the partial dissolution of ferric oxides containing at least some of the I-127 associated with sediment solid phases. The rate of I-127 release from sediments (presumed from Fe-oxides and possibly other phases) was 1 to 3 orders of magnitude more rapid when the sediment was dithionite treated in contrast to untreated sediments (Table 6.5).

Table 6.5. Iodine release rates from sediments.

Sediment	Treatment	Exp. Type	Reaction Time (hr)	I-127 Released (μg/g)	$Fe^{II}CO_3$, FeS (mg/g)	I-127 Release Rate (μmol IO_3 h^{-1} $mol^{-1}Fe^{II}$)
C9487 58.2 - 59.2’	None	1D leach	750	1.12E-02	0.859	7.65E-03
	None	Batch	1000	8.11E-03	0.859	4.15E-03
	Dithionite	Batch	170	1.94E-02	1.873	2.69E-02
C9507 94.1-95.1'	None	Batch	1000	7.00E-03	0.337	9.13E-03
	Dithionite	Batch	170	2.32E-02	1.21	9.48E+01
	Dithionite	Batch	300	3.45E-02	1.21	4.02E+00
	Dithionite	Batch	1000	4.11E-02	1.21	4.36E-01
	None	1D leach	525	1.39E-02	1.21	9.61E-03
	Dithionite	1D leach	743	3.67E-01	1.21	8.28E+01
C9507 104.4-105.4'	None	Batch	1000	5.76E-02	1.32	1.92E-02
	Dithionite	Batch	170	4.86E-01	2.50	5.93E+02
	Dithionite	Batch	300	8.61E-01	2.50	6.44E+01
	Dithionite	Batch	1000	1.05E+00	2.50	6.03E+00
	None	1D leach	525	7.93E-02	2.50	2.66E-02
	Dithionite	1D leach	743	1.26E+00	2.50	4.32E+01
C9507 137.1-138.1'	None	Batch	1000	1.01E-02	2.68	1.66E-03
	Dithionite	Batch	170	4.06E-02	5.48	1.92E-02
C9510 114.3-115.3'	None	Batch	1000	3.02E-02	0.062	2.14E-01
	Dithionite	Batch	170	3.43E-01	0.891	1.11E+03
	Dithionite	Batch	300	5.61E-01	0.891	1.05E+02
	Dithionite	Batch	1000	6.87E-01	0.891	1.13E+01
	None	1D leach	525	3.17E-02	0.062	4.28E-01
	Dithionite	1D leach	743	8.63E-01	0.891	2.60E+01
C9414 283.3-284.5'	None	1D leach	750	1.17E-02	0.24	2.89E-02
	Dithionite	Batch	170	1.08E-02	1.44	1.94E-02
C9415 316.8-327.8'	None	1D leach	750	2.53E-02	0.268	5.54E-02
	Dithionite	Batch	170	1.37E-02	1.40	2.53E-02
C9412 296.4-297.4'	None	1D leach	750	1.71E-02	0.179	5.60E-02
	Dithionite	Batch	170	1.42E-02	1.72	2.14E-02
C9602 375.8-376.5'	None	1D leach	750	1.31E-02	0.204	3.77E-02
	Dithionite	Batch	170	1.24E-02	0.63	5.09E-02
C9510 114.3-115.3'	None	1D leach	750	1.33E-02	0.051	1.53E-01
	Dithionite	Batch	170	3.39E-01	0.878	9.99E-01

If the iodine release rate from the sediment was mainly controlled by Fe-oxides, then there should be a correlation between the concentration of ferrous iron phases (described in Section 6.2.4.1) and the I-127 release rate. However, while greater mass of FeS/$FeCO_3$ (one of several ferrous iron phases) resulted in greater I-127 release rates from the sediment, the correlation was poor, as the release rates in different dithionite-treated sediments varied up to 3 orders of magnitude with the same mass of ferrous iron (Figure 6.15a). This result implies ferrous phases are poorly characterized and/or are not controlling a significant portion of the iodine release from the sediment. While iron extractions have been used in other studies to characterize mass of ferrous and ferric phases, ferrous iron concentrations are low in these Hanford sediments.

There was a moderate correlation between the I-127 mass released from the sediment and the I-127 release rate (Figure 6.15b). Calculated release rates for three sediments that were extensively studied showed generally the highest release rate at 170 h experiments, with decreasing rates by 300 h, 1000 h, and in 750 h long 1-D column leaching. This indicates that the efficiency of I-127 removal decreases, possibly as amorphous Fe oxides are initially (and rapidly dissolved), followed by slower dissolution of more crystalline Fe oxides, both of which contain some iodine.

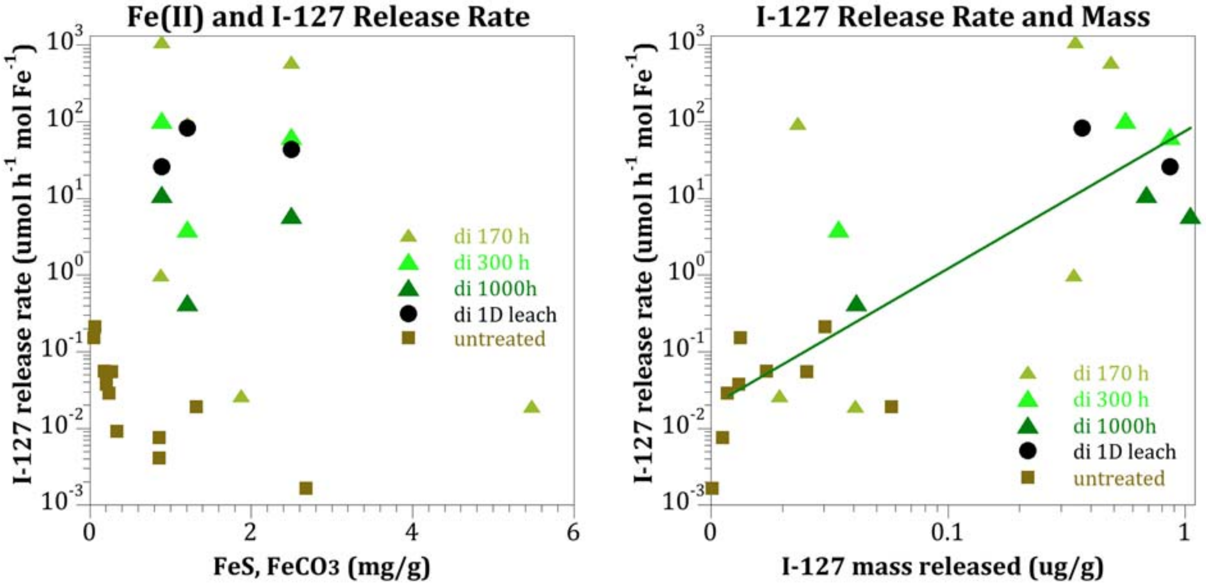

Figure 6.15. Iodine release rates in sediments as a function of a) FeS/$FeCO_3$ concentration, and b) iodine released mass.

7.0 Materials for Iodine Immobilization

Aboveground treatment of iodine, such as in the 200 West Area P&T system, is a potential groundwater remedial option for I-129 in the 200-UP-1 OU if materials with suitable properties can be identified. As a general target, based on the concentration range of I-129 in the 200-UP-1 OU, treatment to meet the required discharge standards would need to reduce I-129 from a maximum concentration of about 30 to 1 pCi/L (30-fold reduction). In addition, materials would need to achieve this reduction in the presence of I-127 concentrations that are typically about 1000 times higher than the I-129 concentration (Levitskaia et al. 2017). Thus, information about performance of treatment materials must consider this context for their deployment.

Potential engineered materials for specific uptake and sequestration of iodine for the range of expected iodine conditions have been evaluated. Materials were evaluated in terms of iodine uptake capacity, selectivity, affinity, and material stability. Material performance was compared with that for the materials currently in use at the 200W P&T system: (i) Purolite A530E ion exchange resin and (ii) Carbon Activated Corporation 011-55 granulated activated carbon. The following material categories were included in the evaluation: (i) iron oxide-influenced redox reactions and sorption, (ii) sulfide phases, (iii) reactions with bismuth-based materials, (iv) organoclays, (v) aerogels, and (vi) metal organic frameworks (MOFs). This effort represents an initial laboratory scoping evaluation of candidate materials to select those that show sufficient promise for continued evaluation.

7.1 Experimental Methods

Bench-scale tests were conducted to evaluate the efficacy of materials for treating targeted contaminants. Tests were conducted using methodologies reported in Mattigod et al. 2010a and 2010b such that direct comparisons could be made to performance characteristics of materials previously evaluated and/or already in use. Candidate materials that met threshold screening criteria were further evaluated in a column configuration as an initial step in evaluating field-scale deployment.

7.1.1 Synthetic Groundwater

A synthetic groundwater was prepared for use in the experimental work using the recipe (Truex et al. 2017) shown earlier in Table 2.2.

7.1.2 Materials

7.1.2.1 Ion Exchange Resin

Purolite A530E (Purolite Company, Bala Cynwyd, PA) ion exchange resin was cleaned to remove residual metals left over from the manufacturing process by centrifuge washing two times for 15 minutes with distilled deionized water at a solution-to-solid ratio of 3:1, followed by centrifugation at 1700 rpm for 5 minutes. The resin is shipped in the chloride form and the excess chloride was removed by soaking the resin in distilled deionized water for 24 hours. The resin was not centrifuged prior to decanting the water. The resin was rinsed once with distilled deionized, the water decanted and then the resin was stored wet in a sealed poly bottle at room temperature while the moisture content was determined. The resin moisture content was determined using EPA Method 1314. The moisture content of the resin was calculated by weighing, nominally 1 to 3 g of wet resin in an individually tarred aluminum weighing boat and then the resin was dried in an oven for 24 hours at 105±2°C. The dried resin was weighed and returned to the oven for 2 hours. This step was repeated until a constant weight was obtained. The dry weight of the resin was used as the basis to determine the solution-to-solid ratios, and to calculate the loading capacity. Thus, the dry weight of the resin used in the tests are reported along with the test results. Per the manufacturer's information, the total resin exchange capacity is 0.6 eq/L Cl^-.

7.1.2.2 Granulated Activated Carbon (GAC)

Carbon Activated Corporation (CAC) 011-55 (coconut shell) GAC was selected since it is currently used in the 200 West P&T Facility. The GAC was used "as-received," which is comparable to current P&T operations.

7.1.2.3 Iron Oxides

Iron oxides were selected to represent a range of redox conditions from completely oxidized Fe(III) in ferrihydrite ($Fe(III)_5O_8H$), to mixed Fe(II)/Fe(III) in magnetite ($Fe(II)Fe(III)_2O_4$), to completely reduced Fe(II) in ferrous hydroxide ($Fe(II)OH_2$).

Synthetic 2-line ferrihydrite was prepared by titrating 0.092M $FeCl_3$ solution with 2M NaOH to a neutral pH (7.0). The precipitate that rapidly formed was agitated in a shaker overnight followed by one last pH adjustment with 0.2M NaOH to the neutral pH. After three rinses with de-ionized water and centrifugations at 5000 g, ferrihydrite was resuspended in deionized Milli-Q water and suspension density was calculated by dissolving a volume of ferrihydrite into 4M HCl, reducing it with 10% hydroxylamine hydrochloride at pH 7, and analyzing Fe^{2+} using the ferrozine method (Stookey 1970)

The synthesis protocol for nano-magnetite has been reported in detail in Pearce et al. (2012). Briefly, Fe_3O_4 nanoparticles were synthesized under ambient conditions and in aqueous suspension by co-precipitating a stoichiometric mixture of $FeCl_2$ and $FeCl_3$ in 0.3 M HCl (pH < 1) with ammonium hydroxide (NH_4OH) solution in an anoxic glovebox. The precipitated nanoparticles were magnetically separated from the aqueous phase and washed twice with degassed and deionized milli-Q (>18 MΩ cm resistivity) water (DDW) to remove possible impurities, such as residual metal chlorides. After washing, the nanoparticles were resuspended in water prepared equivalently and stored inside the glovebox. The suspensions naturally equilibrated to a solution pH of ~8.5.

Micromagnetite particles were prepared following the method of Schwertmann and Cornell (2000). Oxidation of the $FeSO_4$ in an alkaline solution of KNO_3 at 90°C under a N_2 atmosphere yielded the magnetite particles, which were dried and stored under N_2 until analysis. Analysis following a new hybrid oxidi-colorimetric method by Amonette and Matyáš (in review) revealed that micromagnetite was close to stoichiometric (~92%), with a composition of 70.96±0.41 wt% Fe_{Total} and 21.84±0.23 wt% Fe(II).

To synthesize ferrous hydroxide, $FeCl_2$ $4H_2O$ (14.00g, >95%, Fisher Scientific) was dissolved in DDW (400 g) in an anoxic glovebox. NaOH (10M, 8.2 mL) was added to the solution with shaking and it was left overnight to precipitate. The precipitated $Fe(OH)_2$ was filtered and dried for 24 to 48 hours. Immediately prior to use, the dark oxidized surface layer was scraped off to reveal the white-green $Fe(OH)_2$, and the amount needed for testing was ground with a mortar and pestle.

7.1.2.4 Sulfide Phases

To synthesize iron sulfide (FeS) (1.0 g) in degassed, deionized water in an anoxic glovebox, a solution of Fe(II)Cl_2•$2H_2O$ (1.65 g, 10 mL) was added to a solution of Na_2S (0.888g, 30 mL) to form a black precipitate. The precipitate was centrifuged (3000 rpm x 10 min) and washed with degassed, deionized water.

Potassium tin sulfide ($K_{2x}Mg_xSn_{3-x}S_6$, $x = 0.5$-1) was prepared by solid-state synthesis. A mixture of Sn (8.9 mmol, 1055 mg), Mg (4.7 mmol, 113 mg), K_2S (4.6 mmol, 204 mg), and S (15.7 mmol, 512 mg) was sealed under vacuum (10^{-4} Torr) in a fused silica tube and heated (10°C/h) to 550°C for 48 h, followed by cooling to room temperature at 100°C/h. The yellow polycrystalline product obtained was washed several times with water, acetone, and ether (in that order) (2 g, ~ 85% yield based on Sn). EDS analysis gave the average formula "$K_{1.3}Mg_{0.95}Sn_{2.1}S_6$" (Fard et al. 2015).

In a general procedure for tin sulfide (SnS), a mixture of solid $SnCl_2$•$2H_2O$ (2.5 mmol) and $SnCl_4$•$5H_2O$ (2.5 mmol) was suspended in 10 mL de-ionized water and the pH was adjusted to 12 by addition of NaOH while stirring. In a separate beaker, Na_4S•$9H_2O$ (15 mmol) was slowly added to 10 mL de-ionized water , and pH was adjusted first to 8 by drop-wise addition of 0.5 M NaOH, and then 12 by drop-wise addition of 2 M NaOH. The resulting Na_2S solution was slowly added to the Sn suspension, and the pH is adjusted to 12. The solution was stirred for 3 days at room temperature, transferred to a Teflon-lined autoclave, and kept at 110°C ± 5°C for 72 hours to yield the aggregate. The obtained solid was gravity-filtered, washed with excess water until a neutral pH of the rinse water was obtained, and dried. The dried solid was ground into a fine powder using a mortar and pestle.

7.1.2.5 Bismuth-Based Materials

A typical synthesis for bismuth (oxy) hydroxide of the general structure $(BiO)_x(OH)(NO_3)_m(CO_3)_n$ involved suspending $Bi(NO_3)_3 \cdot 5H_2O$ and urea (2.7 mmol) in 50 mL ethylene glycol with stirring as described elsewhere (Qin et al. 2012). The mixture was subjected to solvothermal treatment at 150°C for five hours in the Teflon liner of an autoclave vessel. The reaction mixture was allowed to cool to room temperature, and the ethylene glycol supernatant was decanted. The solid reaction product was collected via centrifugation (3500 rpm for 10 minutes). The solid was re-suspended in ultrapure water (10 mL/0.1 g sorbent), vortexed for one minute, and collected by centrifugation. The washing procedure was repeated with ultrapure water for a total of five washes. The solid was then suspended in 100% methanol (10 mL/0.1 g sorbent), vortexed for one minute, and collected by centrifugation. The methanol wash step was repeated twice more, and the product allowed to dry at room temperature.

The modified synthetic protocol for preparation of bismuth-cobalt-aluminum hydrotalcites was adapted from hydrothermal syntheses reported elsewhere (Byrappa and Yoshimura 2001). In a general procedure, the nitrate or chloride salts of Bi^{3+}, Co^{2+}, and Al^{3+} were dissolved in ~50 mL deionized water at a 2.5:2.5:1 molar ratio. The solution was stirred for about an hour, followed by the addition of 0.5 M NaOH solution while stirring until a pH of 8 – 9 was achieved. The mixture was stirred at room temperature for 3 days, transferred to a Teflon-lined autoclave, and kept at 110°C ± 5°C for 72 hours to yield the aggregate. The obtained solid was gravity-filtered, washed with excess water until a neutral pH of the rinse water was achieved, and dried.

7.1.2.6 Organoclays

Two ORGANOCLAY® proprietary granular adsorption media samples were obtained from CETCO Mineral Technologies (Hoffman Estates, IL), CETCO MRM Organoclay and CETCO PM-200.

Organoclays are composed of sodium bentonite that has been chemically altered to increase its sorption capacity for certain types of contaminants. MRM is a sulfur-impregnated organophilic clay granular filtration media that adsorbs non-aqueous phase liquids (NAPL) and dissolved low-solubility organics. It also sequesters mercury and arsenic from water. MRM has been formulated for use in groundwater pump and treat filtration, as permeable reactive barrier (PRB) media, and as a solidification/stabilization additive to Portland cement. MRM contains a minimum of 25% quaternary amine loading. PM-199 is a granular adsorption media effective in removing oils, greases, other NAPL, and other dissolved high molecular weight/low solubility organics. PM-199 has been formulated for use in organophilic filtration media, bulk sediment capping, and as a solidification/stabilization additive. PM-199 contains 25% to 33% minimum quaternary amine loading.

7.1.2.7 Aerogels

Copper-functionalized silica aerogel was synthesized using a previously developed procedure (Matyáš et al. 2011). Briefly, granules of silica aerogel were hydrated in humidity-saturated air for two days. Following hydration, 3-(mercaptopropyl)trimethoxysilane [3-MPTMS; $HS(CH_2)_3Si(OCH_3)_3$, 95%] (Sigma Aldrich, St. Louis, MO) was distributed throughout the granules using a syringe at ~30 mL per 17 g of unhydrated sample. The wetted material was loaded into a 1 L high-pressure vessel, heated to 150°C, the vessel was filled with supercritical CO_2 at 24 MPa, and the sample cooked for 24 h. Following this process, the thiol-modified aerogel (~12.5 g) was altered by installing the Cu(II) ions through treatment with 360 mL of 10 % $CuSO_4 \cdot 5H_2O$ (99%, Sigma Aldrich) solution. About 60 mL of methanol was added to the solution to facilitate wetting of the moderately hydrophobic thiol-modified aerogel. The Cu^0 nanoparticles were produced on the silica aerogel pore surfaces by reducing the copper thiolate adduct ions at 165 °C for 2 h under a 25 mL min^{-1} stream of 2.7% H_2 in Ar in a glass column.

7.1.2.8 Metal Organic Frameworks (MOFs) and Cationic Polymeric Networks (CPNs)

MOFs and CPNs with demonstrated efficient and selective anion capture were obtained from external collaborators for testing; SCU-101, SCU-102 and SCU-CPN-1-Cl were obtained from Professor Shuao Wang, Soochow University, China; Fe-BTC/PDA was obtained from Professor Wendy Queen, École Polytechnique Fédérale de Lausanne (EPFL), Switzerland.

1. SCU-101 and SCU-102 are a hydrolytically stable and radiation-resistant cationic MOF. SCU-101 has the chemical formula $[Ni_2(tipm)_2(C_2O_4)](NO_3)_2 \cdot 2H_2O$ (tipm = tetrakis[4-(1-imidazolyl)phenyl]methane). These compounds exhibit fast removal kinetics, high sorption capacity, and unique molecular recognition derived sorption selectivity toward pertechnetate (TcO_4^-), and the anion exchange mechanism, shown in Figure 7.1a, is anticipated to be similar for IO_3^- (Zhu et al. 2017). The structure of SCU-102 is given in Figure 7.1b.
2. The synthesis of SCU-CPN-1-Cl is reported in Li et al. (2018). Briefly, SCU-CPN-1-Br, derived from the quaternization reaction between 1,1,2,2-tetrakis(4-(imidazolyl-4-yl) phenyl)ethene (TIPE) and 1,4-bis(bromomethyl)benzene (BBB), was soaked in saturated sodium chloride (NaCl) solution for 12 h to yield SCU-CPN-1-Cl. SCU-CPN-1-Cl demonstrates fast sorption kinetics and high sorption capacity for anions and the exchange mechanism, shown in Figure 7.1c for ReO_4^-, is anticipated to be similar for IO_3^- (Li et al. 2018).
3. Fe-BTC (BTC = 1,3,5-benzenetricaboxylate) was prepared by heating a solution of iron(III) chloride hexahydrate (9.72 g) and trimesic acid (3.36 g) in DDW (120 mL) in a Teflon autoclave at 130 °C for 72 hours (Sun et al. 2018). The resulting solid was washed and purified prior to polymerization with polydopamine (PDA), and the structure is shown in Figure 7.1d. Fe-BTC

exhibits rapid, selective removal of anions, such as Cr(VI)O_4^-, so it is anticipated to exhibit similar affinity for IO_3^- (Sun et al. 2018).

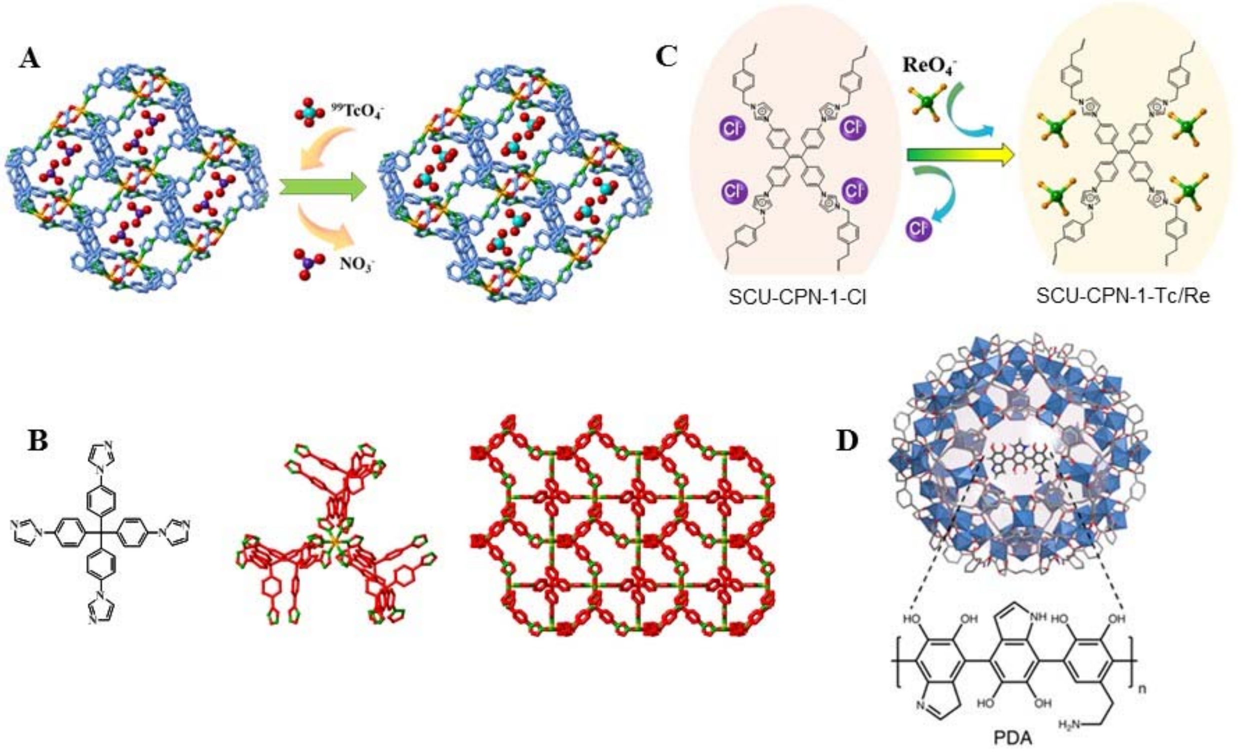

Figure 7.1. (A) Anion (TcO_4^-) exchange mechanism for SCU-101(atom color: Ni-orange; O-red; C-blue; N-green); (B) Structure of SCU-102 (atom color: Ni-orange; C-red; N-green); (C) Anion (ReO_4^-) exchange mechanism for SCU-CPN-1; (D) Polyhedral view of a large cage in the Fe-BTC with PDA embedded inside the channels

7.1.3 Batch Loading Tests

Solutions were prepared by adding the appropriate amount of sodium iodate (Fisher Scientific, Pittsburgh, PA) to simulated ground water to obtain 1.0 mg/L iodine. The pH of the starting solution containing iodate prior to addition of materials was 7.96.

Batch loading tests were conducted per Pacific Northwest National Laboratory (PNNL) Technical Procedure ESG-BSE-001, Rev 3, where a mass of material and the appropriate amount of iodate solution to achieve the target ratio were placed into a 125 mL bottle or 50 mL falcon tube. The size of the bottles and tubes were chosen in an attempt to minimize headspace issues and volatilization concerns. Process blanks included solution blanks (initial iodate solution with no material) and material blanks (material in simulated groundwater with no iodate). Process blanks were prepared and handled in the same manner as all other loading tests. The bottles were sealed and placed on a shaker table set at 125 rpm to ensure the materials and iodate solution remained well mixed for the required 24-hour period. All loading tests and process blanks were kept at room temperature. After the 24-hour contact time, the bottles were removed from the shaker table and the solid materials were allowed to settle for 15 minutes. A 0.45 µm syringe filter was then used to separate the aqueous matrix from the sorbent. A 10 mL aliquot was removed, approximately 5 mL was pushed through the filter to prime the filter, and the remaining solution was placed into a 20 mL liquid scintillation vial.

Total iodine was analyzed on two different ICP-MS instruments based on equipment availability. The first instrument was an X-Series II ICP Mass Spectrometer from ThermoFisher Scientific and the second instrument was an ELAN DRC II ICP Mass Spectrometer from PerkinElmer. The detection limit for total iodine is 0.0126 µg/L for both instruments. Two solution to solid ratios (200 and 1000) were used to span the range of predicted iodate uptake by the different materials. Actual material masses and solution volumes used in the batch tests were recorded and the tests were conducted in duplicate. After the 24-hour sampling, the tubes from each test were returned to the shaker and re-sampled to obtain the > 30-day iodine loading sample. On additional tube for each test was prepared at a solution to solid ratio of 200.

After the 24-hour batch loading test, the solid phase was extracted by centrifugation and analyzed by I K-edge X-ray absorption spectroscopy (XAS) on 20-BM-B at the Advanced Photon Source, Argonne National Laboratory to determine the species of iodine present on the solid phase. Additional solid phase characterization included XRD to confirm the structure of the starting materials and scanning electron microscopy after reaction to examine the interaction between the iodine and the material.

7.2 Results

7.2.1 Iodine Loading Results

The initial and final iodine concentrations, the amount of dry material, and solution volumes are shown in Table 7.1 for the tests conducted at a solution to solid ratio of 200 and Table 7.2 for the tests conducted as a solid to solution ratio of 1000.

Table 7.1. Iodate loading results for materials (solution to solid ratio = 200).

Material Tested	Iodine Initial Concentration (mg/L)	Iodine Final Concentration 0-1 day (mg/L)	Iodine Final Concentration >0-30 days (mg/L)	Mass of Material-Dry (g)	Soln. Vol. (mL)	Iodine Loading 0-1 day (mg/g)	Iodine Loading >0-30 days (mg/g)	Kd after 1 day (mL/g)	Iodine Species on Solid*	pH After Reaction
530E resin	1.01	0.73	0.74	0.10	20.00	0.06	0.05	78.24	I^-	7.58
CAC GAC	1.01	0.73	0.68	0.11	21.11	0.06	0.07	76.68	I^-/IO_3^-	8.12
Ferrihydrite	1.02	0.05	0.04	0.10	17.11	0.17	0.17	3230.89	I^-/IO_3^-	7.26
Nano-magnetite	1.01	0.79	0.75	0.10	19.72	0.04	0.05	54.60	I^-	7.83
Ferrous Hydroxide	1.01	0.93	0.79	0.10	19.80	0.02	0.04	16.34	-	8.00
Potassium Tin Sulfide	1.01	1.01	0.99	0.10	20.81	0.00	0.00	0.00	-	8.54
Iron Sulfide	1.01	1.01	0.98	0.10	20.31	0.00	0.01	0.00	-	7.52
Tin Sulfide	0.99	0.79	0.82	0.10	20.08	0.04	0.03	51.97	-	7.33
Bismuth (oxy)hydroxide	1.01	0.00	0.00	0.11	21.01	0.20	0.20	201903.90	IO_3^-	8.04
Bi-Co-Al	0.99	0.02	0.00	0.10	20.18	0.19	0.20	12800.47	IO_3^-	7.75
Organoclay (PM-199)	1.02	0.82	0.79	0.10	20.78	0.04	0.05	51.95	I^-	7.95
Organoclay (MRM)	1.02	0.78	0.47	0.11	21.57	0.05	0.11	61.85	I^-	5.55
Cu-Silica Aerogel	1.01	0.85		0.11	21.47	0.03		37.35	IO_3^-	6.64
SCU-101 (MOF)	1.02	0.82	0.72	0.11	21.10	0.04	0.06	49.16	I^-	7.71
SCU-102 (MOF)	1.02	0.76	0.73	0.10	20.86	0.05	0.06	67.37	I^-	7.90
SCU-CPN (MOF)	1.02	0.24	0.23	0.11	21.17	0.16	0.16	635.77	I^-/IO_3^-	7.27
FeBTC-PDA (MOF)	1.02	0.41	0.25	0.11	21.42	0.12	0.15	287.36	I^-/IO_3^-	5.65

[*] Iodine species on the solid after 24-hour batch sorption. Iodine speciation could not be determined for some materials as: (i) the amount of iodine was below the detection limit of I K-edge XAS; and (ii) tin caused interference in the absorption spectrum at the I K-edge energy (33.17 KeV)

Table 7.2. Iodate loading results for materials (solution to solid ratio = 1000).

Material Tested	Iodine Initial Concentration (mg/L)	Iodine Final Concentration 0-1 day (mg/L)	Iodine Final Concentration >0-30 days (mg/L)	Mass of Material-Dry (g)	Soln. Vol. (mL)	Iodine Loading 0-1 day (mg/g)	Iodine Loading >0-30 days (mg/g)	Kd after 1 day (mL/g)
530E resin	1.01	0.97	0.96	0.10	100.00	0.04	0.05	43.39
CAC GAC	1.01	0.81	0.78	0.12	105.80	0.21	0.23	254.66
Ferrihydrite	1.02	0.57	0.48	0.10	97.11	0.44	0.55	763.61
Nano-magnetite	1.01	0.82	0.80	0.10	99.72	0.19	0.21	232.56
Ferrous Hydroxide	1.01	1.00	0.98	0.10	99.50	0.01	0.03	11.96
Potassium Tin Sulfide	1.01	1.01	0.99	0.10	103.15	0.00	0.02	4.00
Iron Sulfide	1.01	1.00	1.00	0.10	100.18	0.01	0.01	12.05
Tin Sulfide	0.99	0.80	0.79	0.10	100.20	0.19	0.19	237.80
Bismuth (oxy)hydroxide	1.01	0.19	0.09	0.10	101.55	0.82	0.92	4204.12
Bi-Co-Al	0.99	0.45	0.37	0.10	101.05	0.54	0.62	1218.09
Organoclay (PM-199)	1.02	0.83	0.81	0.11	110.50	0.19	0.21	229.96
Organoclay (MRM)	1.02	0.83	0.28	0.11	111.10	0.19	0.74	225.96
Cu-Silica Aerogel	1.01	0.99	0.94	0.11	105.40	0.02	0.07	22.27
SCU-101 (MOF)	1.02	0.85	0.80	0.11	105.60	0.17	0.22	195.04
SCU-102 (MOF)	1.02	0.81	0.77	0.11	110.50	0.21	0.25	254.61
SCU-CPN (MOF)	1.02	0.66	0.65	0.11	105.30	0.36	0.37	554.88
FeBTC-PDA (MOF)	1.02	0.85	0.53	0.10	100.55	0.17	0.49	198.27

7.3 Discussion

7.3.1 Material Evaluation

7.3.1.1 Baseline P&T Materials (Purolite A530E Ion Exchange Resin and Carbon Activated Corporation GAC)

The baseline materials currently deployed at the 200 West Area P&T, Purolite A530E ion exchange resin and Carbon Activated Corporation GAC, had similar distribution coefficients of 78 and 77 mL/g, respectively for iodate at a solution to solid ratio of 200. The performance was lower for the A530E at the higher solution to solid ratio of 1000. The resin appears to have been at capacity for the solution to solid ratio of 200, consistent with results by Levitskaia et al. (2017), where spent resin from the P&T Facility showed an I-127 loading of 44 – 58 µg/g. The CAC-GAC material showed additional capacity in the solution to solid ratio of 1000, with a loading increase by over a factor of 3. The higher surface area of the CAC-GAC compared to the resin may have contributed to this increased capacity. While the CAC-GAC and the A520E materials have capacity to remove iodine from solution, batch experiments indicate that the removal efficiency is significantly below that required to reduce concentrations of I-129 from ~30 pCi/L to 1 pCi/L considering the total iodine concentration loading that will be present due to I-127 in the groundwater at about 1000 times the I-129 concentration (Levitskaia et al. 2017). Column tests with relevant influent concentrations are needed to verify removal efficiency. Removal rate appears to be rapid, with the 1-day iodine loading on the CAC-GAC and the A520E similar to that for >30 days sample loading.

Analysis of the solid phase after reaction by I K-edge XAS revealed that the iodine speciation was no longer iodate, as was present in the starting solution, but was iodide for A530E and predominantly iodide, with a slight shift in the absorption edge due to the presence of some iodate, for CAC-GAC. This suggests that iodine loading onto the solid was not solely due to sorption, but changes in the solution chemistry caused reduction of a small fraction of the iodate to iodide, and this was preferentially sorbed onto the A530E and CAC-GAC. This is in agreement with previous studies by Parker et al. (2014), in which sorption of iodine was affected by iodine speciation in the 200W groundwater. In this study, iodine loading on resins was increased by an order of magnitude when the iodine was converted to iodide.

7.3.1.2 Iron Oxides

The best performing iron oxide material was ferrihydrite ($Fe(III)_5O_8H$), with loading values of 166 and 436 µg/g and K_d values of 3231 and 764 mL/g, at solution to solid ratios of 200 and 1000, respectively. The K_d value of 3231 mL/g at a solution to solid ratio of 200 is lower than that obtained for the batch sorption with ferrihydrite at a solution to solid ratio of 500 in Section 5 (K_d = 7826 mL/g), but those experiments were conducted in DDW and did not have the competing effects of the other ions present in the synthetic groundwater used here. Because loading on ferrihydrite increased for the solution to solid ratio of 1000 compared to the solution to solid ratio of 200, it was not at capacity at the solution to solid ratio of 200, also demonstrated by the near complete removal of iodine from solution in those tests. The observed batch-test removal efficiency in the solution to solid ratio of 200 (~20-fold) may be sufficient to reduce concentrations of I-129 from 30 pCi/L to 1 pCi/L even in the presence of the total iodine concentration loading due to I-127 in the groundwater at about 1000 times the I-129 concentration (Levitskaia et al. 2017). Column tests with relevant influent concentrations would be needed to verify removal efficiency. Removal rate appears to be rapid, with the 1-day iodine loading on the ferrihydrite similar to that for >30 days of loading.

Analysis of the ferrihydrite solid phase after reaction by I K-edge XAS revealed that the iodine speciation was predominantly iodate, with a reduction in the intensity of the white line due to the presence of some iodide. The amount of iodate remaining in solution decreased slightly over the longer >30 day sorption test, and thus, iodate was not released back into solution, despite that fact that ferrihydrite is unstable and likely undergoing transformation to goethite.

Nano-magnetite (Fe_3O_4) performed less well, with loading values of 40 µg/g and K_d values of 55 mL/g, at a solution to solid ratio of 200 and an iodine loading of 190 µg/g and a K_d of 233 mL/g at the higher solution to solid ratio of 1000. These materials have a relatively high surface area hat helps contribute to higher loading, although loading is not as high as for the ferrihydrite. The amount of iodate removed from solution did not change substantially over longer contact times. Analysis of the solid phase after reaction by I K-edge XAS revealed that the mechanism of iodine removal was by reduction of iodate to iodide.

Ferrous hydroxide ($Fe(OH)_2$) performed the worst of the iron oxides tested, with loading values of 20 and 10 µg/g, and K_d values of 16 and 12 mL/g, at solution to solid ratios of 200 and 1000, respectively. The iodine loading improved slightly with longer contact times. Iodine speciation on the solid could not be determined due to the low iodine loading.

These results suggest that sorption onto, or incorporation into, amorphous Fe(III)-bearing oxy(hydr)oxides, predominantly as iodate, is a promising option. Removal of iodate from solution by Fe(II)-bearing oxide-induced reduction to iodide is not an efficient process. There are challenges associated with deploying an amorphous Fe(III)-bearing oxides oxy(hydr)oxide, such as ferrihydrite, in the P&T system. The instability of ferrihydrite, and its gradual transformation to goethite over time, could affect iodine removal performance, although the lack of release of iodate into solution in the long-term tests performed here is promising. The nature of the ferrihydrite material requires that it be mixed with or coated on a support matrix, like silica sand. This process is of importance along with column configuration (e.g., the need for filters at each end) for deployment.

7.3.1.3 Sulfide Phases

Iron sulfide (FeS) and potassium tin sulfide ($K_{2x}Mg_xSn_{3-x}S_6$, $x = 0.5\text{-}1$, KMS) exhibited virtually no capacity for iodate update, with a very low iodine loading of <0.02 mg/g, irrespective of solution to solid ratio or contact time. Both materials have a significant reducing capacity and, in a sorption test conducted under the same conditions, demonstrated good loading capacity with respect to another potential oxyanion, pertechnetate (TcO_4^-). This highlights the importance of the uptake mechanism and reaction product for predicting material performance, e.g. technetium, as a transition metal, can be reduced to form a low solubility technetium sulfide, but, if the iodate is reduced to iodide in this system, it is out-competed by the excess sulfide for available sorption sites.

7.3.1.4 Bismuth-Based Materials

The bismuth-based materials demonstrated the best performance of all the materials tested with respect to iodate immobilization. Bismuth (oxy)hydroxide had loading values of 200 and 820 µg/g and K_d values of 20,1904 and 4204 mL/g, at solution to solid ratios of 200 and 1000, respectively. Because loading on bismuth (oxy)hydroxide increased for the solution to solid ratio of 1000 compared to the solution to solid ratio of 200, it was not at capacity at the solution to solid ratio of 200, which was also demonstrated by the complete removal of iodine from solution in those tests. The observed batch-test removal efficiency in the solution to solid ratio of 200 (>1000-fold) is more than sufficient to reduce concentrations of I-129 from 30 pCi/L to 1 pCi/L, even in the presence of a total iodine concentration loading due to I-127 in the groundwater at about 1000 times the I-129 concentration (Levitskaia et al. 2017). Given the high performance of this material, an additional test was conducted under the same conditions, but at an iodate concentration more relevant to the concentrations of I-129 present in groundwater (0.6 µg/L). The bismuth oxy(hydroxide) completely removed the iodate from solution to below the detection limit of the instrument at a solution to solid ratio of 200. This indicates that bismuth oxy(hydroxide) is a very promising material, but column tests would be needed to verify removal efficiency. At the lower solution to solid ratio (200), the rate of removal is good, with almost all of the iodate removed from solution within the first 24-hour test period. The stability of the material is such that none of the iodine is released back into solution over the extended batch sorption tests (>30 days). At the higher solution to solid ratio (1000), 81% of the iodate was removed from solution in the first 24 hours, and increased to 92% over the extended sorption test, suggesting that after the initial surface sorption sites become saturated, a kinetically slower process, possibly involving replacement of the interlayer anions (hydroxide, nitrate and carbonate) by the iodate, continues to remove iodate from solution. The speciation of iodine on the solid phase after the 24-hour sorption test is iodate, confirming that redox-driven processes are not involved in the iodine immobilization mechanism.

Bismuth-cobalt-aluminum out-performed the rest of the materials tested, but was slightly less efficient than bismuth (oxy)hydroxide. Bismuth-cobalt-aluminum had loading values of 190 and 540 µg/g and K_d values of 12800 and 1218 mL/g, at solution to solid ratios of 200 and 1000, respectively. The observed batch-test removal efficiency is more than sufficient to reduce concentrations of I-129 from 30 pCi/L to 1 pCi/L, even in the presence of a total iodine concentration loading due to I-127 in the groundwater at about 1000 times the I-129 concentration At the lower solution to solid ratio (200), 97% of the iodate is removed from solution within the first 24-hour test period, and the remaining 3% removed over the extended batch sorption tests (>30 days). At the higher solution to solid ratio (1000), 54% of the iodate was removed from solution in the first 24 hours, increasing slightly to 62% over the extended sorption test. The speciation of iodine on the solid phase after the 24-hour sorption test was iodate. Removal rate appeared to be rapid, with the 1-day iodine loading on the ferrihydrite similar to that for >30 days of loading.

7.3.1.5 Organoclays

The two organoclays tested here, PM-100 and MRM, did not remove significant amounts of iodate from solution, despite a high capacity for iodide and pertechnetate removal reported in the literature (Li et al., 2014). Organoclay PM-100 had loading values of 40 and 190 µg/g and K_d values of 52 and 230 mL/g, at solution to solid ratios of 200 and 1000, respectively. This material removed virtually the same amount of iodate from solution, irrespective of the higher solution to solid ratio, suggesting that it was at capacity at the solution to solid ratio of 200. Much like the ion exchange resin, the performance of organoclay PM-100 did not significantly improve over the extended batch sorption tests. This is likely because organoclay PM-100 is functionalized with quaternary amine groups, as in the ion exchange resin, so any removal of iodate from solution is rapid. The observed batch-test removal efficiency in the solution to solid ratio of 200 was not sufficient to reduce concentrations of I-129 from 30 pCi/L to 1 pCi/L. As with the ion exchange resin, the iodine speciation on the solid was iodide, suggesting that changes in the solution chemistry, induced by the material, caused reduction of a small fraction of the iodate to iodide, and this was preferentially adsorbed onto the organoclay.

Organoclay MRM performed similarly in the 24-hour sorption tests, with loading values of 50 and 190 µg/g and K_d values of 62 and 226 mL/g, at solution to solid ratios of 200 and 1000, respectively. Unlike organoclay PM-100, however, the performance of organoclay MRM did significantly improved over the longer sorption time of >30 days, with loading values increasing to 110 and 740 µg/g, at solution to solid ratios of 200 and 1000, respectively. Even with this improvement, however, the removal efficiency (3.6-fold) is still an order of magnitude too low. This improvement is likely related to a different mechanism for iodate immobilization, related to the sulfur in the sulfur-impregnated organoclay MRM. The speciation of iodine on the solid phase was iodide, implying reduction of iodate prior to immobilization on the organoclay, but the sulfur must remain associated with the clay as, in this case, it does not out-compete the iodide for sorption sites.

7.3.1.6 Aerogels

Despite literature precedent for aerogels to immobilize iodine (in the form of iodide and gaseous iodine), the copper-functionalized aerogel tested here was not able to remove significant quantities of iodate from solution. The aerogel had loading values of 30 and 20 µg/g and K_d values of 27 and 22 mL/g, at solution: solid ratios of 200 and 1000, respectively. This material removed similar amounts of iodate from solution, irrespective of the higher solution to solid ratio, suggesting that it was at capacity at the solution to solid ratio of 200. The speciation of iodine on the solid phase was iodate.

7.3.1.7 Metal Organic Frameworks (MOFs) and Cationic Polymeric Networks (CPNs)

The MOFs and CPNs demonstrated variable performance with respect to iodate immobilization. The CPN (SCU-CPN) performed the best, with loading values of 160 and 360 µg/g and K_d values of 636 and 557 mL/g, at solution to solid ratios of 200 and 1000, respectively. The observed batch-test removal efficiency in the solution to solid ratio of 200 (~4-fold) may not be sufficient for use in aboveground treatment. However, column tests with relevant influent concentrations are needed to verify removal efficiency. Removal rate appears to be rapid, with the 1-day iodine loading on the CPN only slightly less than that for >30 days of loading. The speciation of iodine on the solid phase was predominantly iodate, but a reduction in the intensity of the white line in the I K-edge XAS indicated that some iodide was also present. This result is of interest, as iodine is present as both iodate and iodide in Hanford groundwater. Many materials are selective for either iodate or iodide, but SCU-CPN demonstrated the capacity to immobilize both species on the solid phase.

FeBTC-PDA had loading values of 120 and 170 µg/g and K_d values of 287 and 198 mL/g, at solution to solid ratios of 200 and 1000, respectively. The observed batch-test removal efficiency is significantly below that required to reduce concentrations of I-129 from ~30 pCi/L to 1 pCi/L. However, column tests with relevant influent concentrations would be needed to verify removal efficiency. The performance of FeBTC-PDA did improve over longer loading times, especially at the high solution to solid ratio, with the extent of removal increasing from 17% at one day to 48% at > 30 days. Similar to SCU-CPN, the speciation of iodine on the solid phase was predominantly iodate, but with some iodide.

SCU-102 slightly outperformed SCU-101 at the low solution to solid ratio, with loading values of 50 µg/g and 40 µg/g and K_d values of 67 mL/g and 49 mL/g, respectively. However, they both reached the same loading value of 60 µg/g over the longer loading time. SCU-101 and SCU-102 behaved similarly at the higher solution to solid ratio with loading values of ~200 µg/g after 1 day and > 30 days. Because loading on SCU-101 and SCU-102 increased for the solution to solid ratio of 1000 compared to the solution to solid ratio of 200, it was not at capacity at the solution to solid ratio of 200. The speciation of iodine on the solid phase was iodide for both of these MOFs. This may explain the lower performance than that observed with SCU-CPN and FeBTC-PDA, as SCU-101 and SCU-102 could only immobilize the small amount of iodate that was reduced to iodide, whereas SCU-CPN and FeBTC-PDA could immobilize both iodate and iodide.

None of the MOFs/CPNs tested here were specifically designed for immobilization of iodate, so the fact that they removed some iodate from solution, and that the extent of removal depended on the structure and removal mechanism, suggests the MOF/CPN structure could be modified to improve performance with respect to immobilization of both iodate and iodide. However, given that these materials are relatively new, and that the synthesis can be complex, obtaining sufficient quantities for scaled-up testing will likely be difficult.

8.0 Conclusions and Path Forward for Promising Technologies

Laboratory-based technology screening was conducted on five in situ treatment technologies and a suite of materials for ex situ removal of iodine from groundwater. Key findings from each of these efforts are summarized in the sections below. For the most promising technologies, additional detail is provided to outline an approach for further evaluation of the technology to determine the technology's efficacy and implementability under Hanford Site conditions.

8.1 Co-Precipitation with Calcite

Co-precipitation of iodate with calcium carbonate was investigated using three methods. The first method, based on a study by Podder et al. (2017), showed that silica gel was effective at slowing the rate of calcite precipitation. It took approximately 2 weeks for the silica gel to form within the batch reactors. Subsequently, calcite crystals became visible in the batch reactors after another 2 weeks of equilibration in the silica gel. Separation of the calcite crystals from the silica gel proved to be challenging, confounding quantification of iodate loading within the newly formed calcite material. However, analysis of the silica gel/calcite precipitate demonstrated that the technology consistently removed approximately 60% of iodate from solution. It is interesting to note that this occurred across a wide range of iodate starting solution concentrations, from 100 to 396 mg/L. This finding indicates that the iodate removed from solution was largely associated with the silica gel vs. the calcite crystals.

The second method tested explored precipitating calcium carbonate in Hanford VZPW and AGW, which was based on previous testing that had shown an increase in iodate uptake when calcite forming solutions were made in VZPW. Results from batch tests showed that 65% to 71% of iodine was removed with calcite in VZPW compared to 45% to 48% in AGW and 33% to 38% in DDI (for concentrations 100 to 500 µg/L). Very little iodate was removed from any of the matrices when starting solution concentrations were high, i.e., 396 mg/L iodate. SEM analysis of calcium carbonate precipitates from the various solution matrices showed the presence of only calcite crystals in the DDI and AGW batch reactors. Conversely, SEM characterization of precipitates formed in the tests using VZPW as the contacting solution revealed calcite crystals, as well as needle-like crystals of the calcite polymorph aragonite. Due to their needle-like shape, aragonite crystals have a much higher surface area to mass ratio vs. calcite crystals, which could explain the greater iodate removal in the VZPW vs. the other two matrices tested.

The final approach tested involved the formation of nano-calcite crystals. The nano-calcite was synthesized under elevated temperature and pressure following a method by Montes-Hernandez et al. (2007). Results showed that 76% to 83% of calcite was removed from solution (starting solutions concentrations ranged from 100 to 500 µg/L) over a period of 24 hours. However, nearly all the uptake occurred prior to the first sample collected, which was collected 4 hours after beginning the reaction. SEM images of precipitates from these tests revealed the presence of both large and nano-sized calcite crystals. Although this technique achieved the highest percentage of iodate removal from solution, the need for elevated pressure and temperature limits the practical implementation of this technology for in situ iodate removal.

Evaluation of the three calcite precipitation techniques clearly demonstrated the ability to remove iodate from Hanford-representative solutions at relevant total iodine solution concentrations. However, none of the approaches were effective at a high percentage (>90%) of the iodate from solution. This presents a serious shortcoming for in situ application, as technologies being considered for field deployment should be capable of order of magnitude (90% or greater) reduction in aqueous concentrations. Therefore, further testing of in situ formation of calcite for remediation of ^{129}I is not recommended.

8.2 Incorporation into Apatite/Carbonated Apatite

Precipitation of initially amorphous calcium-phosphate (which slowly crystallized into apatite) inconsistently removed a small amount of iodate from solution at pH 11 and above, and none at pH 9.0 and 7.5 (Figure 8.1a). The Campayo et al. (2011) paper hypothesize that iodate substitutes for OH- in the hydroxyapatite. In the 40 experiments performed as part of our study, many showed greater uptake during initial amorphous calcium phosphate precipitation, and less iodate uptake as the precipitate crystallizes to hydroxyapatite. The uptake from solution resulted in some adsorbed iodate (0% to 4%) and some iodate incorporated into apatite (0% to 6.5%), as measured by ion exchanging iodate off the apatite (for adsorbed), then dissolving the apatite in acid to measure the incorporated mass. The iodate loading in apatite ranged from 0.1 to as high as 10 mg iodate/g apatite starting with unrealistically high aqueous iodate solutions, but 11 to 30 µg iodate/g apatite starting with 200 µg/L iodate. Although this loading is reasonable for field-scale use, none of the 40 experiments showed iodate removal to 1.0 µg/L detection limits.

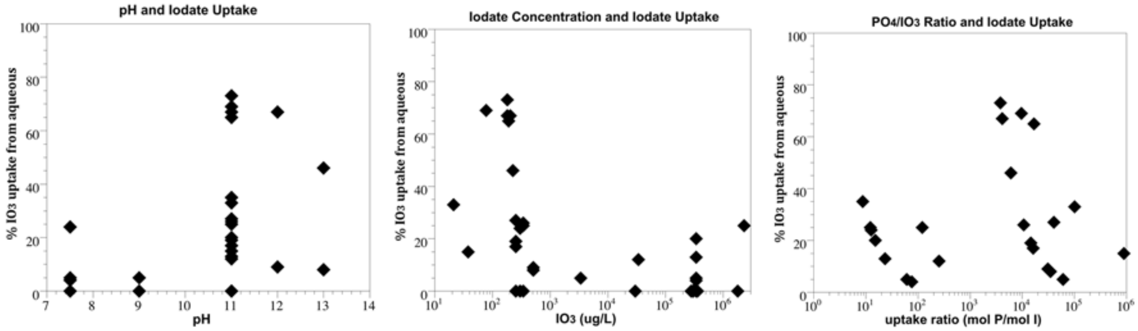

Figure 8.1. Iodate uptake from batch experiments as a function of a) pH, b) iodate concentration, and c) P/I ratio.

The rate of iodate removal from solution was calculated in time-course experiments and plotted as a function of the ratio of iodine to phosphate (Figure 8.2). A clear trend is observed where the most rapid iodate removal rates are observed in systems with the highest (>1000x) phosphate to iodate ratio.

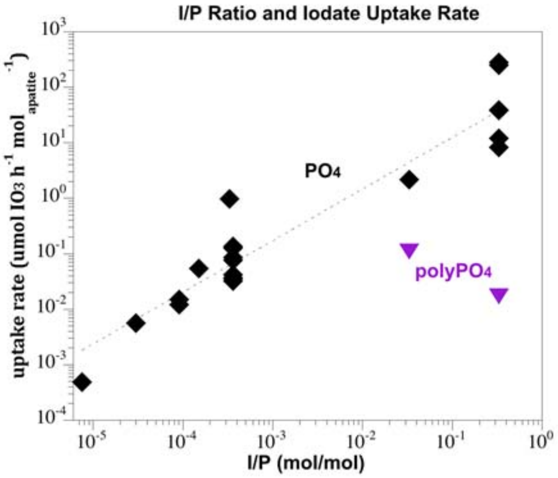

Figure 8.2. Iodate uptake rate as a function of the I/P ratio.

To deploy in the field, iodate concentrations need to be reduced to < 1 µg/L. The phosphate (orthophosphate and polyphosphate) and carbonate-substituted apatite would not be successful in achieving this concentration reduction. While there is some uptake of iodate observed in laboratory batch experiments specifically at pH > 10 and low (< 200 µg/L) iodate concentration with high phosphate concentration, none of the experiments removed all of the iodate from aqueous solution. The most successful phosphate solution used only orthophosphate, which immediately precipitated, making it less practical for field-scale deployment. High phosphate concentrations have been successfully injected into Hanford sediments, including a polyphosphate solution (90% orthophosphate, 10% pyrophosphate at 70 mM) in the 300 area, but only 1 of the 10 polyphosphate experiments performed as part of our study showed any iodate uptake. A Ca-citrate-phosphate solution has also been deployed at field scale (45 mM phosphate) in the 100N area, but our laboratory studies with this solution mobilized more iodine due to the reducing conditions created.

As tested, little iodate was removed from solution via either sorption onto or incorporation into apatite; therefore, further testing of this technology for remediation of ^{129}I is not recommended.

8.3 Enhanced Sorption by Organic Carbon

A series of batch adsorption/desorption experiments was conducted to determine the effectiveness of several organic materials for sequestering iodate and iodide from Hanford groundwater. The organic materials that were evaluated in this study were chitin, lignin, and humic acid sorbed to a representative Hanford sediment. The results indicate that significant sorption of iodide occurred on chitin, with an average K_d value of 74.9 ± 4.3 mL/g. Sorption of iodate to chitin was minimal (K_d = 3.2 ± 4.0 mL/g). Sorption of both iodide and iodate to lignin was also minimal (K_d = 3.6 ± 3.5 and 4.8 ± 4.8 mL/g). Similarly, sorption of both iodide and iodate to HA treated sediments was also minimal. Iodide K_d values for HA treated sediment were 0.46 ± 0.05 mL/g, only slightly higher than that of untreated sediment 0.34 ± 0.05 mL/g. For iodate, HA treated sediment had a K_d value of 0.58 ± 0.27 mL/g, which was lower than that of the untreated sediment 1.13 ± 0.06 mL/g. It is possible that the humic acid acted as a competitor for iodate adsorption sites on the sediment; however, these differences are small.

Of the three organic carbon materials tested, only chitin showed potential as an in situ remediation technology for iodide (average K_d value of 74.9 ± 4.3 mL/g). However, iodine within the groundwater at

200-UP-1 is primarily in the form of iodate, which would limit the effectiveness of chitin as a removal technology. As such, further testing of this technology is not recommended.

8.4 Co-Precipitation with Iron Oxides

The highest sorption capacity was found for HFO or goethite synthesized in a DDI water system followed by the iron oxides synthesized in AGW. Iodine sorption to HFO synthesized in AGW with sediments was also relatively high with the iodine remaining adsorbed for prolonged periods. This is promising because this system most closely mimics actual Hanford field conditions. Co-precipitation results showed that > 98% of the spiked iodate was removed from all three solution systems with initial concentrations in the range of 5 to 200 ppb, resulting in iodine loadings in the range of 0.22 to 7.97 mg/kg. For iodide, the removal efficiency was about 50% to 80%, and the calculated loading values were up to 1.10 mg/kg. 1-D column results showed that iodate transport was strongly retarded by sorption. Particle-facilitated iodine transport was demonstrated to not occur at flow rates as high as ~1.5 m/day, which were much higher than the typical groundwater flowrates at the Hanford site. Successful precipitation of HFO through natural Hanford calcite buffering demonstrated its potential for in situ HFO precipitation in the field.

Laboratory results collected to date indicate that iodate/iodide could be effectively removed from Hanford groundwater by iron oxides, especially HFO, either through sorption or co-precipitation processes. Further testing of this technology is recommended based on the high sorption capacity at neutral pH conditions, low cost, and likely ability to precipitate HFO in situ, indicate that this approach could be good candidate for iodate remediation in the 200-UP-1 OU.

8.5 Dithionite-Enhanced Mobility

Whereas most in situ treatment technologies are designed to immobilize iodine, the Na-dithionite reduction technology is designed to enhance iodine mobility. The Na-dithionite mobilizes significant iodine due to Fe oxide dissolution in sediments and is designed to enhance pump and treat system efficiency. This technology is targeted at accelerating the removal of iodine from the surface by P&T in areas where sorption limits extraction efficiency. Leaching behavior of vadose zone and aquifer sediments under B, T, and S complexes have shown that only 55% of iodine mass is mobilized in the first 10 pore volumes (aqueous and adsorbed iodine), with the remainder removed over the next 100 pore volumes due to the slow dissolution of iodine from precipitates. Sediment characterization shows that only a small fraction (i.e., 2% to 15%) of the iodate and iodide are adsorbed to the sediment, with the remainder present in one or more precipitates. The iodate and iodide associated with sediments may be bound to immobile natural organic matter, incorporated in calcite, incorporated in Fe oxides, or in other minerals.

Dithionite treatment of sediment enabled much greater (4x or more) and rapid (one to three orders of magnitude) leaching of iodine from the sediment compared to leaching of untreated sediment. However, it was expected that after Fe-oxides were dissolved and iodide advected from the sediments, ^{127}I concentrations in the dithionite-treated sediments should eventually be lower than untreated sediments. Unfortunately, leaching experiments have shown continued elevated iodine concentrations for dithionite treated sediments compared to untreated sediments for 100 to 150 pore volumes post treatment. Given that ^{127}I present in the sediments tested as part of this study is a combination of natural and Hanford-released iodine, it is not a perfect analogue for ^{129}I, which is nearly entirely Hanford-derived. This is primarily due to the fact that the initial speciation of Hanford–derived iodine could be different from that of naturally occurring iodine and the rates at which these species reestablish thermodynamic equilibrium is poorly known. Additionally, the source of elevated ^{127}I at Hanford is unknown (Truex et al. 2017), and could be from a different waste stream than some, or all, the ^{129}I. This variability in possible source terms for stable iodine could have a dramatic impact on the leachability of ^{129}I vs. ^{127}I from Hanford sediments, as ^{129}I from Hanford operations could be much less recalcitrant than ^{127}I present in the sediments tested to date. Further, unlike other treatment technologies that focus on removal of total iodine from solution, which must consider both ^{127}I and ^{129}I, dithionite only needs to be effective for removal of radioactive iodine, as stable iodine is not regulated as a groundwater contaminant. Based on this, in combination with the results generated to date, this technology is recommended to be further evaluated as a possible in situ treatment technology. Future testing will focus on evaluating the removal of ^{129}I from contaminated sediments in both batch and 1-D column tests. Emphasis will be placed upon determining total removal efficiencies for ^{129}I, as well as the kinetics of ^{129}I removal.

8.6 Materials for Iodine Immobilization

A wide range of materials were tested for capacity to remove iodate from synthetic groundwater containing competing anions. Ferrihydrite, bismuth oxy(hydroxide) and bismuth-cobalt-aluminum are the most promising materials, and the observed batch-test removal efficiency is sufficient to reduce concentrations of I-129 from 30 to 1 pCi/L, even in the presence of total iodine concentration loading due to I-127 in the groundwater at about 1000 times the I-129 concentration. Although the synthetic bismuth-based materials are currently only available in gram-quantities, efforts are underway to scale-up their synthesis. These most promising materials are recommended for additional column testing with relevant influent concentrations to verify removal efficiency.

9.0 Quality Assurance

The results presented in this report originate from work governed by the PNNL Nuclear Quality Assurance Program (NQAP). The NQAP implements the requirements of the United States Department of Energy Order 414.1D, *Quality Assurance*, and 10 CFR 830 Subpart A, *Quality Assurance Requirements*. The NQAP uses ASME NQA-1-2012, *Quality Assurance Requirements for Nuclear Facility Applications*, as its consensus standard and NQA-1-2012 Subpart 4.2.1 as the basis for its graded approach to quality.

Two quality grading levels are defined by the NQAP:

Basic Research - The required degree of formality and level of work control is limited. However, sufficient documentation is retained to allow the research to be performed again without recourse to the original researcher(s). The documentation is also reviewed by a technically competent individual other than the originator.

Not Basic Research - The level of work control is greater than basic research. Approved plans and procedures govern the research, software is qualified, calculations are documented and reviewed, externally sourced data is evaluated, and measuring instrumentation is calibrated. Sufficient documentation is retained to allow the research to be performed again without recourse to the original researcher(s). The documentation is also reviewed by a technically competent individual other than the originator.

The work supporting the results presented in this report was performed in accordance with the *Basic Research* grading level controls.

10.0 References

10 CFR 830, Subpart A. 2011. *Quality Assurance Requirements*. Code of Federal Regulations, U.S. Department of Energy, Washington, D.C.

ASME NQA-1-2012. *Quality Assurance Requirements for Nuclear Facility Applications*. The American Society of Mechanical Engineers, New York, NY.

Bird GA and W Schwartz. 1997. "Distribution coefficients, K(d)s, for iodide in Canadian Shield lake sediments under oxic and anoxic conditions." *J. Environ. Radioact.* 3:261- 279.

Byrappa K, and M Yoshimura. 2001. *Handbook of Hydrothermal Technology: A Technology for Crystal Growth and Materials Processing.* Norwich. In: Noyes Publications/William Andrew Publishing LLC.

Campayo L, A Grandjean, A Coulon, R Delorme, D Vantelon, and D Laurencin. 2011. "Incorporation of iodates into hydroxyapatite: a new approach for the confinement of radioactive iodine." *J. Mater Chem.* 21:17609-17611.

Cantrell KJ, RJ Serne, and GV Last. 2003. *Hanford Contaminant Distribution Coefficient Database and Users Guide*. PNNL-13895, Rev. 1, Pacific Northwest National Laboratory, Richland, WA.

Chao TT, and L Zhou. 1983. "Extraction techniques for selective dissolution of amorphous iron oxides from soils and sediments 1." *Soil Sci. Soc. Am. J.* 47:225-232.

Couture RA and MG Seitz. 1983. "Sorption of anions of iodine by iron oxides and kaolinite." *Nuclear and Chemical Waste Management* 4:301-306.

Denham M and C Eddy-Dilek. 2016. Sustainable Remediation of Radionuclide by a Common Sense Approach to Ehanced Attenuation – 16441. WM2016 Conference, March 6-10, Phoenix, AZ.

DOE. 1996. *Iodine-129 Contamination: Nature, Extent, and Treatment Technologies*. DOE/RL-95- 89, U.S. Department of Energy, Richland, WA.

DOE. 2012. *Record of Decision for Interim Remedial Action Hanford 200 Area Superfund Site 200-UP-1 Operable Unit*. 12-AMRP-0171, U.S. Department of Energy, Richland Operations Office, Richland, WA. Available at https://pdw.hanford.gov/arpir/index.cfm/viewDoc?accession=0091413.

DOE. 2017. *UP-1 Evaluation Plan for Iodine.* DOE/RL-2015-69, Rev. 0., U U.S. Department of Energy, Richland Operations Office, Richland, WA.

DOE. 2016. *Hanford Site Groundwater Monitoring Report for 2016*. DOE/RL-2016-67, U.S. Department of Energy, Richland, WA.

DOE Order 414.1D. 2011. *Quality Assurance*. U.S. Department of Energy, Washington, D.C. Approved 4/25/2011.

Du TB, D Tamoli, Y Luo, and V Desai. 2004. "Electrochemical characterization of copper chemical mechanical planization in KIO_3 slurry." *Applied Surface Science* 390:412-421.

Fard ZH, CD Malliakas, JL Mertz, and MG Kanatzidis. 2015. “Direct Extraction of Ag^+ and Hg^{2+} from Cyanide Complexes and Mode of Binding by the Layered $K_2MgSn_2S_6$ (KMS-2).” *Chemistry of Materials* 27(6):1925-1928.

Fuhrmann M, S Bajt, and M Schoonen. 1998. “Sorption of iodine on minerals investigated by x-ray adsorption near edge structure (XANES) and 125-I tracer sorption experiemnts.” *Applied Geochem* 13:127-141.

Hartman MJ, LJ Morasch, and WD Webber. 2004. *Hanford Site Groundwater Monitoring for Fiscal Year 2003*. PNNL- 14548, Pacific Northwest National Laboratory, Richland, WA.

Heron G, C Crouzet, AC Bourg, TH Christensen. 1994. “Speciation of Fe(II) and Fe(III) in Contaminated Aquifer Seiments Using Chemical Extraction Techniques. *Environ. Sci. Technol.* 28(9), 1698-1705.

Hou XL, CL Fogh, J Kucera, KG Andersson, H Dahlgaard, and SP Nielsen. 2003. “Iodine-129 and cesium-137 in Chernobyl contaminated soil and their chemical fractionation.” *Sci. Total Environ.* 308:97-109.

Kekl, A, A Aldahan, M Meili, G Possnert, N Buraglio, and R Stepanauskas. 2003. “I-129 in Swedish rivers: distribution and sources.” *Sci. Total Environ.* 309:1610-172.

Lee BD, JE Szecsody, N Qafoku, EM McElroy, SR Baum, M Snyder, and AR Lawter, et al. 2017. "Contaminant Attenuation and Transport Characterization of 200-UP-1 Operable Unit Sediment Samples." PNNL-26894, Pacific Northwest National Laboratory, Richland, WA.

Levitskaia TG, EL Campbell, SD Chatterjee, and GB Hall. 2017 *Analysis of Technetium Ion Exchange Resin from the 200 West Pump-and-Treat Facility*. PNNL-26933; RPT-DVZ-AFRI-049, Rev. 0, Pacific Northwest National Laboratory, Richland, WA.

Li D, DI Kaplan, AS Knox, KP Crapse, and DP Diprete. 2014. “Aqueous ^{99}Tc, ^{129}I and ^{137}Cs removal from contaminated groundwater and sediments using highly effective low-cost sorbents.” *Journal of Environmental Radioactivity* 136:56-63.

Li K, Y Zhao, P Zhang, C He, J Deng, S Ding, and W Shi. 2016. “Combined DFT and XPX investigation of iodine anions adsoprtion on the sulfur terminated (0001) chalcopyrite surface.” *Applied Surface Science* 390:412-421.

Li J, X Dai, and L Zhu, et al. 2018. “$^{99}TcO_4^-$ remediation by a cationic polymeric network.” *Nature Communications* 9:3007.

Mattigod SV, EC Golovich, DM Wellman, EA Cordova, and RM Smith 2010a. *Uranium Adsorption on Ion-Exchange Resins - Batch Testing*. PNNL- 20135, Pacific Northwest National Laboratory, Richland, WA.

Mattigod SV, EC Golovich, DM Wellman, EA Cordova, and RM Smith 2010b. *Tc-99 Adsorption on Selected Activated Carbons Batch Testing Results*. PNNL- 20136, Pacific Northwest National Laboratory, Richland, WA.

Matyáš J, GE Fryxell, BJ Busche, K Wallace, LS Fifield. 2011. *Ceram. Eng. Sci.: Ceram. Mater. Energy Appl.*, H-T Lin, Y Katoh, KM Fox, I Belharouak, S Widjaja, D Singh*, Wiley-The American Ceramic Society,* Daytona Beach, FL, 32:23.

Mehta S. 2017. “Geochemical evaluation of uranium sequestration from field-scale infiltration and injection of polyphosphate solutions in contaminated Hanford sediments.” Applied Geochemistry 84:133-153.

Montes-Hernandez, G, F Renard, N Geoffroy, L Charlet, and J Pironon. 2007. “Calcite precipitation from CO_2–H_2O–Ca $(OH)_2$ slurry under high pressure of CO_2. *Journal of Crystal Growth* 308(1):228-236.

Parker KE, EC Golovich, and DM Wellman. 2014. *Iodine Adsorption on Ion-Exchange Resins and Activated Carbons– Batch Testing*. PNNL-23730; RPT-DVZ-AFRI-021, Rev. 0, Pacific Northwest National Laboratory, Richland, WA.

Pearce CI, O Qafoku, J Liu, E Arenholz, SM Heald, RK Kukkadapu, CA Gorski, CMB Henderson, and KM Rosso. 2012. “Synthesis and properties of titanomagnetite (Fe3-xTixO4) nanoparticles: A tunable solid-state Fe(II/III) redox system.” *Journal of Colloid and Interface Science* 387:24-38.

Podder J, J Lin, W Sun, SM Botis, J Tse, N Chen, Y Hu, D Li, J. Seaman, and Y Pan. 2017. “Iodate in calcite and vaterite: Insights from synchrotron X-ray absorption spectroscopy and first-principles calculations.” *Geochimica et Cosmochimica Acta* 198:218-228.

Qin F, GF Li, RM Wang, JLWu, HZ Sun, and R Chen. 2012. “Template-Free Fabrication of Bi_2O_3 and $(BiO)_2CO_3$ Nanotubes and Their Application in Water Treatment.” *Chem-Eur J* 18:16491-16497.

Qafoku NP, AR Lawter, DH Bacon, L Zheng, J Kyle, CF Brown. 2017. “Review of the impacts of leaking CO_2 gas and brine on groundwater quality.” *Earth-science reviews*, 169:69-84.

Schwertmann U and RM Cornell. 2000. *Iron Oxides in the Laboratory*. John Wiley & Sons.

Serne R.J., J.H. Westsik, B.D. Williams, H.B. Jung, and G. Wang. 2015. "Extended Leach Testing of Simulated LAW Cast Stone Monoliths." PNNL-24297. Pacific Northwest National Laboratory Richland, WA.

Sheppard, MI, DH Thibault, J McMurry, and PA Smith. 1995. “Factors affecting the soil sorption of iodine.” *Water Air Soil Poll.* 83:51-67.

Shigeno Y, K Kondo, and K Takemoto. 1980. “Functional monomers and polymers. LXX. On adsoption of iodine onto chitosan.” *Journal of Applied Polymer Science* 25(5):731-738.

Stookey LL. 1970. “Ferrozine – A New Spectrophotometric Reagent for Iron.” *Analytical Chemistry* 42: 779-781.

Strickland CE, AR Lawter, NP Qafoku, JE Szecsody, MJ Truex, and G Wang. 2017a. *Evaluation of Iodine Remediation Technologies in Subsurface Sediments: Interim Status Report*. PNNL-26957, Pacific Northwest National Laboratory, Richland, WA.

Strickland CE, CD Johnson, BD Lee, N Qafoku, JE Szecsody, MJ Truex, and VR Vermeul. 2017b. *Identification of Promising Remediation Technologies for Iodine in the UP-1 Operable Unit*. PNNL-26934, Pacific Northwest National Laboratory, Richland, WA.

Stucki JW, DC Golden, CB Roth. 1984. “Effects of oxidation state of octahedral iron on clay swelling..” *Clays Clay Miner.* 32:191-197.

Sumner ME. 2000. “Soil Fertility and Plant Nutrition.” Section D in Handbook of Soil Science, CRC Press, Boca Raton, Florida.

Sun DT, L Peng, WS Reeder, et al. 2018. “Rapid, Selective Heavy Metal Removal from Water by a Metal–Organic Framework/Polydopamine Composite.” *ACS Central Science* 4(3):349-356.

Szecsody JE, KM Krupka, MD Williams, KJ Cantrell, CT Resch, and JS Fruchter. 1998. "Uranium Mobility During In Situ Redox Manipulation of the 100 Areas of the Hanford Site." PNNL-12048, Pacific Northwest National Laboratory, Richland, WA.

Szecsody J.E., J.S. Fruchter, M.A. Mckinley, C.T. Resch, and TJ Gilmore. 2001. "Feasibility of In Situ Redox Manipulation of Subsurface Sediments for RDX Remediation at Pantex." PNNL-13746, Pacific Northwest National Laboratory, Richland, WA.

Szecsody JE, JS Fruchter, MD Williams, VR Vermeul, and DS Sklarew. 2004. "In Situ Chemical Reduction of Aquifer Sediments: Enhancement of Reactive Iron Phases and TCE Dechlorination." *Environmental Science & Technology* 38(17):4656-4663.

Szecsody JE, BD Lee, AR Lawter, N Qafoku, CT Resch, SR Baum, and II Leavy, et al. 2017. "Effect of Co-Contaminants Uranium and Nitrate on Iodine Remediation." PNNL-26955, Pacific Northwest National Laboratory, Richland, WA.

Truex MJ, BD Lee, CD Johnson, N Qafoku, GV Last, MH Lee, and DI.Kaplan. 2015. "Conceptual Model of Iodine Behavior in the Subsurface at the Hanford Site." PNNL-24709, Pacific Northwest National Laboratory, Richland, WA.

Truex MJ, BD Lee, CD Johnson, NP Qafoku, JE Szecsody, JE Kyle, M Tfaily, MMV Snyder, AR Lawter, M Oostrom, G Tartakovsky, II Leavy, EM McElroy, D Appriou, R Sahajpal, MM Carroll, GV Last, MH Lee, and DI Kaplan. 2016. *Conceptual Model of Iodine Behavior in the Subsurface at the Hanford Site*. PNNL-24709, Rev. 1, Pacific Northwest National Laboratory, Richland, WA.

Truex MJ, JE Szecsody, N Qafoku, CE Strickland, JJ Moran, BD Lee, and M Snyder. 2017. *Contaminant Attenuation and Transport Characterization of 200-DV-1 Operable Unit Sediment Samples*. PNNL-26208; RPT-DVZ-AFRI-037, Pacific Northwest National Laboratory, Richland, WA.

Um W and RJ Serne. 2005. “Sorption and transport behavior of radionuclides in the proposed low-level radioactive waste repository at the Hanford site, Washington.” *Radiochim. Acta.* 93:57-63.

Vermeul VR, MD Williams, JE Szecsody, JS Fruchter, CR Cole, and JE Amonette. 2002. "Creation of a Subsurface Permeable Reactive Barrier Using In Situ Redox Manipulation." In Handbook of Groundwater Remediation using Permeable Reactive Barriers: Applications to Radionuclides, Trace Metals, and Nutrients, edited by David L. Naftz, et al. 163-192. San Diego, California:Academic Press.

Wellman DM, JP Icenhower, AP Gamerdinger, and SW Forrester. 2006. "Effects of pH, temperature, and aqueous organic material on the dissolution kinetics of meta-autunite minerals, $(Na, Ca)_{2-1}[(UO_2)(PO_4)]_2 \cdot 3H_2O$." *The American Mineralogist* 91(1):143-158.

Xu C, D Kaplan, S Zhang, M Athon, Y Ho, H Li, C Yeager, K Schwehr, R Grandbois, D Wellman, and P Santschi. 2015. “Radioiodine sorption/desorption and speciation transformation by subsurface sediments from the Hanford Site.” *J. Env. Radioactivity* 139:43-55.

Yamashita t and P Hayes. 2008. “Analysis of XPS spectra of Fe^{2+} and Fe^{3+} ions in oxide materials.” *Applied Surface Science* 254:2441-2449.

Zhu L D Sheng, C Xu, et al. 2017. “Identifying the Recognition Site for Selective Trapping of $^{99}TcO_4^-$ in a Hydrolytically Stable and Radiation Resistant Cationic Metal–Organic Framework.” *Journal of the American Chemical Society* 139(42):14873-14876.

Pacific Northwest
NATIONAL LABORATORY

www.pnnl.gov

902 Battelle Boulevard
P.O. Box 999
Richland, WA 99352
1-888-375-PNNL (7665)

U.S. DEPARTMENT OF
ENERGY